CIVIL ENGINEERING STUDIES

STRUCTURAL RESEARCH SERIES NO. 323



# A LARGE DEFLECTION ANALYSIS METHOD FOR ELASTIC-PERFECTLY PLASTIC CIRCULAR PLATES



by

J. G. CROSE

and

A. H.-S. ANG

Issued as a Technical Report
of a Research Program Carried Out
under
NATIONAL SCIENCE FOUNDATION
Research Grant No. NSF-GK589

UNIVERSITY OF ILLINOIS
URBANA, ILLINOIS
JUNE 1967

# A LARGE DEFLECTION ANALYSIS METHOD FOR ELASTIC-PERFECTLY PLASTIC CIRCULAR PLATES

by

J. G. Crose
and
A. H.-S. Ang

Issued as a Technical Report
of a Research Program Carried Out under

NATIONAL SCIENCE FOUNDATION
Research Grant No. NSF-GK 589

UNIVERSITY OF ILLINOIS
URBANA, ILLINOIS

June 1967

# ACKNOWLEDGMENT

The results presented herein were obtained as a part of a research program on the development of mathematical models for solid media being conducted in the Department of Civil Engineering, University of Illinois, and sponsored by the National Science Foundation under Research Grant NSF-GK589. This report is based on a doctoral thesis by Dr. James G. Crose, submitted to the Graduate College of the University of Illinois in partial fulfillment of the requirements for the degree of Doctor of Philosophy. The work was done under the immediate direction of Dr. A. H.-S. Ang, Professor of Civil Engineering.

The authors wish to acknowledge Dr. L. A. Lopez, Assistant Professor of Civil Engineering, Lehigh University and Dr. J. H. Rainer, Assistant Professor of Civil Engineering for fruitful discussions throughout the course of the investigation and Dr. J. W. Melin, Assistant Professor of Civil Engineering, for the use of his efficient computer subroutine to solve linear simultaneous equations. Also gratefully acknowledged is the cooperation of the Department of Computer Science in the use of the IBM 7094 computing system.

TABLE OF CONTENTS

LIST OF FIGURES

# I. INTRODUCTION

## 1.1 Object and Scope

The classical theory of plates which assumes small deflections and linearly elastic material behavior is noticeably deficient in describing the behavior of thin plates and plates made of ductile materials. When lateral deflections exceed one-half of the thickness of a plate (1)*, the prediction of the classical theory of plates is erroneous.

Solutions for the large deflection analysis of elastic plates are based on Von Karman's non-linear equations (1)(2)(3). These equations include the effects of membrane forces and the second order effects of vertical displacements in the associated stain-displacement equations.

There have been many recent efforts to determine the load carrying capacity of elastic-perfectly plastic plates. Ang and Lopez (4) found solutions for square plates that compared favorably with upper and lower bound theories of perfectly plastic plates (5). In addition, deflections, and stresses were found as a function of load. The general approach of Ang and Lopez is used in the present study.

Haythornthwaite (6), Ohashi and Murakami (7) found solutions for elastic-perfectly plastic plates and showed that membrane forces play an important role in the behavior of these plates even with relatively small deflections. Cooper and Shifrin (8) showed experimentally that the ultimate load carrying capacity of mild steel plates is considerably higher than indicated by upper bound theories which are based on small deflections.

*Numbers in parentheses refer to entries in the bibliography.

Ang and Lopez (4) demonstrated the feasibility of using a lumped parameter model to solve non-linear plate problems. The model is essentially a finite difference physical analogue of the governing differential equations of the corresponding continuous plate.

The objective of this thesis is to develop a numerical method for analyzing plates that will take into account all non-linearities involving displacements and material behavior. Such a method is to be used to determine the behavior of thin to medium thick plates throughout the entire range of loading.

## 1.2 Assumptions

The present development is valid only for axially symmetric plates. In addition, the variation of displacements and stresses through the thickness of the plate is simplified by adopting a sandwich configuration. Theoretical equations are developed with the following assumptions:

1. The plate is composed of three layers. The top and bottom layers are identical and are assumed to be characterized by a state of plane stress. They are composed of an elastic-perfectly plastic material. Yielding is governed by the von Mises yield criterion and plastic flow follows the Prandtl-Reuss flow rule. The middle layer, referred to as a shear core, has constant thickness, is infinitely stiff with respect to transverse shearing forces, and provides no resistance to flexural and extensional forces. Such a plate can be proportioned to exactly simulate a solid elastic plate and a plastic membrane.

2. The Kirchoff-Love hypothesis, which states that for thin plates and shells, a normal to the middle surface remains normal during deflection. This assumption is not related to material behavior, but is a direct consequence of the geometry of thin plates and shells (9). The effect of this assumption is to neglect shear deformations normal to the middle surface of the plate or shell. These deformations are negligible when compared with the rotations of a flexible body such as a thin plate or shell.
3. The principal loading of the plate is normal to the plane of the plate.
4. The stress rate-strain rate equations of plasticity are valid for small, but finite increments of load.
5. Hooke's law is valid for large deflections.

## 1.3 Notation

| | |
|---|---|
| C | stress-strain coefficient matrix |
| D | strain-displacement coefficient matrix |
| E | Young's Modulus |
| E ($\Delta X$) | residual load corresponding to $\Delta X = 0$, otherwise an element of the equilibrium equation |
| F | internal force vector |
| h | half-thickness of the sandwich plate |
| $J_2$ | second invariant of the deviatoric stresses |
| k | yield limit of material in simple shear |
| $M_r$, MR, $MR_i$ | radial bending moments per unit width |

| | |
|---|---|
| $M_t$, $MT$, $MT_i$ | tangential bending moments per unit width |
| $N_r$, $NR$, $NR_i$ | radial membrane forces per unit width |
| $N_t$, $NT$, $NT_i$ | tangential membrane forces per unit width |
| $n$ | number of discrete points of the plate, or the number of the point on the boundary |
| $p$ | scalar quantity proportional to the intensity of load |
| $P$ | load vector prescribing the load distribution |
| $P_n$, $P_N$ | loads per unit area normal to the middle surface of the plate |
| $P_t$, $P_T$ | loads per unit area tangent to the middle surface of the plate (must be directed radially when projected on the r-θ plane) |
| $P_v$, $\overline{P}_v(i)$ | total vertical load on an element of the plate within a given radial distance |
| $Q$, $Q_i$ | shear force per unit width |
| $R$ | coefficient matrix of internal forces in the equilibrium equations |
| $S$, $S_i$ | extension of middle surface |
| $t$ | thickness of the sheets in the sandwich plate |
| $T$ | coefficient matrix of the stress-force transformation equations |
| $u$, $u_i$, $u_i^t$, $u_i^b$ | horizontal displacements; t refers to top sheet and b refers to bottom sheet |
| $w$, $w_i$, $w_i^t$, $w_i^b$ | vertical displacements; t refers to top sheet and b refers to bottom sheet |
| $\mathring{W}$ | rate of work of the deviatoric stresses in distorting the material |
| $X$ | displacement vector |

| | |
|---|---|
| $\Delta$ | as a prefix, represents any incremental quantity, e.g., $\Delta X$ is an incremental displacement corresponding to an incremental load, $\Delta p$ |
| $\overline{\Delta R}$ | an approximation of R |
| $\widetilde{\Delta R}\ \Delta X$ | $= \overline{\Delta R}$ |
| $\varepsilon_r$, $\varepsilon_r^t$, $\varepsilon_r^b(i)$, etc. | radial strain |
| $\mathring{\varepsilon}_r$ | radial strain rate |
| $\varepsilon_t$, $\varepsilon_t^t$, $\varepsilon_t^b(i)$, etc. | tangential strain |
| $\mathring{\varepsilon}_t$ | tangential strain rate |
| $\lambda$ | radial mesh length of the undeformed model |
| $\mu$ | Poisson's ratio |
| $\sigma_r$, $\sigma_r^t$, $\sigma_r^b(i)$, etc. | radial stress |
| $\mathring{\sigma}_r$ | radial stress rate |
| $\sigma_t$, $\sigma_t^t$, $\sigma_t^b(i)$, etc. | tangential stress |
| $\mathring{\sigma}_t$ | tangential stress rate |
| $0\ (\lambda^j)$ | an error proportional to $\lambda^j$ |
| $\overline{\sigma}_r$, $\overline{\sigma}_t$, etc. | barred stresses indicate a stress somewhere between $\sigma_r$ and $\sigma_r + \Delta\sigma_r$ or $\sigma_t$ and $\sigma_t + \Delta\sigma_t$, etc. |
| $\frac{qa^4}{Eh^4}$ | a nondimensional load parameter where q is the normal load per unit area, a is the radius of the plate, h is the total thickness of an equivalent solid plate, and E is Young's Modulus |
| $w_o/h$ | a nondimensional displacement parameter where $w_o$ is the vertical displacement at the center of the plate and h is the total thickness of an equivalent solid plate |

$\frac{\sigma a^2}{Eh^2}$ a nondimensional stress parameter where $\sigma$ is the sum of the maximum fibre bending stress and membrane stress, a is the radius of the plate, h is the thickness of the equivalent solid plate and E is Young's Modulus (Bending stresses in the sandwich plate are multiplied by $\sqrt{3}$ to correspond to the extreme fiber bending stresses of a solid plate)

# II. THEORETICAL EQUATIONS

## 2.1 Equilibrium

Fig. 1 shows an infinitesimal element of a circular plate in its unloaded state A and in its deformed state A* with the loads and forces acting on it. Since the displacements and rotations of such an element may be large, the equations of equilibrium must be satisfied in its deformed position (9). The resulting expressions are similar to the shell equations of equilibrium except that the geometry of the shell is a function of the displacements.

Fig. 2 shows the projection of A* on an r-z plane. The loads $P_n$ and $P_t$, and the forces $M_r$, $M_t$, $N_r$, $N_t$, and Q are the forces acting on the element. The displacement functions u and w determine the deformed shape of the plate and as such determine the radius of curvature R at A*. Summation of forces in the r-z plane and in a direction tangent to the plate in its deformed state yields

$$
\begin{aligned}
&[(r + u) + \frac{1 + \frac{\partial u}{\partial r}}{2} dr]\,[N_r + \frac{\partial N_r}{\partial r}\frac{dr}{2} \cos \frac{d\phi}{2}\, d\theta] \\
&- [(r + u) - \frac{1 + \frac{\partial u}{\partial r}}{2} dr]\,[N_r - \frac{\partial N_r}{\partial r}\frac{dr}{2} \cos \frac{d\phi}{2}\, d\theta] \\
&- [(r + u) + \frac{1 + \frac{\partial u}{\partial r}}{2} dr]\,[Q + \frac{\partial Q}{\partial r}\frac{dr}{2} \sin \frac{d\phi}{2}\, d\theta] \qquad (1) \\
&- [(r + u) - \frac{1 + \frac{\partial u}{\partial r}}{2} dr]\,[Q - \frac{\partial Q}{\partial r}\frac{dr}{2} \sin \frac{d\phi}{2}\, d\theta] \\
&- 2\, R d\phi\, N_t \sin \frac{d\theta}{2} \cos \phi + P_t\, R d\phi\, (r + u)\, d\theta = 0
\end{aligned}
$$

while summing moments in the r-z plane about the center of the element leads to

$$
\begin{aligned}
&[(r + u) + \frac{1 + \frac{\partial u}{\partial r}}{2} dr] [M_r + \frac{\partial M_r}{\partial r} \frac{dr}{2}] d\theta \\
&- [(r + u) - \frac{1 + \frac{\partial u}{\partial r}}{2} dr] [M_r - \frac{\partial M_r}{\partial r} \frac{dr}{2}] d\theta \\
&- 2 R d\phi \, M_t \sin \frac{d\theta}{2} \cos \phi \qquad (2) \\
&+ [(r + u) + \frac{1 + \frac{\partial u}{\partial r}}{2} dr] [Q + \frac{\partial Q}{\partial r} \frac{dr}{2}] \frac{R d\phi}{2} d\theta \\
&+ [(r + u) - \frac{1 + \frac{\partial u}{\partial r}}{2} dr] [Q - \frac{\partial Q}{\partial r} \frac{dr}{2}] \frac{R d\phi}{2} d\theta = 0
\end{aligned}
$$

Dividing the above equations by $dr d\theta$, and neglecting higher order terms, Eqs. (1) and (2) become, respectively,

$$
\begin{aligned}
&(1 + \frac{\partial u}{\partial r}) N_r + (r + u) \frac{\partial N_r}{\partial r} - \frac{(r + u) S}{R} Q - (1 + \frac{\partial u}{\partial r}) N_t \\
&+ (r + u) S P_t = 0 \qquad (3)
\end{aligned}
$$

and,

$$
(1 + \frac{\partial u}{\partial r}) M_r + (r + u) \frac{\partial M_r}{\partial r} - (1 + \frac{\partial u}{\partial r}) M_t + (r + u) S Q = 0 \qquad (4)
$$

where $$S = \sqrt{\left(\frac{\partial w}{\partial r}\right)^2 + \left(1 + \frac{\partial u}{\partial r}\right)^2}$$

and $$R = \frac{\left[\left(1 + \frac{\partial u}{\partial r}\right)^2 + \left(\frac{\partial w}{\partial r}\right)^2\right]^{3/2}}{\left[\left(1 + \frac{\partial u}{\partial r}\right)\frac{\partial^2 w}{\partial r^2} - \frac{\partial w}{\partial r}\frac{\partial^2 u}{\partial r^2}\right]}$$

The shear force Q can be found by considering the equilibrium of a section of the symmetrically loaded plate within the radius r. Fig. 3 shows this section in the r-z plane. Summation of forces in the z direction yields

$$Q = \frac{S\,\overline{P}_v}{2\pi(r + u)\left(1 + \frac{\partial u}{\partial r}\right)} - \frac{\frac{\partial w}{\partial r} N_r}{\left(1 + \frac{\partial u}{\partial r}\right)} \tag{5}$$

where $\overline{P}_v$ is the total vertical load from r = 0 to r = r.

Substitution of Eq. (5) into Eqs. (3) and (4) yields, respectively,

$$\left[1 + \frac{\partial u}{\partial r} + \frac{(r + u)\,S\,\frac{\partial w}{\partial r}}{R\left(1 + \frac{\partial u}{\partial r}\right)}\right] N_r + (r + u)\frac{\partial N_r}{\partial r} - \left(1 + \frac{\partial u}{\partial r}\right) N_t$$
$$+ \frac{S^2}{2\pi R\left(1 + \frac{\partial u}{\partial r}\right)}\overline{P}_v + (r + u)\,S\,P_t = 0 \tag{6}$$

and

$$(1 + \frac{\partial u}{\partial r}) M_r + (r + u) \frac{\partial M_r}{\partial r} - (1 + \frac{\partial u}{\partial r}) M_t - \frac{(r + u) S \frac{\partial w}{\partial r}}{1 + \frac{\partial u}{\partial r}} N_r$$

$$- \frac{S^2}{2\pi(1 + \frac{\partial u}{\partial r})} \overline{P}_v = 0 \tag{7}$$

which are the final equilibrium equations for the plate.

## 2.2 Variation of Stresses on a Cross-Section of the Plate

In order to treat the plate as a two-space problem, it is idealized as a sandwich plate (4). The result of this idealization is to eliminate the effect of yielding throughout the thickness of the plate. Fig. 4 is a schematic representation of the sandwich plate. It is assumed that the thin sheets are in plane stress; i.e., all stress components lie within the plane of the sheets and are distributed uniformly across their thickness. Shear forces resulting from the bending of the plate are carried only by the shear core. The resultant forces per unit width acting on a cross-section of the plate are related to the stresses by

$$\begin{aligned} M_r &= (\sigma_r^{\ t} - \sigma_r^{\ b})\ ht \\ M_t &= (\sigma_t^{\ t} - \sigma_t^{\ b})\ ht \\ N_r &= (\sigma_r^{\ t} + \sigma_r^{\ b})\ t \\ N_t &= (\sigma_t^{\ t} + \sigma_t^{\ b})\ t \end{aligned} \tag{8}$$

where the subscripts b and t, respectively, refer to the bottom and top sheets of the plate; h is the half thickness of the plate, and t is the thickness of the sheets.

## 2.3 Stress-Strain Relations

### 2.3.1 Hooke's Equations

The material of the plate is assumed to be an elastic-perfectly plastic solid. In the elastic range the material behavior is described by Hooke's law, while beyond the elastic limit, this is replaced by an elastic-plastic law. Throughout the range of elastic behavior of the plate, Hooke's law is used to relate stresses to strains. For an elastic isotropic material under plane stress conditions, Hooke's equations in polar coordinates are

$$\sigma_r = \frac{E}{1 - \mu^2} (\varepsilon_r + \mu \ \varepsilon_t)$$

$$\sigma_t = \frac{E}{1 - \mu^2} (\varepsilon_t + \mu \ \varepsilon_r) \tag{9}$$

where E is Young's modulus, $\mu$ is Poisson's ratio, and $\varepsilon_r$ and $\varepsilon_t$ are the strains in the radial and tangential directions, respectively.

### 2.3.2 Elastic-Plastic Equations

Hooke's equations are not valid when the state of stress exceeds the elastic limit as given by the von Mises yield condition. The behavior of the material beyond this state is governed by the elastic-plastic equations of Prandtl-Reuss. It is characterized as being elastic-perfectly plastic.

A loading function, $\phi$, may be defined as follows:

$$\phi = \phi\ (\sigma_r, \sigma_t)$$

If $\phi < k^2$, where k is the yield limit of the material in simple shear, the material is elastic and is governed by Hooke's law. If $\phi = k^2$, the material will undergo plastic flow and a plastic stress-strain law is used. The condition $\phi > k^2$ is not permissible for perfectly plastic material. If, after plastic flow has occurred at a point, the state of stress becomes such that $\phi < k^2$, the material is said to have unloaded from a prior plastic state and its behavior is incrementally elastic.

In the von Mises yield criterion $\phi = J_2$, the second invariant of the deviatoric stresses. For the case of plane stress with axial symmetry, the yield condition becomes

$$J_2 \equiv \frac{1}{3}\left(\sigma_r^{\,2} - \sigma_r\sigma_t + \sigma_t^{\,2}\right) = k^2 \tag{10}$$

Appendix A contains a derivation of the associated flow rule of Prandtl-Reuss. In rate form,

$$\overset{\circ}{\sigma}_r = \frac{E\left[(2\sigma_t - \sigma_r)^2\,\overset{\circ}{\varepsilon}_r - (2\sigma_t - \sigma_r)(2\sigma_r - \sigma_t)\,\overset{\circ}{\varepsilon}_t\right]}{(2\sigma_t - \sigma_r)^2 + (2\sigma_r - \sigma_t)^2 + 2\mu(2\sigma_t - \sigma_r)(2\sigma_r - \sigma_t)} \tag{11a}$$

$$\overset{\circ}{\sigma}_t = \frac{E\left[(2\sigma_r - \sigma_t)^2\,\overset{\circ}{\varepsilon}_t - (2\sigma_t - \sigma_r)(2\sigma_r - \sigma_t)\,\overset{\circ}{\varepsilon}_r\right]}{(2\sigma_t - \sigma_r)^2 + (2\sigma_r - \sigma_t)^2 + 2\mu(2\sigma_t - \sigma_r)(2\sigma_r - \sigma_t)} \tag{11b}$$

$$\overset{\circ}{W} = \frac{2(\sigma_r^2-\sigma_r\sigma_t+\sigma_t^2)\{[(2\sigma_r-\sigma_t)-\mu(2\sigma_t-\sigma_r)]\ \overset{\circ}{\varepsilon}_r+[(2\sigma_t-\sigma_r)-\mu(2\sigma_r-\sigma_t)]\ \overset{\circ}{\varepsilon}_t\}}{(2\sigma_r-\sigma_t)^2+(2\sigma_t-\sigma_r)^2+2\mu(2\sigma_r-\sigma_t)(2\sigma_t-\sigma_r)} \tag{12}$$

where $\overset{\circ}{W}$ is interpreted as the rate of work of the deviatoric stresses in distorting the material. Eqs. (11a, b) are the constitutive relations for the material in the plastic range and remain valid as long as

$$J_2 = k^2$$

$$\overset{\circ}{W} > 0$$

If $\overset{\circ}{W} < 0$, the state of unloading has occurred and Hooke's law in incremental form must be used in place of Eqs. (11a, b).

## 2.4 Strain-Displacement Relations

The magnification of an infinitesimal line element is used as the basis for defining strain as a function of displacements. Strain is defined as

$$\varepsilon_L = \frac{1}{2}\left[\left(\frac{ds^*}{ds}\right)^2 - 1\right] \tag{13a}$$

where ds is the infinitesimal length of the line element L before deformation and ds* is the infinitesimal length after deformation.

For the case of axial symmetry,

$$\varepsilon_r = \frac{\partial u}{\partial r} + \frac{1}{2}\left[\left(\frac{\partial u}{\partial r}\right)^2 + \left(\frac{\partial w}{\partial r}\right)^2\right]$$

$$\varepsilon_t = \frac{u}{r} + \frac{1}{2}\left(\frac{u}{r}\right)^2 \qquad (13)$$

where $\varepsilon_r$ is the strain in the radial direction, $\varepsilon_t$ is the strain in the tangential direction, u is the radial displacement and w is the vertical displacement of a point.

## 2.5 Transformation of Displacements to the Middle Surface

The variables, u, w, r in Eq. (13) are evaluated at a point, say r = a, to yield the strain $\varepsilon_r$ at "a" and $\varepsilon_t$ at "a". As a result of the Kirchoff-Love assumption, the displacement of any point in a plate may be expressed in terms of the displacement functions of the middle surface. Accordingly, the displacement of a point in the top sheet of the plate can be expressed in terms of the displacement functions of the middle surface evaluated at the corresponding point on the middle surface. The displacement of a point in the bottom sheet can be expressed similarly.

Fig. 5 shows the sandwich plate in the r-z plane. The shape of the middle surface is determined by the two displacement functions u and w. Corresponding displacements of the top sheet are expressed as $u^t$ and $w^t$ and the displacements of the bottom sheet are expressed as $u^b$ and $w^b$. According to the Kirchoff-Love hypothesis, the line element "$a^t a^b$" which is normal to the middle surface at "a" in the unloaded state remains normal to the middle surface at "a" in the deformed state.

Therefore:

$$u^t = u + h \times \frac{\frac{\partial w}{\partial r}}{\sqrt{(\frac{\partial w}{\partial r})^2 + (1 + \frac{\partial u}{\partial r})^2}}$$

$$w^t = w - h \times \frac{1 + \frac{\partial u}{\partial r}}{\sqrt{(\frac{\partial w}{\partial r})^2 + (1 + \frac{\partial u}{\partial r})^2}} + h$$

$$u^b = u - h \times \frac{\frac{\partial w}{\partial r}}{\sqrt{(\frac{\partial w}{\partial r})^2 + (1 + \frac{\partial u}{\partial r})^2}} \tag{14}$$

$$w^b = w + h \times \frac{1 + \frac{\partial u}{\partial r}}{\sqrt{(\frac{\partial w}{\partial r})^2 + (1 + \frac{\partial u}{\partial r})^2}} - h$$

Eq. (14), therefore, expresses the displacements of the top and bottom sheets of the plate in terms of the displacements of the middle surface.

## 2.6 Combination of Equations

The solution to the problem, therefore, consists of obtaining the displacement functions $u = u(r)$ and $w = w(r)$ of the middle surface of the plate at every level of loading. These functions must be smooth and continuous through their first derivatives to insure that the assumption of compatibility is satisfied.

The above equations, Eqs. (6) through (9), and Eqs. (13) and

(14) may be combined to form two partial differential equations in terms of the unknown displacement functions, $u = u(r)$, and $w = w(r)$ of the middle surface. These equations are valid as long as no portion of the plate yields. The solution of the two partial differential equations over the region of the plate, together with suitable boundary conditions constitute the solution to a laterally loaded elastic plate.

When the load on the plate reaches a level that will cause yielding of some region of the plate according to von Mises' yield criterion, Eq. (10), Eq. (9) must be replaced by Eq. (11). When plastic flow occurs, the problem becomes more difficult because the stress-strain equations are functions of the instantaneous stresses; e.g., at some level of load, say P, the stresses are $\sigma_r$, and $\sigma_t$. At a higher load level, $P + \Delta P$, the stresses are $\sigma_r + \Delta\sigma_r$, and $\sigma_t + \Delta\sigma_t$. Therefore in getting from load level P to $P + \Delta P$, the stress-strain law must be variable in $\sigma_r$ and $\sigma_t$. In other words, the correct stresses in Eq. (11) are evaluated somewhere between $(\sigma_r, \sigma_t)$ and $(\sigma_r + \Delta\sigma_r, \sigma_t + \Delta\sigma_t)$. However, if $\Delta P$ is small, the stresses $\sigma_r$, $\sigma_t$ at load level P may be used (4) in Eq. (11). An alternative approximation is derived in Appendix A.

## 2.7 An Incremental Approach to the Solution of Equations

Eqs. (6), (7), (11), (12), (13), (14) are non-linear in the variables $u = u(r)$ and $w = w(r)$. Therefore, the traditional techniques used for the solution of linear analysis problems cannot be applied directly. Since Eq. (11) is expressed in rate form, it has been suggested (4) that an incremental approach may be taken. The basic approach is to linearize the equations within small increments of load.

The approach presented herein applies the same technique for handling the plastic stress-strain relations, but includes the non-linear geometrical relationships. However, the solution of the corresponding non-linear elastic problems is not restricted to "small" increments of loading.

# III. THE MATHEMATICAL MODEL

## 3.1 Background

A mathematically consistent lumped parameter model is used herein to formulate the equations in terms of the unknown displacement functions u and w. This type of model was first suggested by Newmark and formally developed by Ang (10). Each physical element of the model is point-wise compatible with a corresponding quantity in the continuum. The model is, in fact, a physical discretization of the continuum.

Ang has established the criterion of mathematical consistency in his models. The equations resulting from the model must correspond to a finite difference form of the differential equations of the continuum. The advantage of this criterion is that questions concerning uniqueness, convergence, stability, and errors can be related to similar questions in the theory of finite differences.

The primary advantage realized in using a model approach is that the resulting equations can be derived through the use of elementary mechanics and simple geometry. Also, the equations are physically meaningful when related to the model.

## 3.2 Description of the Model

The model described herein satisfies the Kirchoff-Love assumptions for the theory of plates and shells in finite difference form, and is mathematically consistent with the finite difference expressions of the differential equations of the corresponding continuum.

Fig. 6 is a schematic representation of the model. The essential elements are a network of mass points interconnected by generalized axial and shear springs possessing properties identical with whatever behavioral properties are ascribed to the solid.

The total mass of the solid continuum is concentrated at the mass points. Each mass point contains the mass of the solid corresponding to an elemental volume of $r_m \cdot \Delta\theta \cdot \lambda \cdot t$. All displacements are defined only at the mass points (10).

A stress point is the point of definition of the average stress and strain tensors of the solid within an elemental volume of $r_s \cdot \Delta\theta \cdot \lambda \cdot t$. The material in this volume, therefore, is implicitly in homogeneous states of stress and strain. The deformability, or conversely, the resistance, of a continuum is represented by that of a finite number of stress points.

The entire mass of the continuum is assumed to be in the top and bottom sheets of the sandwich configuration. Stress-strain relationships are also established for the top and bottom sheets only, while shear forces on a cross-section are assumed to be a direct consequence of equilibrium of the plate. Accordingly, the model is made up of two layers of mass points and stress points, which are tied together by the Kirchoff-Love assumption of normality and the assumption that the shear core is incompressible across the thickness of the plate. These assumptions force the mass points to remain on a normal to the imaginary middle surface and a constant distance h from it during deformation.

Therefore, the locations of the mass points after deformation are determined by the displacements of the middle surface. Stresses are then determined from relative displacements of the mass points of the top or bottom sheets.

It should be noted that the mathematical model presented herein is essentially the same as that presented by Ang and Lopez (4) as well as Mohraz and Schnobrich (11). Their conceptual presentation of the model was in terms of "rigid bars" and "deformable nodes" whereas the presentation described herein retains the "mass point-stress point" notation. The resulting mathematical models are identical in every way except that normal loads are applied somewhat differently here. In the rigid bar - deformable node representation of Ang and Lopez, and Mohraz and Schnobrich, the normal loads are applied at the nodes while tangential loads are applied at the centers of the rigid bars. In the present model, both normal and tangential loads are applied at the centers of the rigid bars. Consistent with the Kirchoff-Love hypothesis the vertical displacements of the middle surface are located at the "stress points" or "deformable nodes." Horizontal displacements are defined at the "mass points" or the center of the "rigid bars." Horizontal forces are applied to "mass points" or the center of the "rigid bars." The internal stresses computed from the model are applied at "stress points" or "nodal points" of the model.

# IV. DEVELOPMENT OF MODEL EQUATIONS

## 4.1 Equilibrium of a Mass Point

Fig. 7 is an r-z plane of the deformed model. The load at mass point i is resolved into a normal force $P_N$ and a tangential force $P_T$. The internal forces, NR, MR, and Q which are evaluated at stress point i-1 act on mass point i. Similarly, the internal forces, NR, MR, and Q which are evaluated at stress point i+1 act on mass point i. The internal forces MT and NT which are evaluated at stress point i (see Fig. 6) also act on mass point i.

The summation of moments about i in the r-z plane yields

$$\Big\{-Q_{i-1}\frac{\lambda S_{i-1}}{2}\Big[\frac{(i-1)\lambda}{2}+u_{i-1}\Big]-Q_{i+1}\frac{\lambda S_{i+1}}{2}\Big[\frac{(i+1)\lambda}{2}+u_{i+1}\Big]$$
$$+MR_{i-1}\Big[\frac{(i-1)\lambda}{2}+u_{i-1}\Big]-MR_{i+1}\Big[\frac{(i+1)\lambda}{2}+u_{i+1}\Big] \tag{15}$$
$$+MT_i\,[\lambda+u_{i+1}-u_{i-1}]\Big\}\,\Delta\theta=0$$

and summation of forces in the direction r* yields

$$\Big\{-Q_{i-1}\,\mathrm{SIN}\,\phi_{i-1}\Big[\frac{(i-1)\lambda}{2}+u_{i-1}\Big]-Q_{i+1}\,\mathrm{SIN}\,\phi_{i+1}\Big[\frac{(i+1)\lambda}{2}+u_{i+1}\Big]$$
$$-NR_{i-1}\,\mathrm{COS}\,\phi_{i-1}\Big[\frac{(i-1)\lambda}{2}+u_{i-1}\Big]+NR_{i+1}\,\mathrm{COS}\,\phi_{i+1}$$
$$\Big[\frac{(i+1)\lambda}{2}+u_{i+1}\Big]-NT_i\,[\lambda+u_{i+1}-u_{i-1}] \tag{16}$$
$$+P_T\frac{\lambda S_i}{2}[i\lambda+u_{i-1}+u_{i+1}]\Big\}\Delta\theta=0$$

where

$$\text{SIN } \phi_{i-1} = \frac{1}{\lambda^2 S_i S_{i-1}} [\lambda(w_{i+1} - w_{i-1} - w_i + w_{i-2})$$

$$+ w_{i+1} u_i - w_{i+1} u_{i-2} - w_{i-1} u_i + w_{i-1} u_{i-2}$$

$$- w_i u_{i+1} + w_i u_{i-1} + w_{i-2} u_{i+1} - w_{i-2} u_{i-1}]$$

$$\text{SIN } \phi_{i+1} = \frac{1}{\lambda^2 S_i S_{i+1}} [\lambda(w_{i+2} - w_i - w_{i+1} + w_{i-1})$$

$$+ w_{i+2} u_{i+1} - w_{i+2} u_{i-1} - w_i u_{i+1} + w_i u_{i-1}$$

$$- w_{i+1} u_{i+2} + w_{i+1} u_i + w_{i-1} u_{i+2} - w_{i-1} u_i]$$

$$\text{COS } \phi_{i-1} = \frac{1}{\lambda^2 S_i S_{i-1}} [\lambda^2 + \lambda(u_{i+1} - u_{i-1} + u_i - u_{i-2})$$

$$+ u_{i+1} u_i - u_{i+1} u_{i-2} - u_{i-1} u_i + u_{i-1} u_{i-2}$$

$$+ w_{i+1} w_i - w_{i+1} w_{i-2} - w_{i-1} w_i + w_{i-1} w_{i-2}]$$

$$\text{COS } \phi_{i+1} = \frac{1}{\lambda^2 S_i S_{i+1}} [\lambda^2 + \lambda(u_{i+2} - u_i + u_{i+1} - u_{i-1})$$

$$+ u_{i+2} u_{i+1} - u_{i+2} u_{i-1} - u_i u_{i+1} + u_i u_{i-1}$$

$$+ w_{i+2} w_{i+1} - w_{i+2} w_{i-1} - w_i w_{i+1} + w_i w_{i-1}]$$

$$S_i = \sqrt{\left(1 + \frac{u_{i+1} - u_{i-1}}{\lambda}\right)^2 + \left(\frac{w_{i+1} - w_{i-1}}{\lambda}\right)^2} \tag{17}$$

$S_{i-1}$ and $S_{i+1}$ are found by replacing i with i-1 and i+1, respectively.

$\lambda$ = undeformed radial mesh length (Fig. 6)

The shear force $Q_i$ at any stress point i is obtained from the equilibrium of normal forces of the plate from the center to i. The resulting equation is used to eliminate $Q_{i-1}$ and $Q_{i+1}$ from Eqs. (15) and (16). Fig. 8 is a schematic representation of such a section of the model in the r-z plane. The total vertical load on the plate is determined by summing the vertical components of the loads $P_N(i)$ and $P_T(i)$ from the center of the plate and is given by

$$\overline{P}_v(i) = \pi\lambda \sum \overline{k}\, [(\lambda + u_{k+1} - u_{k-1})\, P_N(k) + (w_{k+1} - w_{k-1})\, P_T(k)]$$

$$\begin{aligned} k = \overline{k} &= 1, 3, 5 \ldots\ldots\ldots i \ \underline{\text{if}}\ i \text{ is odd} \\ k &= 0, 2, 4 \ldots\ldots\ldots i \ \underline{\text{if}}\ i \text{ is even} \\ \overline{k} &= .25, 2, 4 \ldots\ldots i \ \underline{\text{if}}\ i \text{ is even} \end{aligned} \tag{18}$$

Therefore, summing the forces in the z direction yields

$$\overline{P}_v(i-1) + Q_i \frac{\lambda + u_{i+1} - u_{i-1}}{\lambda\ S_i} \pi\lambda i + NR_i \frac{w_{i+1} - w_{i-1}}{\lambda\ S_i} \pi\lambda i = 0 \tag{19}$$

Substituting Eq. (18) evaluated at i-1 into Eq. (19) and solving for $Q_i$

$$Q_i = \frac{- S_i \sum_k \bar{k} \, [(\lambda+u_{k+1}-u_{k-1}) \, P_N(k) + (w_{k+1}-w_{k-1}) \, P_T(k)]}{i(\lambda + u_{i+1} - u_{i-1})} - \frac{w_{i+1} - w_{i-1}}{\lambda + u_{i+1} - u_{i-1}} NR_i \tag{20}$$

where the summation is carried to k = i-1 as in Eq. (18).

By eliminating the shear forces $Q_{i-1}$ and $Q_{i+1}$ from Eq. (15) by using Eq. (19), the dquilibrium of moments becomes

$$\begin{aligned} & NR_{i-1}\{[\frac{\lambda S_{i-1} (w_i - w_{i-2})}{2(\lambda + u_i - u_{i-2})}][\frac{(i-1)\lambda}{2} + u_{i-1}]\} \\ & + NR_{i+1}\{[\frac{\lambda S_{i+1} (w_{i+2} - w_i)}{2(\lambda + u_{i+2} - u_i)}] [\frac{(i+1)\lambda}{2} + u_{i+1}]\} \\ & + MR_{i-1} [\frac{(i-1)\lambda}{2} + u_{i-1}] - MR_{i+1} [\frac{(i+1)\lambda}{2} + u_{i+1}] \\ & + MT_i [\lambda + u_{i+1} - u_{i-1}] \\ & + \bar{P}_v(i-2)\{[\frac{\lambda S_{i-1}^2}{2\pi(i-1)(\lambda + u_i - u_{i-2})}] [\frac{(i-1)\lambda}{2} + u_{i-1}]\} \\ & + \bar{P}_v(i)\{[\frac{\lambda S_{i+1}^2}{2\pi(i+1)(\lambda + u_{i+2} - u_i)}] [\frac{(i+1)\lambda}{2} + u_{i+1}]\} = 0 \end{aligned} \tag{21}$$

and by eliminating $Q_i$ from Eq. (16), the equilibrium of in-plane forces becomes

$$- NR_{i-1}\{[\cos\phi_{i-1} - \sin\phi_{i-1}\frac{w_i - w_{i-2}}{(\lambda + u_i - u_{i-2})}]\,[\frac{(i-1)\lambda}{2} + u_{i-1}]\}$$

$$+ NR_{i+1}\{[\cos\phi_{i+1} + \sin\phi_{i+1}\frac{(w_{i+2} - w_i)}{(\lambda + u_{i+2} - u_i)}]\,[\frac{(i+1)\lambda}{2} + u_{i+1}]\}$$

$$- NT_i\,(\lambda + u_{i+1} - u_{i-1}) \tag{22}$$

$$+ \overline{P}_v(i-2)\,\{\frac{S_{i-1}\sin\phi_{i-1}}{\pi(i-1)(\lambda + u_i - u_{i-2})}\,[\frac{(i-1)\lambda}{2} + u_{i-1}]\}$$

$$+ \overline{P}_v(i)\,\{\frac{S_{i+1}\sin\phi_{i+1}}{\pi(i+1)(\lambda + u_{i+2} - u_i)}\,[\frac{(i+1)\lambda}{2} + u_{i+1}]\}$$

$$+ P_T(i)\,\frac{\lambda\,Si}{2}\,(i\lambda + u_{i+1} - u_{i-1}) = 0$$

Eqs. (21) and (22) can be written in a more abbreviated form, respectively, as follows:

$$(A_{i-1,\,1})(MR_{i-1}) + (A_{i-1,\,3})(NR_{i-1}) + (A_{i,\,6})(MT_i)$$
$$+ (A_{i+1,\,9})(MR_{i+1}) + (A_{i+1,\,11})(NR_{i+1}) = P_{i1} \tag{23}$$

and

$$(B_{i-1,\,3})(NR_{i-1}) + (B_{i,\,8})(NT_i) + (B_{i+1,\,11})(NR_{i+1}) = P_{i2} \tag{24}$$

where $A_{k,j}$ and $B_{k,j}$ are coefficients of the forces determined from the equilibrium equations, Eqs. (21) and (22), evaluated at point i. By writing Eqs. (23) and (24) for all points of the plate, equilibrium can be expressed in matrix form as

$$R\,F = pP \tag{25}$$

where F is a 4n vector of internal forces, $F = [MR_0, MT_0, NR_0, NT_0, MR_1, MT_1, NR_1, NT_1, ---MR_i, MT_i, NR_i, NT_i, ---MR_n, MT_n, NR_n, NT_n]$, R is a 2n x 4n matrix of coefficients, and P is a 2n vector of external forces. These correspond to the n discrete points along a radial line of the plate. p is a scalar which is a measure of the load on the plate, while P determines the shape of the load distribution.

## 4.2 Force-Stress Relations

The internal forces $MR_i$, $MT_i$, $NR_i$, and $NT_i$ are derived from considering the stresses $\sigma_r^t(i)$, $\sigma_r^b(i)$, $\sigma_t^t(i)$, $\sigma_t^b(i)$ acting over the thickness of the top and bottom sheets. $\sigma_r^t(i)$ is the radial stress in the top sheet at stress point i and acts over a thickness of t. $\sigma_r^b(i)$ is the radial stress in the bottom sheet at stress point i and acts over a thickness of t. $\sigma_t^t(i)$ and $\sigma_t^b(i)$ are the tangential stresses. The center of the top and bottom sheets are located at a distance h from the middle surface. Therefore,

$$\begin{aligned} MR_i &= [\sigma_r^t(i) - \sigma_r^b(i)]\ th \\ MT_i &= [\sigma_t^t(i) - \sigma_t^b(i)]\ th \\ NR_i &= [\sigma_r^t(i) + \sigma_r^b(i)]\ t \\ NT_i &= [\sigma_t^t(i) + \sigma_t^b(i)]\ t \end{aligned} \tag{26}$$

The internal stresses are arranged as a 4n vector, or $\sigma = [\sigma_r^{\,t}(0),$ $\sigma_r^{\,b}(0),\ \sigma_t^{\,t}(0),\ \sigma_t^{\,b}(0),\ \sigma_r^{\,t}(1),\ \sigma_r^{\,b}(1),\ \sigma_t^{\,t}(1),\ \sigma_t^{\,b}(1),\text{---}\sigma_r^{\,t}(i),\ \sigma_r^{\,b}(i),$ $\sigma_t^{\,t}(i),\ \sigma_t^{\,b}(i),\text{---}\sigma_r^{\,t}(n),\ \sigma_r^{\,b}(n),\ \sigma_t^{\,t}(n),\ \sigma_t^{\,b}(n)]$. The 4n stress vector, $\sigma$ can be transformed into the 4n force fector, F by a 4n x 4n transformation matrix, T, or

$$T\ \sigma = F \tag{27}$$

T is composed of n identical 4 x 4 submatrices along the main diagonal, or

$$T = \begin{bmatrix} \begin{bmatrix} th & -th & 0 & 0 \\ 0 & 0 & th & -th \\ t & t & 0 & 0 \\ 0 & 0 & t & t \end{bmatrix} & \text{---}0\text{---} & \\ \begin{matrix} \vdots \\ 0 \\ \vdots \end{matrix} & \begin{bmatrix} th & -th & 0 & 0 \\ 0 & 0 & th & -th \\ t & t & 0 & 0 \\ 0 & 0 & t & t \end{bmatrix} & \text{---}0\text{---} \\ & \begin{matrix} \vdots \\ 0 \\ \vdots \end{matrix} & \end{bmatrix} \tag{28}$$

## 4.3 Stress-Strain Relations

Hooke's law as given by Eq. (9) is used for all stress points that are in the elastic state of stress. For all stress points that undergo plastic flow, Eq. (11) is used to represent the stress-strain relationship. Since the plastic stress-strain relation is expressed in rate form, only an instantaneous relationship between stress rate and strain rate can be found from Eq. (11). For a small change in load on the plate, the plastic stress rate-strain rate relation can be considered linear. Expressing these in incremental form (4), Eq. (9) becomes

$$\Delta\sigma_r = \frac{E}{1-\mu^2}[\Delta\varepsilon_r + \mu\Delta\varepsilon_t]$$

$$\Delta\sigma_t = \frac{E}{1-\mu^2}[\Delta\varepsilon_t + \mu\Delta\varepsilon_r]$$

or, taking into consideration the discrete nature of the formulation, at a stress point i,

$$\begin{aligned}
\Delta\sigma_r^{\,t}(i) &= \frac{E}{1-\mu^2}[\Delta\varepsilon_r^{\,t}(i) + \mu\Delta\varepsilon_t^{\,t}(i)] \\
\Delta\sigma_r^{\,b}(i) &= \frac{E}{1-\mu^2}[\Delta\varepsilon_r^{\,b}(i) + \mu\Delta\varepsilon_t^{\,b}(i)] \\
\Delta\sigma_t^{\,t}(i) &= \frac{E}{1-\mu^2}[\Delta\varepsilon_t^{\,t}(i) + \mu\Delta\varepsilon_r^{\,t}(i)] \\
\Delta\sigma_t^{\,b}(i) &= \frac{E}{1-\mu^2}[\Delta\varepsilon_t^{\,t}(i) + \mu\Delta\varepsilon_r^{\,b}(i)]
\end{aligned} \tag{29}$$

Similarly, the plastic stress-strain equations become

$$\Delta\sigma_r^{\,t}(i) = \frac{E}{a_t^{\,2} + b_t^{\,2} + 2\mu a_t b_t}\left[b_t^{\,2}\ \Delta\varepsilon_r^{\,t}(i) - a_t b_t\ \Delta\varepsilon_t^{\,t}(i)\right]$$

$$\Delta\sigma_r^{\,b}(i) = \frac{E}{a_b^{\,2} + b_b^{\,2} + 2\mu a_b b_b}\left[b_b^{\,2}\ \Delta\varepsilon_r^{\,b}(i) - a_b b_b\ \Delta\varepsilon_t^{\,b}(i)\right]$$

$$\Delta\sigma_t^{\,t}(i) = \frac{E}{a_t^{\,2} + b_t^{\,2} + 2\mu a_t b_t}\left[a_t^{\,2}\ \Delta\varepsilon_t^{\,t}(i) - a_t b_t\ \Delta\varepsilon_r^{\,t}(i)\right] \qquad (30)$$

$$\Delta\sigma_t^{\,b}(i) = \frac{E}{a_b^{\,2} + b_b^{\,2} + 2\mu a_b b_b}\left[a_b^{\,2}\ \Delta\varepsilon_t^{\,b}(i) - a_b b_b\ \Delta\varepsilon_r^{\,b}(i)\right]$$

where,

$$a_t = 2\bar{\sigma}_r^{\,t}(i) - \bar{\sigma}_t^{\,t}(i)$$

$$a_b = 2\bar{\sigma}_r^{\,b}(i) - \bar{\sigma}_t^{\,b}(i)$$

$$b_t = 2\bar{\sigma}_t^{\,t}(i) - \bar{\sigma}_r^{\,t}(i)$$

$$b_b = 2\bar{\sigma}_t^{\,b}(i) - \bar{\sigma}_r^{\,b}(i)$$

and the barred quantities are obtained from

$$\bar{\sigma}_r = \frac{\sqrt{3}\ k\ (\sigma_r + \frac{\Delta\sigma_r}{2})}{\sqrt{(\sigma_r + \frac{\Delta\sigma_r}{2})^2 - (\sigma_r + \frac{\Delta\sigma_r}{2})(\sigma_t + \frac{\Delta\sigma_t}{2}) + (\sigma_t + \frac{\Delta\sigma_t}{2})^2}}$$

$$\bar{\sigma}_t = \frac{\sqrt{3}\ k\ (\sigma_t + \frac{\Delta\sigma_t}{2})}{\sqrt{(\sigma_r + \frac{\Delta\sigma_r}{2})^2 - (\sigma_r + \frac{\Delta\sigma_r}{2})(\sigma_t + \frac{\Delta\sigma_t}{2}) + (\sigma_t + \frac{\Delta\sigma_t}{2})^2}}$$

which are derived in Appendix A, Sect. A.2.

It can be seen that Eqs. (29) and (30) can be expressed in the following form,

$$\Delta\sigma_r^{\,t}(i) = C_{11}\ \Delta\varepsilon_r^{\,t}(i) + C_{13}\ \Delta\varepsilon_t^{\,t}(i)$$

$$\Delta\sigma_r^{\,b}(i) = C_{22}\ \Delta\varepsilon_r^{\,b}(i) + C_{24}\ \Delta\varepsilon_t^{\,b}(i)$$

$$\Delta\sigma_t^{\,t}(i) = C_{33}\ \Delta\varepsilon_t^{\,t}(i) + C_{31}\ \Delta\varepsilon_r^{\,t}(i)$$

$$\Delta\sigma_t^{\,b}(i) = C_{44}\ \Delta\varepsilon_t^{\,b}(i) + C_{42}\ \Delta\varepsilon_r^{\,b}(i)$$

where the coefficients $C_{ij}$ are determined from Eq. (29) or (30) depending on whether a stress point is elastic or plastic, respectively. Therefore, the 4n vector of incremental stresses, $\Delta\sigma$, is related to the 4n vector of incremental strains, $\Delta\varepsilon$, by the matrix equation,

$$\Delta\sigma = C\cdot\Delta\varepsilon \tag{31}$$

where C is a 4n x 4n matrix which is made up of coefficients from Eq. (29) or (30).

### 4.4 Strain-Displacement Relations

Strain is defined by Eq. (13a). Fig. 9 shows two mass points, i-1 and i+1, connected by the stress point i in the top sheet of the plate before and after deformation. Initially the two mass points i-1 and i+1 are a distance $\lambda$ apart, but after deformation they are separated by a distance,

$$\sqrt{(w_{i+1}^t - w_{i-1}^t)^2 + (\lambda + u_{i+1}^t - u_{i-1}^t)^2}$$

From Eq. (13a),

$$\varepsilon_r^{\,t}(i) = \frac{1}{2}\left[\frac{(w_{i+1}^t - w_{i-1}^t)^2 + (\lambda + u_{i+1}^t - u_{i-1}^t)^2}{\lambda^2} - 1\right]$$

or, simplifying,

$$\varepsilon_r^{\,t}(i) = \frac{u_{i+1}^t - u_{i-1}^t}{\lambda} + \frac{1}{2\lambda^2}\left[(u_{i+1}^t - u_{i-1}^t)^2 + (w_{i+1}^t - w_{i-1}^t)^2\right] \tag{32a}$$

Similarly,

$$\varepsilon_r^{\,b}(i) = \frac{u_{i+1}^b - u_{i-1}^b}{\lambda} + \frac{1}{2\lambda^2}\left[(u_{i+1}^b - u_{i-1}^b)^2 + (w_{i+1}^b - w_{i-1}^b)^2\right] \tag{32b}$$

$$\varepsilon_t^{\,t}(i) = \frac{2\,u_i^{\,t}}{i\lambda} + \frac{2(u_i^{\,t})^2}{i^2\,\lambda^2} \tag{32c}$$

$$\varepsilon_t^{\,b}(i) = \frac{2\,u_i^{\,b}}{i\lambda} + \frac{2(u_i^{\,b})^2}{i^2\,\lambda^2} \tag{32d}$$

The displacements $u_i^{\,t}$, $w_i^{\,t}$ of the top sheet and $u_i^{\,b}$, $w_i^{\,b}$ of the bottom sheet are related to the displacements $u_i$, $w_i$ of the middle surface as required by the Kirchoff-Love hypothesis of normality. Fig. 10 shows this graphically. The displacements $u_i^{\,t}$ and $w_i^{\,t}$ are determined from the displacement $u_i$, $w_i$ by proceeding a distance h from the middle surface in a direction perpendicular to an imaginary line drawn through the points i-1 and i+1 on the middle surface. The result of this geometric construction is:

$$u_i^t = u_i + \frac{h\,(w_{i+1} - w_{i-1})}{\lambda\sqrt{\left(\frac{w_{i+1} - w_{i-1}}{\lambda}\right)^2 + \left(1 + \frac{u_{i+1} - u_{i-1}}{\lambda}\right)^2}} \tag{33a}$$

$$u_i^b = u_i - \frac{h\,(w_{i+1} - w_{i-1})}{\lambda\sqrt{\left(\frac{w_{i+1} - w_{i-1}}{\lambda}\right)^2 + \left(1 + \frac{u_{i+1} - u_{i-1}}{\lambda}\right)^2}} \tag{33b}$$

$$w_i^t = w_i - \frac{h\,(\lambda + u_{i+1} - u_{i-1})}{\lambda\sqrt{\left(\frac{w_{i+1} - w_{i-1}}{\lambda}\right)^2 + \left(1 + \frac{u_{i+1} - u_{i-1}}{\lambda}\right)^2}} + h \tag{33c}$$

$$w_i^b = w_i + \frac{h\,(\lambda + u_{i+1} - u_{i-1})}{\lambda\sqrt{\left(\frac{w_{i+1} - w_{i-1}}{\lambda}\right)^2 + \left(1 + \frac{u_{i+1} - u_{i-1}}{\lambda}\right)^2}} - h \tag{33d}$$

The strain at stress points in the top and bottom sheets can be expressed as a function of the displacements of the middle surface by substituting Eq. (33) (which is evaluated at i-1, i, and i+1) into Eq. (32). The resulting strain-displacement equations then become

$$\begin{aligned}
\varepsilon_r^{\,t}(i) = {} & \frac{u_{i+1} - u_{i-1}}{\lambda} + \frac{h}{\lambda}\left[\frac{w_{i+2} - w_i}{\lambda S_{i+1}} - \frac{w_i - w_{i-2}}{\lambda S_{i-1}}\right] \\
& + \frac{1}{2\lambda^2}\left[(u_{i+1} - u_{i-1})^2 + (w_{i+1} - w_{i-1})^2\right] \\
& + 2h\left[(u_{i+1} - u_{i-1})\left(\frac{w_{i+2} - w_i}{\lambda S_{i+1}} - \frac{w_i - w_{i-2}}{\lambda S_{i-1}}\right)\right. \\
& \left. - (w_{i+1} - w_{i-1})\left(\frac{\lambda + u_{i+2} - u_i}{\lambda S_{i+1}} - \frac{\lambda + u_i - u_{i-2}}{\lambda S_{i-1}}\right)\right] \\
& + h^2\left[\left(\frac{w_{i+2} - w_i}{\lambda S_{i+1}} - \frac{w_i - w_{i-2}}{\lambda S_{i-1}}\right)^2\right. \\
& \left. + \left(\frac{\lambda + u_{i+2} - u_i}{\lambda S_{i+1}} - \frac{\lambda + u_i - u_{i-2}}{\lambda S_{i-1}}\right)^2\right]
\end{aligned} \tag{34a}$$

$$\begin{aligned}
\varepsilon_r^{\,b}(i) = {} & \frac{u_{i+1} - u_{i-1}}{\lambda} - \frac{h}{\lambda}\left[\frac{w_{i+2} - w_i}{\lambda S_{i+1}} - \frac{w_i - w_{i-2}}{\lambda S_{i-1}}\right] \\
& + \frac{1}{2\lambda^2}\left[(u_{i+1} - u_{i-1})^2 + (w_{i+1} - w_{i-1})^2\right] \\
& - 2h\left[(u_{i+1} - u_{i-1})\left(\frac{w_{i+2} - w_i}{\lambda S_{i+1}} - \frac{w_i - w_{i-2}}{\lambda S_{i-1}}\right)\right. \\
& \left. - (w_{i+1} - w_{i-1})\left(\frac{\lambda + u_{i+2} - u_i}{\lambda S_{i+1}} - \frac{\lambda + u_{i+2} - u_i}{\lambda S_{i-1}}\right)\right] \\
& + h^2\left[\left(\frac{w_{i+2} - w_i}{\lambda S_{i+1}} - \frac{w_i - w_{i-2}}{\lambda S_{i-1}}\right)^2\right. \\
& \left. + \left(\frac{\lambda + u_{i+2} - u_i}{\lambda S_{i+1}} - \frac{\lambda + u_i - u_{i-2}}{\lambda S_{i-1}}\right)^2\right]
\end{aligned} \tag{34b}$$

$$\varepsilon_t{}^t(i) = \frac{2}{i\lambda}\, u_i + \frac{2h}{i\lambda} \times \frac{w_{i+1} - w_{i-1}}{\lambda S_i} + \frac{2}{i^2\lambda^2}\, u_i{}^2 + \frac{4h}{i^2\lambda^2}\, u_i \times \frac{w_{i+1} - w_{i-1}}{\lambda S_i} + \frac{2h^2}{i^2\lambda^2} \times \frac{(w_{i+1} - w_{i-1})^2}{\lambda^2\; S_i{}^2} \tag{34c}$$

$$\varepsilon_t{}^b(i) = \frac{2}{i\lambda}\, u_i - \frac{2h}{i\lambda} \times \frac{w_{i+1} - w_{i-1}}{\lambda S_i} + \frac{2}{i^2\lambda^2}\, u_i{}^2 - \frac{4h}{i^2\lambda^2}\, u_i \times \frac{w_{i+1} - w_{i-1}}{\lambda S_i} + \frac{2h^2}{i^2\lambda^2} \times \frac{(w_{i+1} - w_{i-1})^2}{\lambda^2\; S_i{}^2} \tag{34d}$$

where $S_i = \sqrt{\left(\frac{w_{i+1} - w_{i-1}}{\lambda}\right)^2 + \left(1 + \frac{u_{i+1} - u_{i-1}}{\lambda}\right)^2}$, and

$S_{i-1}$ and $S_{i+1}$ are the same as $S_i$ except i is replaced by i-1 and i+1, respectively.

## 4.5 An Incremental Form of the Field Equations of the Model

It was pointed out in Sect. 2.7 that the stress-strain equations must be in incremental form because of the use of the incremental theory of plasticity. Therefore, the remainder of the field equations are converted to an incremental form. The form of the equations developed in this section provides an efficient means for their numerical solution.

The technique described in Chapter V takes advantage of the incremental form to find solutions for the equations which are non-linear because of changes in geometry. This technique is efficient in the elastic range of behavior because it is not restricted to small increments of loading.

A simplification is necessary for the treatment of the term $S_i$. It represents the ratio of elongation or shortening of the middle surface to the original (unloaded) dimensions within one mesh length of the model. Its primary effect is in those terms which produce bending stresses. Since bending stresses become less important with larger deformations, it is assumed that $\Delta S_i$ has negligible effect for a small increment of loading. This assumption is supported in Sect. 7.5 where solutions are shown to be practically independent of load increment in the elastic range.

The incremental form of the strain displacement equations at a point i can be expressed as

$$\Delta\varepsilon_i = D_i \, \Delta X_i \tag{33}$$

where $\Delta\varepsilon_i$ is the vector of strains, $[\Delta\varepsilon_r{}^t(i), \Delta\varepsilon_r{}^b(i), \Delta\varepsilon_t{}^t(i), \Delta\varepsilon_t{}^b(i)]$, $\Delta X_i$ is the vector of displacements, $[\Delta u_{i-2}, \Delta w_{i-2}, \Delta u_{i-1}, \Delta w_{i-1} --- \Delta w_{i+2}]$, and $D_i$ is the matrix,

$$D_i = \begin{bmatrix} d_{11} & d_{12} & d_{13} & - - - - - - - - & d_{1,10} \\ d_{21} & \ddots & & & \vdots \\ d_{31} & & \ddots & & \vdots \\ d_{41} & - - - - - - - - - - - - & & & d_{4,10} \end{bmatrix}$$

where:

$$d_{11} = \frac{1}{S_{i-1}} \left(\frac{2h^2\delta_i}{\lambda^2} + \frac{h^2\Delta\delta_i}{\lambda^2}\right)$$

$$d_{12} = \frac{1}{S_{i-1}} \left(\frac{h}{\lambda^2} + \frac{2h\alpha_i}{\lambda} - \frac{2h\beta_i}{\lambda} + \frac{2h^2\Gamma_i}{\lambda^2} + \frac{h^2\Delta\Gamma_i}{\lambda^2}\right)$$

$$d_{13} = - \left(\frac{1}{\lambda} + \frac{\alpha_i}{\lambda^2} + \frac{\Delta\alpha_i}{2\lambda^2} + \frac{2h\Gamma_i}{\lambda} + \frac{2h\Delta\Gamma_i}{\lambda}\right)$$

$$d_{14} = - \left(\frac{\beta_i}{\lambda^2} + \frac{\Delta\beta_i}{2\lambda^2} - \frac{2h\Gamma_i}{\lambda} - \frac{2h\Delta\Gamma_i}{\lambda}\right)$$

$$d_{15} = - d_{11}\, S_{i-1} \left(\frac{1}{S_{i+1}} + \frac{1}{S_{i-1}}\right)$$

$$d_{16} = - d_{12}\, S_{i-1} \left(\frac{1}{S_{i+1}} + \frac{1}{S_{i-1}}\right)$$

$$d_{17} = - d_{13}$$

$$d_{18} = - d_{14}$$

$$d_{19} = d_{11} \times \frac{S_{i-1}}{S_{i+1}}$$

$$d_{1,10} = d_{12} \times \frac{S_{i-1}}{S_{i+1}}$$

and $d_{21}$ through $d_{2,10}$ are the same as $d_{11}$ through $d_{1,10}$, respectively, when h is replaced with -h.

$$d_{31} = 0$$

$$d_{32} = 0$$

$$d_{33} = 0$$

$$d_{34} = -\left[\frac{2h}{i\lambda^2 S_i} + \frac{4h}{i^2\lambda^3 S_i} u_i + \frac{2h^2}{i^2\lambda^4 S_i^2}(2\beta_i + \Delta\beta_i)\right]$$

$$d_{35} = \frac{2}{i\lambda} + \frac{4}{i^2\lambda^2} u_i + \frac{2}{i^2\lambda^2} \Delta u_i + \frac{4h}{i^2\lambda^3 S_i}(\beta_i + \Delta\beta_i)$$

$$d_{36} = 0$$

$$d_{37} = 0$$

$$d_{38} = -\ d_{34}$$

$$d_{39} = 0$$

$$d_{3,10} = 0$$

and, $d_{4,1}$ through $d_{4,10}$ are the same as $d_{3,1}$ through $d_{3,10}$, respectively, when h is replaced with -h.

$$\alpha_i = u_{i+1} - u_{i-1}$$

$$\beta_i = w_{i+1} - w_{i-1}$$

$$\Gamma_i = \frac{w_{i+2} - w_i}{S_{i+1}} - \frac{w_i - w_{i-2}}{S_{i-1}}$$

$$\delta_i = \frac{\lambda + u_{i+2} - u_i}{S_{i+1}} - \frac{\lambda + u_i - u_{i-2}}{S_{i-1}}$$

and,

$$\Delta\alpha_i = \Delta u_{i+1} - \Delta u_{i-1}$$

$$\Delta\beta_i = \Delta w_{i+1} - \Delta w_{i-1}$$

$$\Delta\Gamma_i = \frac{\Delta w_{i+2} - \Delta w_i}{S_{i+1}} - \frac{\Delta w_i - \Delta w_{i-2}}{S_{i-1}}$$

$$\Delta\delta_i = \frac{\Delta u_{i+2} - \Delta u_i}{S_{i+1}} - \frac{\Delta u_i - \Delta u_{i-2}}{S_{i-1}}$$

Now, by applying Eq. (33) to all points of the plate the strain displacement equations can be summarized in the matrix equation,

$$\Delta\varepsilon = D\ \Delta X \tag{34}$$

where $\Delta\varepsilon$ is the 4n vector of strains, $\Delta X$ is the 2n vector of displacements and D is the 4n x 2n matrix obtained by the suitable assemblage of the submatrices $D_i$.

The matrix T in Eq. (27) is composed of constant terms. Therefore, Eq. (27) can be expressed in incremental form directly as

$$\Delta F = T \ \Delta\sigma \tag{35}$$

The equilibrium equation, Eq. (25), is an assemblage of the displacement variables and cannot be converted directly to an incremental form as was done for the other equations. The following form of the equations makes use of the incremental approach, but in a somewhat different form.

A change in loading, say $\Delta p$ is accompanied by a change in the matrix R, $\Delta R$, a change in the vector F, $\Delta F$, and a change in P, $\Delta P$, such that the resulting equilibrium equation becomes

$$(R + \Delta R)(F + \Delta F) = (p + \Delta p)(P + \Delta P)$$

Rearranging terms, this equation becomes

$$(R + \Delta R) \ \Delta F = \Delta p \ (P + \Delta P) + [p(P + \Delta P) - (R + \Delta R)F] \tag{36}$$

The term $\Delta F$ represents the change in internal forces corresponding to an increment of load, $\Delta P$. As plastic straining increases, $\Delta F$ becomes smaller. Additional load carrying capacity of the plate then becomes more a function of the changing shape of the plate. This would cause the left hand side of Eq. (36) to become a null vector. The ideal form of Eq. (36) would be

$$(R + \Delta R) \ \Delta F + \Delta RF = \Delta p(P + \Delta P) + p\Delta P$$

However, the incremental displacement, $\Delta X$ cannot be factored from $\Delta R$, and also $\Delta P$ cannot be computed directly. This difficulty can be overcome by augmenting Eq. (36) with an approximate expression for $\Delta RF$ which is denoted by $\overline{\overline{\Delta RF}}$. The approximate form is found by assuming that the only significant change in shape of the plate is a result of vertical displacements. In this way, the incremental displacements can be factored from the expression $\overline{\overline{\Delta RF}}$. The particular expressions retained in this element are found in the coefficients of the membrane forces in Eq. (21). The predominant change can be seen to be roughly proportional to the finite difference expression for the slope of the deflected plate. Eq. (36) becomes

$$(R + \Delta R)\Delta F + \overline{\overline{\Delta RF}} = \Delta p(P + \Delta P) + [p(P + \Delta P) - (R + \Delta R)F] + \overline{\overline{\Delta RF}} \tag{36a}$$

Eq. (36a) is obtained by adding $\overline{\overline{\Delta RF}}$ to both sides of Eq. (36). On the right hand side of the equation, $\overline{\overline{\Delta RF}}$ is a vector of constants.

Now, if Eqs. (35), (31), and (34) are substituted in Eq. (36a) and the remainder of $\overline{\overline{\Delta RF}}$ after factoring out $\Delta X$ is denoted by $\widetilde{\Delta RF}$, then

$$\begin{aligned} [(R + \Delta R)\ TCD + \widetilde{\Delta RF}]\ \Delta X &= \Delta p(P + \Delta P) \\ &+ [p(P + \Delta P) - (R + \Delta R)\ F] + \widetilde{\Delta RF}\ \Delta X \end{aligned} \tag{37}$$

Equation (37) represents a system of 2n simultaneous nonlinear equations expressed in terms of the unknowns, $\Delta X$ corresponding to an increment of load, $\Delta p$. A vector $\Delta X$ satisfying these equations constitutes a solution to the problem.

## 4.6 Boundary Conditions

Boundary conditions are defined by prescribing appropriate geometric or stress conditions of mass points or stress points on a boundary. These may be described as follows:

The term fixed edge is used to describe the boundary condition in which the vertical displacement at the edge is zero and the slope of a tangent plane to the middle surface of the plate at the edge is also zero. For the case of a mass point n on the boundary, these conditions are given respectively by $w_n = 0$ and $w_{n-2} = w_{n+2}$. For the case of a stress point n on the boundary, $w_{n-1} = 0$ and $w_{n+1} = 0$, prescribe the same conditions of zero displacement and zero slope.

The term simple support is used to describe an edge that is free to rotate but restrained from vertical displacement. For the case of a mass point n on the boundary, these requirements are given by $w_n = 0$ and $MR_n = 0$, respectively. For the case of a stress point at n, continuity of a model element is provided by $w_{n-1} + w_{n+1} = 0$ which also approximates the condition of zero displacement. The equilibrium equation at n is written for a half-mass at n. The tangential stresses act over 1/2 mesh length and the radial moment at n+1 is set to zero.

The term restrained edge refers to a boundary in which no horizontal motion at the edge is allowed. It is prescribed by $u_n = 0$ for a mass point on the boundary and $u_{n-1} + u_{n+1} = 0$ for a stress point on the boundary. Conversely, the term unrestrained edge refers to an edge which is free to move horizontally. This is prescribed by setting $NR_n = 0$ for the case of a stress point on the boundary, and by neglecting the effect of all membrane forces outside the boundary when determining in-plane equilibrium of a mass point on the boundary.

Special conditions are required at the center of the plate because an apparent singularity exists as the radius of the plate tends to zero. Rotational symmetry requires $u_o = 0$, $u_1 + u_{-1} = 0$, $w_{-1} - w_{+1} = 0$, and $w_{-2} - w_2 = 0$. The equations that have vanishing denominators are expressions for internal forces at the center. The internal forces at the center of the plate are evaluated by taking the limit of their equations as the radius approaches zero. In the limit, the radial strain is equal to the tangential strain since a homogeneous state of strain exists at the center. Therefore, the expressions for tangential strain can be replaced by those for radial strain at the center, giving,

$$\Delta\sigma_t^t(o) = \Delta\sigma_r^t(o) = \frac{E(1 + \mu)}{1 - \mu^2} \Delta\varepsilon_r^t(o)$$

and,

$$\Delta\sigma_r^b(o) = \Delta\sigma_t^b(o) = \frac{E(1 + \mu)}{1 - \mu^2} \Delta\varepsilon_r^b(o)$$

where $\Delta\varepsilon_r^t(o)$ and $\Delta\varepsilon_r^b(o)$ do not contain $r$.

# V. METHOD OF SOLUTION

## 5.1 Reduction of Incremental Equations to a Linear Form

The matrix equation, Eq. (37), when augmented by appropriate boundary conditions expresses the relation between the vector of incremental displacements, $\Delta X$, and the vector of incremental loads, $\Delta p$. The coefficient matrices in Eq. (37) are computed prior to the addition of the load increment. Given a set of incremental loads, $\Delta p$, the solution is assumed to be the set of incremental displacements which satisfy these equations. Now, let

$$F(\Delta X) = (R + \Delta R)\ TCD + \Delta\tilde{R}F$$

$$E(\Delta X) = p(P + \Delta P) - (R + \Delta R)\ F$$

If X is zero, it can be seen that $E(\Delta X) = 0$, since $\Delta P$ and $\Delta R$ would be zero and

$$pP - RF \equiv 0$$

$P + \Delta P$ and $R + \Delta R$ are the coefficients of the equation of equilibrium in the deformed position $X + \Delta X$, and F and P are the internal, and external forces in the deformed position X. Therefore $E(\Delta X)$ is the residual when the "old" forces, F and P, are substituted in the "new" equations. In fact, if $\Delta p = 0$, $E(\Delta X)$ is exactly the residual associated with a given solution to the equations. In other words, if a set of displacements X are in error by $\Delta X$, then $E(\Delta X)$ is the residual force in the equations of equilibrium.

The equations may then be written in the form

$$F(\Delta X)\ \Delta X = \Delta p(P + \Delta p) + E(\Delta X) + \Delta\tilde{R}F\ \Delta X \tag{38}$$

If a value for $\Delta X$ is substituted in $F(\Delta X)$, $(P + \Delta P)$, $E(\Delta X)$, and $\Delta\tilde{R}F\ \Delta X$, the result is a set of simultaneous linear equations in $\Delta X$. If the correct value of $\Delta X$ is used, the equations are satisfied and $\Delta X$ is the incremental solution vector.

## 5.2 Solution of the Simultaneous Equations

The solution of Eq. (38) is obtained for an initial load increment vector, $\Delta p$, by setting $\Delta X$ to zero in the terms $F(\Delta X)$, $(P + \Delta P)$, $E(\Delta X)$, and $\Delta\tilde{R}F\ \Delta X$. The result is a set of simultaneous linear equations in $\Delta X$. These equations are solved by Gauss elimination for a first trial value, $\Delta X_1$. Next, $\Delta X_1$ is used in the calculation of the terms $F(\Delta X)$, $(P + \Delta P)$, $E(\Delta X)$, and $\Delta\tilde{R}F\ \Delta X$ to obtain another set of linear simultaneous equations which are solved by Gauss elimination for a second trial value, $\Delta X_2$. This is continued until two successive trial values $\Delta X_{i-1}$, $\Delta X_i$ agree within a small tolerance. Then, $\Delta X_i$ is assumed to be the solution of Eq. (38) for the first load increment, $\Delta p_1$.

A solution to the problem now exists for the load level, $p = \Delta p_1$, and the complete set of corresponding internal forces, external forces, and displacements are known. Therefore, the equations can be set up for the next load increment, $\Delta p_2$. These equations are solved by the same recursive technique described above. Additional load increments are applied until the desired load level is attained.

The aforementioned procedure is graphically depicted in Fig. 11 which is a plot of the relation between one of the elements in the displacement vector X and the load parameter, p. Setting the element of $\Delta X_1$ to zero for the first iteration will result in a solution corresponding to the linear elastic solution to the same problem, yielding point a in Fig. 11. When this value is used in the second iteration, a solution is obtained along line b-o which is designated as c. Now, when the value at c is used in the third iteration, a solution at e is obtained. This is continued and points e, g, i, etc., are obtained. When two successive trials are sufficiently close to one another, the last value is taken to be the solution. Path o'a'b'c'd'e'f' depicts a subsequent load increment where opposite curvature is encountered. Note that the first trial always follows a path tangent to the curve o-z. Convergence of this iterative scheme appears to be assured. The following observations can be made concerning the magnitude of $\Delta p$:

1. From a computational experiment, it was determined that the effect of $\Delta p$ on the parameter $S + \Delta S$ is insignificant.
2. The efficiency of solving a problem depends on the magnitude of $\Delta p$. If $\Delta p$ is small, the solution must be incremented many times, but convergence for each load increment is rapid. Conversely, if $\Delta p$ is large, fewer increments are needed, but convergence is slow. It was found that in the elastic range, very large increments are most efficient. There does seem to be a limit, however, when successive values of X turn out to be several orders of magnitude apart.

3. If a very large number of increments are used, roundoff errors may be introduced. This was determined to be relatively insignificant due to the automatic correction inherent in the solution. The term $E(\Delta X)$, which is the residual of the equations corresponding to $\Delta X = 0$, serves to correct the solution as the procedure progresses.
4. The only important restriction on p is during plastic flow. If $\Delta p$ is too large, the yield criterion, Eq. (10), will be violated. In fact, $\Delta p$ must be adjusted to a value which will result in a stress relation which meets the yield criterion within a small tolerance, (say, 1% of $J_2$). In addition, during plastic flow, $\Delta p$ must be relatively small in order to insure that the assumption outlined in Sect. 2.5 is valid.
5. The magnitude of $\Delta p$ may also be limited by certain stability requirements of the nonlinear equations. This was observed at latter stages of loading where the solution process appears to be more sensitive to the magnitude of $\Delta P$.

5.3 <u>Separation</u>

A phenomenon which will be called separation occurs in the problem solution as formulated thus far. Separation can best be explained in reference to the solution of a linear elastic problem with the model. For the sake of brevity and clearness of explanation, let the formulation of the problem be designated as

$$FX = P \tag{39}$$

where F is the stiffness matrix for the model, X is the displacement vector and P is the load vector. If only the odd numbered terms in X are taken, the odd values are represented and if only the even numbered terms in X are taken, the even values are represented. These two sets will hereinafter be referred to as the "odd string" and "even string."

It can be shown (12) that the solution of Eq. (39) breaks down into two parts. When the terms in F and P corresponding to the odd string only are retained, the solution will be exactly the same as when all the terms are retained. The same effect occurs when the terms corresponding to the even string are retained. Therefore, the two solutions are independent.

For linear elastic problems, there is no disadvantage associated with separation and it disappears with decreasing mesh size. Also, the two strings appear to bound the true solution of the problem for any mesh size and in this sense it is an advantage.

The fact that the two strings are not identical is caused by the application of inconsistent boundary conditions. For example, the boundary condition associated with the odd string may correspond to that for a stress point on the boundary, while the boundary condition associated with the even string would correspond to a mass point on the boundary, or vice versa. Consequently, the solutions of the two strings will invariably not agree.

In the large deflection problem and in the elastic-plastic problem, the two strings are weakly coupled. However, separation still occurs as evidenced by an examination of the solutions, but in these cases the equations cannot be broken apart. In fact, the equations are coupled by "second order" terms. In the case of large deflections these terms are always of a stiffening nature and in the case of plasticity they are always of a weakening nature.

A typical plot of the solution for the large deflection elastic problem is shown in Fig. 12. Line o-a represents the solution for $X_1$ and line o-b represents the solution for $X_2$. The even string as characterized by o-b can be thought of as being stiffer than the odd string characterized by o-a. As was mentioned, the elements in K which tie the two strings together tend to make K stiffer by an amount related to the magnitude of X. In other words, the greater X is, the stiffer K will be. In addition, the stiffening of the odd string is due to the coupling with the even string and vice versa. The true solution appears to be between lines o-a and o-b; therefore, the values of the weaker string are too large and the values of the stiffer string are too small. As the load increases, the stiffer string tends to become stiffer. Conversely, the weaker string becomes weaker. This is evidenced by the eventual divergence of the two strings.

The opposite effect was observed when an elastic-plastic problem was solved. Lopez (12) circumvented this problem by a clever arrangement of mass points and stress points on the boundary of a square plate. In this case, it is possible to arrange the even and odd strings in an asymmetrical fashion such that the boundary conditions at one edge for one string is compensated by the boundary condition at the other edge. However, this is not possible for a circular plate or for a plate of general shape.

When separation becomes severe, as in the case of the diverging strings shown in Fig. 12, the condition of continuous displacements that is assumed in the derivation of the strain displacement functions is severely violated. The violation of this condition suggests that the problem of separation may be resolved by the addition of a continuity requirement between the displacements of the two strings.

## 5.4 Continuity of Displacements

Since the two strings are tied together loosely with second order terms, each string contains the primary terms in the equation describing a problem. It is suggested that only one string be used in the formulation of the equations; this leaves the displacements of the other string undefined. The displacements of the second string can be related to those of the first string by imposing a continuity requirement. The necessary continuity equations are derived by forcing the second string to assume displacements which will cause the model to deform continuously.

For the purpose of explanation, let the odd string be used for the basic formulation of the problem. This leaves the even string undefined. Let $X_i$, where i is even, be defined by passing a cubic curve through $X_{i-3}$, $X_{i-1}$, $X_{i+1}$, $X_{i+3}$ as in Fig. 13. The result yields

$$X_i = \frac{1}{16} [-X_{i-3} + 9 X_{i-1} + 9 X_{i+1} - X_{i+3}] \tag{40}$$

By applying Eq. (40) to all even numbered points, a complete set of displacements for the second string is obtained. The model, therefore, is forced to deform smoothly. The basic characteristics of the model are retained; that is, the equations remain a finite difference analogue of the governing differential equation, are still physically meaningful, and can be derived through elementary principles of mechanics and basic material equations.

Finite difference operators are derived by applying a Taylor's expansion about a point of the displacement function. The resulting power series is truncated so as to retain all terms within an accuracy of $0(\lambda^2)$. The continuity equation, Eq. (40), can be derived from the same power series about the point $X_i$ by retaining all terms within an accuracy of $0(\lambda^4)$.

It should be noted that a straight line function could be used in place of the cubic displacement function, but it was found that the cubic function gives answers slightly better and with very little additional effort. The straight line equation is equivalent to a truncation of the power series for the displacement function with an accuracy of $0(\lambda^2)$.

# VI. COMPUTER PROGRAMS

## 6.1 Objectives of the Computer Programing

A computer program was written for the IBM 7094 computing system. It was designed to accomplish the following:

1. Efficiency of computations.
2. Restriction to immediate access storage.
3. Minimum input.
4. Flexibility for solving a wide variety of problems.
5. Maximum utilization of output features and simplicity of output format.
6. Automatic adjustment of load increments with provision for manual adjustments through input.

Efficiency of computations was achieved through the elimination of all unnecessary computations. All of the matrices presented in Chapter IV are banded or in other words have zero elements everywhere except near the main diagonal. Only the elements inside the band of each matrix are generated and manipulated during matrix operations. An extremely efficient simultaneous equation solver was used. This routine was developed by John W. Melin of the Department of Civil Engineering at the University of Illinois. It uses Gauss elimination to solve a set of simultaneous equations that are characterized by a banded coefficient matrix. Storage requirements are limited to that for the elements of the band above the main diagonal after elimination, the solution vector, a list equal in length to the number of equations, and a vector of sufficient length to store the non-zero elements of one equation (that is, the elements of one row of the coefficient matrix that lie within the band).

Immediate access storage on the IBM 7094 consists of approximately 32,000 locations. The storage required for this program is roughly proportional to the number of mass points or stress points used to discretize the continuum. The available storage was sufficient to prescribe 120 mass points and stress points along the radius of the plate. This represents an extremely "fine" mesh and is deemed sufficient for all practical problems. For the solution to a linear elastic problem (the first iterate of the large deflection solution), this mesh size will produce answers which are in error by less than .1% of the corresponding exact procedures. The degree of accuracy is approximately inversely proportional to the square of the number of mesh points.

Input to the program consists of:

1. Number of mesh points
2. Number of load increments
3. Maximum number of iterations to be allowed within each load increment
4. The thickness to span ratio of the plate ($\frac{h}{a}$)
5. Poisson's ratio
6. The tolerance on successive iterations
7. The initial load and the load increment
8. Control information which causes more or less information to be output by the program. For example, solution vectors after each iteration and the coefficient matrix generated prior to the solution of the simultaneous

equations can be output.

9. The yield limit in simple shear expressed as a fraction of Young's modulus

10. A tolerance on yielding expressed as a fraction of $J_2$

11. A flag which designates the controlling "string," and a flag which denotes whether the problem is starting or whether it is a continuation of a previous run. If it is a continuation, additional input is needed to describe the load, displacement, and force configuration of the previous run. This is supplied as output at the end of each computer run.

The amount of input is the minimum required for the degree of flexibility desired. In addition to the listed input, a subroutine must be written to describe the desired loading configuration. The load can be specified as a function of the displacements as well as any shape corresponding to the mesh size of the model.

Output varies according to that designated by the input, but it essentially consists of the load, the yield table, horizontal and vertical displacements, and stresses at each point of the mesh for each increment of loading. In addition, the stresses can be output as plotted curves on 35 mm film from the Cathode Ray Tube plotter attachment for the IBM 7094.

Load increments are designated as input. However, during plastic flow, they must be adjusted so as to not "overshoot" the yield criterion. These adjustments are carried out automatically by an interpolation scheme.

## 6.2 Description of the Computer Program

Fig. 14 is a flow diagram of the computer program. The solution begins by incrementing the load and setting the incremental displacements to zero. Then, the equilibrium equations are generated and solved for a new value of the incremental displacements. In general, these do not agree with the old values and are then used to generate a new set of equilibrium equations. The equations are solved recursively until two successive iterates agree within a small specified tolerance. The total displacements and stresses are then computed.

The stresses are examined to determine if any new yielding or unloading has occurred. If a point has values of stresses that are inadmissible on the basis of the yield criterion, the incremental load is reduced by an interpolation process and the above procedure is repeated for the new value of incremental load. If the yield criterion is not violated, the yield table is adjusted to reflect new yielding or unloading. Then, the total stresses at all plastic nodes are corrected because, in general, they will lie outside of the admissible region defined by the yield condition.

Additional load increments are applied and the procedure is repeated. When the last load increment has been added, the program terminates and outputs information which is necessary to continue the problem from that stage at a later time if desired.

# VII. SAMPLE PROBLEMS

## 7.1 Clamped Plate Loaded with a Uniform Pressure

Fig. 15 contains a graph of load versus deflection reproduced from a report by E. T. Onat and R. M. Haythornthwaite (13). A 1/4 inch thick circular plate, 10 inches in diameter and made of mild steel was tested under a uniform pressure. The test was conducted to about three plate thicknesses. The test results clearly show the importance of membrane effects on the behavior and ultimate load carrying capacity of the plate. In addition, the upper bound load predicted (14) on the basis of the small deflection assumption as shown in Fig. 15 is much too low.

Fig. 15 also contains a graph of load versus deflection from the present calculation. The parameters used in the calculations were adjusted to simulate the aforementioned plate. In order to make the sandwich plate behave as a solid plate, the cross-sectional areas and the flexural rigidities of the sandwich plate are taken equal to those of the solid plate. Poisson's ratio was taken to be .28 and Young's modulus was set at 30,000,000 psi; while the tensile yield strength was assumed to be 33,000 psi. The mesh size, $\lambda$, was taken to be 1/25 of the radius. This resulted in 100 equations plus the boundary conditions.

Throughout the elastic range, the behavior of the sandwich plate is similar to that of the solid plate. However, a difference occurs in the plastic range of behavior when the primary resisting forces are flexural. This is because the stresses in the solid plate vary over the thickness whereas those of the sandwich plate are concentrated at the two outer sheets. Because of this, the equivalent sandwich plate yields at a much higher load. After yielding, the sandwich plate becomes more flexible in bending than the solid plate because it is equivalent to a plate yielded all through the cross-section, whereas the solid plate yields only part of the way. At large plastic deflections, the behavior of the solid plate and sandwich plate are very much alike since at large deflections the membrane effect, which is influenced mostly by the cross-sectional areas of the plates, is most significant.

From Fig. 15 it can be seen that a reasonably close agreement is achieved throughout the entire range of the test results. The strains at a deflection of two plate thicknesses are large enough for strain-hardening to become a factor in the test of the real plate. Consequently, the real plate stiffens beyond this point, while in the calculation the material is elastic-perfectly plastic and thus a softening effect is indicated beyond this point. The computations proceeded smoothly with a uniform load increment of

$$\frac{qa^4}{Eh^4} = .009$$

until a load level of approximately

$$\frac{qa^4}{Eh^4} = 4$$

At that point, it was observed that a reduction in the load increment was necessary. This may be attributed to the existence of a stability requirement. Accordingly, the load increments were reduced to

$$\frac{qa^4}{Eh^4} : .003$$

and calculations continued up to a total load of

$$\frac{qa^4}{Eh^4} = 5.26$$

Fig. 16 shows the distributions of the radial stress in the top sheet of the plate at different load levels. Initially, the stresses in the central regions of the plate are compressive. As deflections increase, the character of the plate changes from flexure to membrane and the stresses in the plate become primarily tensile. Because of perfect plasticity, the stresses over a major portion of the plate approach a nearly uniform level at the higher loads.

Fig. 17 shows the corresponding distribution of the radial stresses in the bottom sheet of the plate. The tensile region of the plate grows with increasing load and becomes nearly constant over most of the plate after large plastic deformation.

Fig. 18 is a graph of the radial distribution of the tangential stresses in the top sheet. Initially, the stresses are primarily compressive. As a consequence of plastic flow and large deflection, the stresses approach a constant tensile value over about 75% of the central portion of the plate. Because of the Kirchoff-Love assumption, a point on the top surface of the plate must move toward the center even at very large deflection. Therefore, the tangential stresses must be compressive near the boundary. This region is seen to decrease with increasing loads. The distribution of the same stress in the bottom sheet is shown in Fig. 19. It also approaches a constant tensile value over most of the plate. The unusual pattern near the boundary is again due to the imposition of the Kirchoff-Love requirement.

The heavy lines in Figs. 16 to 19 denote the plastic region of the plate.

The profile of the vertical displacements is shown in Fig. 20. In the elastic range, the slope of the curve is horizontal at the fixed boundary. However, when yielding occurs at the boundary, the support then acts as a hinge. The shape of the deflected surface at a load level of

$$\frac{qa^4}{Eh^4} = 5$$

is almost spherical for most of the central portion of the plate. The corresponding profile for the horizontal displacements of the middle surface is shown in Fig. 21.

The curves in Figs. 16 through 19 are the results for the odd numbered mesh points. The stresses at the odd numbered mesh points satisfy the equilibrium equations at all levels of load. The stresses at the even numbered points are merely computed from the interpolated displacements and consequently may not satisfy equilibrium.

The behavior of an elastic-perfectly plastic plate restrained from inward movement at the edge under uniform pressure can be characterized as follows. The state of stress is approximately constant over

70% of the radius when large plastic flow has occurred; at the latter stage of deformation, the shape of the deflected surface tends to a spherical surface. A spherical state of stress begins at the center and propagates toward the edge with increasing load. It may be deduced that the ultimate load (pressure) carrying capacity of a circular plate would correspond approximately to the pressure inside a sphere of the same radius, producing the same state of stress. This ultimate load and resulting shape cannot be obtained with the technique presented herein because of the computational difficulties near the boundary.

It should be noted that the Kirchoff-Love assumption of normality is inappropriate near the clamped edge boundary after large rotation occurs at the plastic hinge. A more appropriate boundary condition would take into account the variation of stress through the thickness of the plate and shear deformations.

## 7.2 Simply Supported Plate Unrestrained at the Edge with a Concentrated Load at the Center

Fig. 22 contains a graph of load versus central deflection (curve A) from a report by R. M. Cooper and B. A. Shifrin (8). It represents the results from a test of a circular plate .104 inch thick and 17.3125 inches in diameter. The plate is of mild steel and was loaded through a loading rod of 0.6 inch diameter located at the center of the plate. It was supported on a 17-inch diameter ring.

A problem simulating the above test was considered in the analysis. The results of this analysis are also shown in Fig. 22. The boundary was assumed to be simply supported with unrestrained in-plane motion at the edge. The loading was assumed to consist of a uniform pressure applied over a circular area of radius .34625 inch. The diameter of the plate was taken to be 17.3125 inches and the thickness, 0.104 inch. Poisson's ratio is .28 and Young's modulus is 30,000,000 psi. The tensile yield strength is 37,000 psi. All of these material constants are taken to be the same as those of the test specimen.

At first glance, there appears to be some disagreement over the range of loading. This difference is attributable to two causes.

1. The test was started after an initial load was placed on the plate to bring it level with its support.

2. Strain-hardening occurred in the region of the plate directly under the central load.

An analysis was made to determine the effect of an initial load on the test results. Within the early elastic range of behavior it was assumed that the test should compare favorably with an elastic analysis. Accordingly, an initial load of 124 lbs. corresponding to a central deflection of .116 inch was found to account for the differences in the first 200 lbs. of load.

Since the analytical solution assumes perfectly plastic behavior, it was decided to compare results at some distance from the center of the plate. Curve C is a graph of the experimental load-deflection relation for a point at 1.37 inches from the center of the plate. It has been adjusted to take into acocunt the initial load of 124 lbs. Curve D is the corresponding result of the analysis. Agreement appears to be excellent.

In the test, plastic straining was observed in the top of the plate near the edge at a load of 2200 lbs. The analysis indicated the same yielding at a load of about 2,030 lbs. The measured inward in-plane displacement at the edge of the plate was .013 inch at a load of 3,862 lbs. whereas the analysis indicated .0165 inch at approximately the same load. It is expected that friction of the support would restrain this motion somewhat.

Figs. 23 through 26 are graphs showing the distribution of stresses along the radius at increasing load levels. As might be expected, the behavior near the concentrated load is somewhat erratic. This is due to the fact that the mesh size is coarse with respect to the small loading area. The mesh size is .34625 inch which corresponds exactly to the size of the loaded area. As was mentioned in Sect. 7.1, the curves correspond to the calculated results of the odd numbered points. Also, the heavy lines denote the plastic region of the plate.

## 7.3 Elastic Solutions

Several solutions were obtained in the elastic range for the purpose of comparing the present method with existing theories. Fig. 27 is redrawn from the results of pressure tests of clamped plates performed by McPherson, Ramberg, and Levy (15). The tests were made of 5.0 inch diameter, 17S-RT aluminum alloy plates of various thicknesses. The points denoted by circles were obtained from a .0658-inch thick plate. The points denoted by squares were obtained from a .0300-inch plate. The solid square points represent test results where a permanent central deflection greater than .01 inch was observed. Also drawn on this figure are theoretical curves of several investigators. The most accurate of these theoretical curves (represented by the solid line) is generally known to be that corresponding to an extension of Nadai's theory (15).

The points denoted by a triangle were obtained with the method presented here. They compare favorably with Nadai's solution of the theoretical equations. The deviation of the calculated results (the present results and those obtained with Nadai's theory) with the tests of McPherson, Ramberg, and Levy can be attributed to the clamping apparatus and the fact that the experiments were for aluminum alloy which is not a linearly elastic material. It should also be observed that the stresses at the clamped edge were near the yield limit at a load level of only

$$\frac{qa^4}{Eh^4} = 180$$

whereas the experiments indicated that plastic flow occurs only after a permanent set of .01 inch which corresponds to a load level of

$$\frac{qa^4}{Eh^4} = 230$$

Since the stress distribution of a solid plate when compared with that of the sandwich idealization would indicate higher stresses in the outer fibers, first yielding (at the outer edge) of a solid plate could have occurred at load levels even lower than

$$\frac{qa^4}{Eh^4} = 180$$

The solid lines in Fig. 28 are redrawn from the results described by Timoshenko (1). They represent the theoretical results obtained by Federhofer and Egger of simply supported circular plates with immovable edges. Fig. 28 contains a graph of the central deflection, the extreme fiber stress at the center, and the extreme fiber stress in the radial and tangential directions at the edge of the plate. The points denoted by a triangle were obtained by the method presented herein. The agreement between the two solutions is certainly excellent.

Fig. 29 is a similar graph obtained for a simply supported plate with movable edges. The results obtained with the present method are shown with dashed lines. After a deflection of about five plate thicknesses, it is seen that the results obtained herein differ significantly from those of Federhofer and Egger. Fig. 30 is a scale drawing of the deflected plate at a load level of

$$\frac{qa^4}{Eh^4} = 172$$

It can be seen that the horizontal displacements near the edge are very large. They are large enough that second order terms of this displacement are important. The theoretical equations presented by Timoshenko and reportedly used by Federhofer and Egger (1) neglected the second order effects of horizontal displacements, whereas the solutions obtained herein include this effect. The most important difference is in determining the slope of the deflected plate near the edge. The slope is approximated by Timoshenko as

$$\frac{dw}{dr}$$

whereas the exact expression is

$$\frac{\frac{\partial w}{\partial r}}{1 + \frac{\partial u}{\partial r}}$$

The difference in these values is approximately 30% at a load level of

$$\frac{qa^4}{Eh^4} = 172$$

7.4 Convergence of Results with Decreasing Mesh Size

The solutions obtained herein are essentially solutions of the finite difference approximation of the governing differential equations. The error associated with this approximation has been shown to be proportional to the square of the mesh size (16). In the absence of accumulated round-off errors, extrapolation to zero mesh-size should give a value for the computed function that is very close to the exact solution of the governing differential equations. The behavior of results plotted against varying mesh size was examined to determine the degree of accuracy obtained by the method described herein.

There are two distinct questions relating to accuracy obtained by the present method. The first is concerned with the convergence of the solutions obtained with decreasing mesh size to the true solution. The second question is related to the validity of using a continuity relation to avoid the separation discussed in Sect. 5.4. The computer program is designed so that the continuity relation can be imposed on either the odd or even numbered string. In addition, the boundary can be placed at an odd or even numbered point. Therefore, four combinations of boundary conditions with respect to the placement of the boundary and the imposition of the continuity relation are possible. Presumably, any of the four combinations should give valid solutions.

Figs. 31 and 32 were obtained for a simply supported plate restrained at its edge and loaded with a uniform pressure to the level

$$\frac{qa^4}{Eh^4} = 2.566$$

The centerline deflection plotted against varying mesh size is shown in Fig. 31. Fig. 32 is a similar plot for the membrane stress at the edge. The points denoted by a shaded triangle and an open triangle are obtained by placing the boundary at an odd numbered point, while the points denoted by a square and a circle were obtained by placing the boundary at an even numbered point. The points denoted by a shaded triangle and a square were obtained by satisfying the equilibrium equations at the odd numbered mesh points and those denoted by an open triangle and a circle correspond to satisfying equilibrium at the even numbered points. The maximum stress at the center was also found as a function of mesh size. However, the range of solutions was so small ($\sigma a^2/Eh^2 = 1.915$ to $1.918$) that a graph was not prepared.

The convergence of solutions with decreasing mesh size shown in Figs. 31 and 32 gives a strong indication of the validity of the proposed method of solution. It may be observed that the four solutions in Fig. 31 or 32 converge on a common solution at zero mesh length.

## 7.5 The Effect of Load Increment on Errors in the Elastic Range

Solutions were obtained for a simply supported plate restrained at the edge up to a load level of

$$\frac{qa^4}{Eh^4} = 10.264$$

which corresponds to a centerline displacement of $w_o/h = 1.424$. A set of solutions were obtained by incrementing the load 40 times and another set by incrementing the load 2 times. In both cases, successive iterations were required to converge to within 0.1% of one another for each load increment. Displacements, centerline stresses and edge stresses were found to agree within 0.07%, 0.17%, and 0.08%, respectively. The variance is of the same order of magnitude as the iteration tolerance and the error is evidently not cumulative. As was mentioned in Sect. 5.2, the term $E(\Delta X)$, which is the residual corresponding to $\Delta X = 0$, serves to correct the solution as the procedure progresses.

# VIII. SUMMARY AND CONCLUSIONS

A numerical technique has been presented to analyze elastic-plastic plates without the usual assumptions of small deflections. By using a lumped-parameter model the continuous plate is replaced by one with a finite number of degrees of freedom. The field equations are then derived directly from the model for large deflection geometry. These equations turn out to be a finite difference approximation to the corresponding "exact" differential equations. Hence, a solution formulated through the model can be shown to tend to the corresponding problem of a continuum.

In order to make the problem more easily tractable, the plates are assumed to be a sandwich configuration, consisting of a rigid shear core between two thin elastic-perfectly plastic sheets. The shear core is incapable of developing flexural and membrane stresses. The Prandtl-Reuss equation is used to describe the material behavior of the thin sheets which are assumed to be in plane stress.

The plate and its loading are assumed to be axially symmetric, thereby limiting the problem to one independent space variable.

A recursive technique is presented to solve the non-linear equations which are expressed as a function of displacements. Within each iteration, the equations are simultaneously linear and solved by a modified Gauss elimination scheme. Successive iterations converge to a unique solution for each increment of load. Load is added in small increments until a desired level of loading is achieved.

The technique is programmed for the IBM 7094 computing system at the University of Illinois. Three sample problems are presented which compare favorably with test results, and are also shown to be consistent with other theoretical solutions in the elastic range.

In the absence of formal proofs, the problem of convergence of solutions with decreasing mesh size has been studied with respect to the known errors associated with finite difference approximations. The results of this investigation show that a sequence of solutions determined with decreasing mesh size tend to a unique solution. Assuming this solution to be correct, the error is seen to be proportional to the square of the mesh size. The validity of the solutions is supported by the favorable comparison with test results.

Although the solution method is described and used herein for circular plates of elastic-perfectly plastic material, the method is equally applicable for other material equations.

# REFERENCES


1. Timoshenko, S., and Woinowski-Krieger, S., Theory of Plates and Shells, McGraw-Hill Co., New York, 1959.

2. Levy, S., "Large Deflections of Rectangular Plates," NACA, T. N., 846, 1942.

3. Keller, H. B., and Reiss, E. L., "Non-Linear Bending and Buckling of Circular Plates," Proceedings of the Third U. S. National Congress of Applied Mechanics, 1958, pp. 375-385.

4. Ang, A. H.-S., and Lopez, L. A., "Flexural Analysis of Elastic-Plastic Rectangular Plates," Preprint No. 478, ASCE Structural Engineering Conference, Seattle, Wash., May, 1967.

5. Prager, W., and Hodge, P. G., Theory of Perfectly Plastic Solids, John Wiley and Sons, Inc., New York, 1963.

6. Haythornthwaite, R. M., "The Deflections of Plates in the Elastic-Plastic Range," Proceedings of the Second National Congress of Applied Mechanics, Ann Arbor, 1954, pp. 521-526, 1955.

7. Ohashi, Y., and Murakami, S., "The Elasto-Plastic Bending of a Clamped Thin Circular Plate," Proceedings of the Eleventh International Congress of Applied Mechanics, Munich, 1964, pp. 212-223.

8. Cooper, R. M., and Shifrin, G. A., "An Experiment on Circular Plates in the Plastic Range," Proceedings of the Second U. S. National Congress of Applied Mechanics, Ann Arbor, 1954, pp. 527-534.

9. Novozhilov, V. V., Foundations of the Nonlinear Theory of Elasticity, Graylock Press, Rochester, N. Y., 1953.

10. Ang, A. H.-S., and Newmark, N. M., "A Numerical Procedure for the Analysis of Continuous Plates," Second Conference on Electronic Computation, ASCE, September, 1960.

11. Mohraz, B., and Schnobrich, W. C., "The Analysis of Shallow Shell Structures by a Discrete Element System," Civil Engineering Studies, Structural Research Series No. 304, University of Illinois, March, 1966.

12. Lopez, L. A., "Flexural Analysis of Elastic-Plastic Rectangular Plates," Ph.D. Thesis, University of Illinois, 1966.

13. Onat, E. T., and Haythornthwaite, R. M., "The Load-Carrying Capacity of Circular Plates at Large Deflection," Journal of Applied Mechanics, Vol. 23, March, 1956, pp. 49-55.

14. Hodge, P. G., Limit Analysis of Rotationally Symmetric Plates and Shells, Prentice-Hall, Inc., Englewood Cliffs, N. J., 1963.

15. McPherson, A. E., Ramberg, W., and Levy, S., "Normal Pressure Tests of Circular Plates with Clamped Edges," NACA, T. N., 848, 1942.

16. Crandall, S. H., Engineering Analysis, McGraw-Hill Co., New York, 1956.

# APPENDIX A

## A1 Derivation of Plastic Stress-Strain Equations

The following derivation of the stress-strain equations follows the procedure outlined in Reference (5). This derivation is restricted to the assumptions stated in Chapter I.

According to the von Mises yield criterion,

$$J_2 = k^2$$

where $J_2$ is the 2nd invariant of stress deviation and k is the yield limit of the material in simple shear. In terms of polar coordinates where the stresses are symmetric about the z-axis and for the case of plane stress,

$$J_2 = 1/3\ (\sigma_r^2 - \sigma_r\sigma_\theta + \sigma_\theta^2)$$

hence, the von Mises condition becomes

$$\sigma_r^2 - \sigma_r\sigma_\theta + \sigma_\theta^2 = 3k^2 \qquad \text{(A1)}$$

The total strain is assumed to be the sum of the elastic strain according to Hooke's law and the plastic strain denoted by $\varepsilon'$ and $\varepsilon''$, respectively.

For plane stress, the mean normal stress is

$$s = 1/3\ (\sigma_r + \sigma_\theta) \qquad \text{(A2)}$$

and the stress deviator is

$$s_r = \sigma_r - s$$

$$s_\theta = \sigma_\theta - s \tag{A3}$$

$$s_z = - s$$

The mean normal strain is

$$e = 1/3\ (\varepsilon_r + \varepsilon_\theta + \varepsilon_z)$$

and the strain deviation is

$$e_r = \varepsilon_r - e$$

$$e_\theta = \varepsilon_\theta - e \tag{A4}$$

$$e_z = \varepsilon_z - e$$

By assuming that there is no permanent change in volume, the plastic component of the mean normal strain must disappear, or

$$e'' = 1/3\ (\varepsilon_r'' + \varepsilon_\theta'' + \varepsilon_z'') = 0 \tag{A5}$$

Therefore, the plastic strain deviation is identical to plastic strain or

$$e''_r = \varepsilon''_r$$

$$e''_\theta = \varepsilon''_\theta \qquad \text{(A6)}$$

$$e''_z = \varepsilon''_z$$

According to the Prandtl-Reuss theory, the rate of change of the plastic strain deviation is at any instant proportional to the instantaneous stress deviation, or

$$2G\mathring{e}''_r = \Gamma\ s_r$$

$$2G\mathring{e}''_\theta = \Gamma\ s_\theta$$

$$2G\mathring{e}''_z = \Gamma\ s_z$$

where $\Gamma$ is a constant of proportionality and G is given by

$$G = \frac{E}{2(1 + \mu)}$$

where E is Young's modulus and $\mu$ is Poisson's ratio.

According to Hooke's law,

$$2G\mathring{e}'_r = \mathring{s}_r$$

$$2G\mathring{e}'_\theta = \mathring{s}_\theta$$

$$2G\mathring{e}'_z = \mathring{s}_z$$

Therefore, the rate of total strain is

$$2G\mathring{e}_r = \mathring{s}_r + \Gamma\ s_r \tag{A7}$$

$$2G\mathring{e}_\theta = \mathring{s}_\theta + \Gamma\ \mathring{s}_\theta \tag{A8}$$

$$2G\mathring{e}_z = \mathring{s}_z + \Gamma\ s_z \tag{A9}$$

$\Gamma$ may be eliminated from these equations by multiplying Eq. (A7) by $s_r$, Eq. (A8) by $s_\theta$, and Eq. (A9) by $s_z$. Summing the results yields

$$2G\ (\mathring{e}_r s_r + \mathring{e}_\theta s_\theta + \mathring{e}_z s_z) = 2\ \Gamma k^2$$

Therefore,
$$\Gamma = \frac{G\mathring{W}}{k^2} \tag{A10}$$

where

$$\mathring{W} = \mathring{e}_r\ s_r + \mathring{e}_\theta\ s_\theta + \mathring{e}_z\ s_z \tag{A11}$$

The quantity $\overset{\circ}{W}$ may be interpreted as the rate at which the stresses do work in connection with the change of shape. $\overset{\circ}{W}$ must be positive for plastic straining to take place. Otherwise, the material is unloading; in which case, Hooke's law in rate form may be used for elastic unloading.

Substituting (A10) into (A7) through (A9) yields

$$s_r = 2G\ (e_r - \frac{\overset{\circ}{W}}{2k^2} s_r) \tag{A12}$$

$$s_\theta = 2G\ (e_\theta - \frac{\overset{\circ}{W}}{2k^2} s_\theta) \tag{A13}$$

$$s_z = 2G\ (e_z - \frac{\overset{\circ}{W}}{2k^2} s_z) \tag{A14}$$

$\overset{\circ}{W}$ may be expressed in terms of the total stresses and strain rates by substitution of Eqs. (A3) and (A4) into (A11) and taking note that

$$\overset{\circ}{s} = 3\ K\ \overset{\circ}{e}$$

where

$$K = \frac{E}{3(1 - 2\mu)}$$

is the elastic bulk modulus. This yields

$$\overset{\circ}{W} = \sigma_r\ \overset{\circ}{\varepsilon}_r + \sigma_\theta\ \overset{\circ}{\varepsilon}_\theta - \frac{s\overset{\circ}{s}}{K} \tag{A15}$$

Eqs. (A12), (A13), and (A14) can now be expressed in terms of total stresses, strains, stress rates and strain rates. The stress rates can then be determined as follows:

$$\overset{\circ}{\sigma}_r = \frac{E\,[(2\sigma_\theta - \sigma_r)^2\,\overset{\circ}{\varepsilon}_r - (2\sigma_\theta - \sigma_r)(2\sigma_r - \sigma_\theta)\,\overset{\circ}{\varepsilon}_\theta]}{(2\sigma_\theta - \sigma_r)^2 + (2\sigma_r - \sigma_\theta)^2 + 2\mu(2\sigma_\theta - \sigma_r)(2\sigma_r - \sigma_\theta)}$$

(A16)

$$\overset{\circ}{\sigma}_\theta = \frac{E\,[(2\sigma_r - \sigma_\theta)^2\,\overset{\circ}{\varepsilon}_\theta - (2\sigma_\theta - \sigma_r)(2\sigma_r - \sigma_\theta)\,\overset{\circ}{\varepsilon}_r]}{(2\sigma_\theta - \sigma_r)^2 + (2\sigma_r - \sigma_\theta)^2 + 2\mu(2\sigma_\theta - \sigma_r)(2\sigma_r - \sigma_\theta)}$$

If Eq. (A2) and its derivative are substituted into Eq. (A15) and using Eq. (A16), $\overset{\circ}{W}$ may be expressed as follows:

$$\overset{\circ}{W} = \frac{2(\sigma_r^2 - \sigma_r\sigma_\theta + \sigma_\theta^2)\,\{[(2\sigma_r - \sigma_\theta) - \mu(2\sigma_\theta - \sigma_r)]\,\overset{\circ}{\varepsilon}_r + [(2\sigma_\theta - \sigma_r) - \mu(2\sigma_r - \sigma_\theta)]\,\overset{\circ}{\varepsilon}_\theta\}}{(2\sigma_r - \sigma_\theta)^2 + (2\sigma_\theta - \sigma_r)^2 + 2\mu(2\sigma_r - \sigma_\theta)(2\sigma_\theta - \sigma_r)}$$

(A17)

The yield criterion, Eq. (A1), the stress rate-strain rate equation, Eq. (A16) and Eq. (A17) are the basic equations of perfect plasticity used in the solution of the problems described herein. Geometrically, the state of stress is represented by a point in stress space of $\sigma_r$ and $\sigma_\theta$ in the present case. Yielding of the material occurs when the stress state is on the boundary of the stress space defined by the yield criterion. No state of stress outside of this region is permissible for a perfectly plastic material. For plastic straining (according to the plastic stress rate-strain rate equations) to take place, $\overset{\circ}{W}$ must be positive.

## A2 An Incremental Form of the Plastic Stress-Strain Equations

Eq. (A16) represents the instantaneous stress rate-strain rate relation corresponding to a state of stress, $\sigma_r$, $\sigma_\theta$. It is assumed that the stress-strain law is time independent. Therefore, the rates can be taken with respect to the instantaneous load on the plate. In other words,

$$\overset{\circ}{\sigma}_r = \frac{\partial \sigma_r}{\partial p}$$

$$\overset{\circ}{\sigma}_\theta = \frac{\partial \sigma_\theta}{\partial p}$$

$$\overset{\circ}{\varepsilon}_r = \frac{\partial \varepsilon_r}{\partial p}$$

$$\overset{\circ}{\varepsilon}_\theta = \frac{\partial \varepsilon_\theta}{\partial p}$$

The solution technique employed herein requires that the load be increased in finite increments. Therefore,

$$\frac{\partial \sigma_r}{\partial p} \cong \frac{\Delta \sigma_r}{\Delta p}$$

$$\frac{\partial \sigma_\theta}{\partial p} \cong \frac{\Delta \sigma_\theta}{\Delta p}$$

$$\frac{\partial \varepsilon_r}{\partial p} \cong \frac{\Delta \varepsilon_r}{\Delta p}$$

$$\frac{\partial \varepsilon_\theta}{\partial p} \cong \frac{\Delta \varepsilon_\theta}{\Delta p}$$

Now, for a finite increment of loading, the stress-strain relation at a point changes during the load increment because the state of stress changes during the increment. At load level p, the functional stress-strain relation can be stated as

$$\mathring{\sigma} = f(\sigma)\ \mathring{\varepsilon}$$

while at load level $p + \Delta p$,

$$\mathring{\sigma} = f(\sigma + \Delta\sigma)\ \mathring{\varepsilon}$$

For a finite load increment, the finite increments, $\Delta\sigma$, $\Delta\varepsilon$ must be related by some function $\bar{\bar{\sigma}}$, where $\sigma \leq \bar{\bar{\sigma}} \leq \sigma + \Delta\sigma$. In other words,

$$\Delta\sigma = f(\bar{\bar{\sigma}})\ \Delta\varepsilon$$

It is proposed that $\bar{\sigma}$ be evaluated on the basis of

$$\left.\frac{\partial\sigma_r}{\partial\sigma_\theta}\right|_{\bar{\sigma}_r,\ \bar{\sigma}_\theta} = \frac{\Delta\sigma_r}{\Delta\sigma_\theta} \tag{A18}$$

and that the three stress states $(\sigma_r, \sigma_\theta; \bar{\sigma}_r, \bar{\sigma}_\theta; \sigma_r + \Delta\sigma_r, \sigma_\theta + \Delta\sigma_\theta)$ satisfy the yield criterion.

Let $\bar{\sigma}_r$ and $\bar{\sigma}_\theta$ be related by

$$\bar{\sigma}_\theta = \bar{\sigma}_r \frac{\sigma_\theta + \frac{\Delta\sigma_\theta}{2}}{\sigma_r + \frac{\Delta\sigma_r}{2}} \tag{A19}$$

where Eq. (A19) is the equation of a straight line from $\sigma_r = \sigma_\theta = 0$ passing through the bisector of the chord between $(\sigma_r, \sigma_\theta)$ and $(\sigma_r + \Delta\sigma_r, \sigma_\theta + \Delta\sigma_\theta)$. Substituting Eq. (A19) into the yield criterion, Eq. (A1), yields

$$\bar{\sigma}_r = \frac{\sqrt{3}\ k\ (\sigma_r + \frac{\Delta\sigma_r}{2})}{\sqrt{(\sigma_r + \frac{\Delta\sigma_r}{2})^2 - (\sigma_r + \frac{\Delta\sigma_r}{2})(\sigma_\theta + \frac{\Delta\sigma_\theta}{2}) + (\sigma_\theta + \frac{\Delta\sigma_\theta}{2})^2}} \tag{A20a}$$

$$\bar{\sigma}_\theta = \frac{\sqrt{3}\ k\ (\sigma_\theta + \frac{\Delta\sigma_\theta}{2})}{\sqrt{(\sigma_r + \frac{\Delta\sigma_r}{2})^2 - (\sigma_r + \frac{\Delta\sigma_r}{2})(\sigma_\theta + \frac{\Delta\sigma_\theta}{2}) + (\sigma_\theta + \frac{\Delta\sigma_\theta}{2})^2}} \tag{A20b}$$

The slope of the yield function evaluated at the above $\bar{\sigma}_r$, $\bar{\sigma}_\theta$ can be shown to be

$$\left.\frac{\partial\sigma_r}{\partial\sigma_\theta}\right|_{\bar{\sigma}_r,\ \bar{\sigma}_\theta} = -\frac{2\bar{\sigma}_\theta - \bar{\sigma}_r}{2\bar{\sigma}_r - \bar{\sigma}_\theta} \tag{A21}$$

and if Eqs. (A20) are substituted in Eq. (A21),

$$\left.\frac{\partial\sigma_r}{\partial\sigma_\theta}\right|_{\bar{\sigma}_r,\ \bar{\sigma}_\theta} = \frac{2\sigma_\theta - \sigma_r + \Delta\sigma_\theta - \frac{\Delta\sigma_r}{2}}{2\sigma_r - \sigma_\theta + \Delta\sigma_r - \frac{\Delta\sigma_\theta}{2}} \tag{A22}$$

Now, the stresses $\sigma_r + \Delta\sigma_r$ and $\sigma_\theta + \Delta\sigma_\theta$ also satisfy the yield criterion. From this the following can be shown:

$$\frac{\Delta\sigma_r}{\Delta\sigma_\theta} = -\frac{2\sigma_\theta - \sigma_r + \Delta\sigma_\theta - \frac{\Delta\sigma_r}{2}}{2\sigma_r - \sigma_\theta + \Delta\sigma_r - \frac{\Delta\sigma_\theta}{2}} \tag{A23}$$

Therefore, from Eqs. (A22) and (A23), Eq. (A18) is proved to be correct.

$$\left.\frac{\partial\sigma_r}{\partial\sigma_\theta}\right|_{\bar{\sigma}_r,\ \bar{\sigma}_\theta} = \frac{\Delta\sigma_r}{\Delta\sigma_\theta}$$

For a finite increment of loading, the terms $\bar{\sigma}_r$ and $\bar{\sigma}_\theta$ are substituted for $\sigma_r$ and $\sigma_\theta$ respectively in the stress-strain equation, Eq. (A16), and the stress rates and strain rates become finite increments,

$$\Delta\sigma_r = \frac{E\,[(2\bar{\sigma}_\theta - \bar{\sigma}_r)^2\,\Delta\varepsilon_r - (2\bar{\sigma}_\theta - \bar{\sigma}_r)(2\bar{\sigma}_r - \bar{\sigma}_\theta)\,\Delta\varepsilon_\theta]}{(2\bar{\sigma}_\theta - \bar{\sigma}_r)^2 + (2\bar{\sigma}_r - \bar{\sigma}_\theta)^2 + 2\mu(2\bar{\sigma}_\theta - \bar{\sigma}_r)(2\bar{\sigma}_r - \bar{\sigma}_\theta)} \tag{A24a}$$

$$\Delta\sigma_\theta = \frac{E\,[(2\bar{\sigma}_r - \bar{\sigma}_\theta)^2\,\Delta\varepsilon_\theta - (2\bar{\sigma}_\theta - \bar{\sigma}_r)(2\bar{\sigma}_r - \bar{\sigma}_\theta)\,\Delta\varepsilon_r]}{(2\bar{\sigma}_\theta - \bar{\sigma}_r)^2 + (2\bar{\sigma}_r - \bar{\sigma}_\theta)^2 + 2\mu(2\bar{\sigma}_\theta - \bar{\sigma}_r)(2\bar{\sigma}_r - \bar{\sigma}_\theta)} \tag{A24b}$$

where $\bar{\sigma}$ and $\bar{\sigma}_\theta$ are evaluated by Eq. (A20).

It should be noted that Eq. (A24) is non-linear in terms of $\Delta\sigma_r$ and $\Delta\sigma_\theta$. It is solved by letting $\Delta\sigma_r = 0$, $\Delta\sigma_\theta = 0$ for the first iterate in the solution scheme described in Sect. 5.2. Successive iterations use the old value of $\Delta\sigma_r$, $\Delta\sigma_\theta$ in the right side of Eq. (A24). When convergence is obtained, all of the equations are satisfied and $\sigma_r + \Delta\sigma_r$, $\sigma_\theta + \Delta\sigma_\theta$ satisfy the yield criterion. $\bar{\sigma}_r$ and $\bar{\sigma}_\theta$ as well as $\sigma_r$ and $\sigma_\theta$, always satisfy the yield criterion.

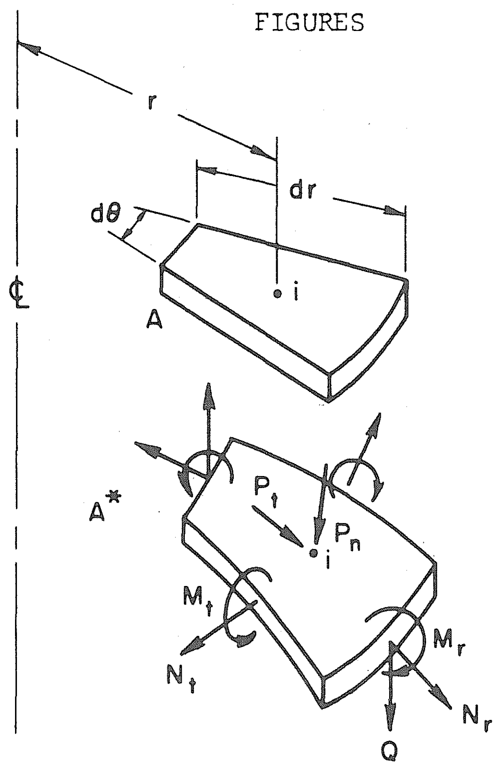


Figure 1. Infinitesimal element of a circular plate.

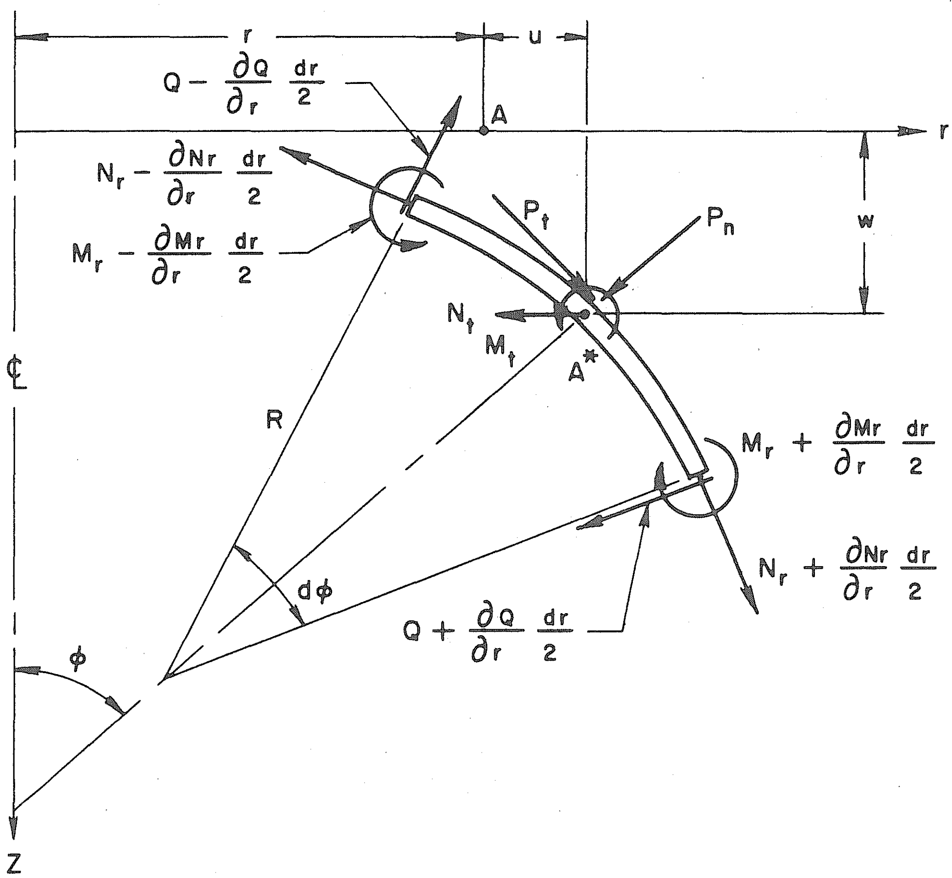


Figure 2. Projection of an infinitesimal element on the r-z plane.

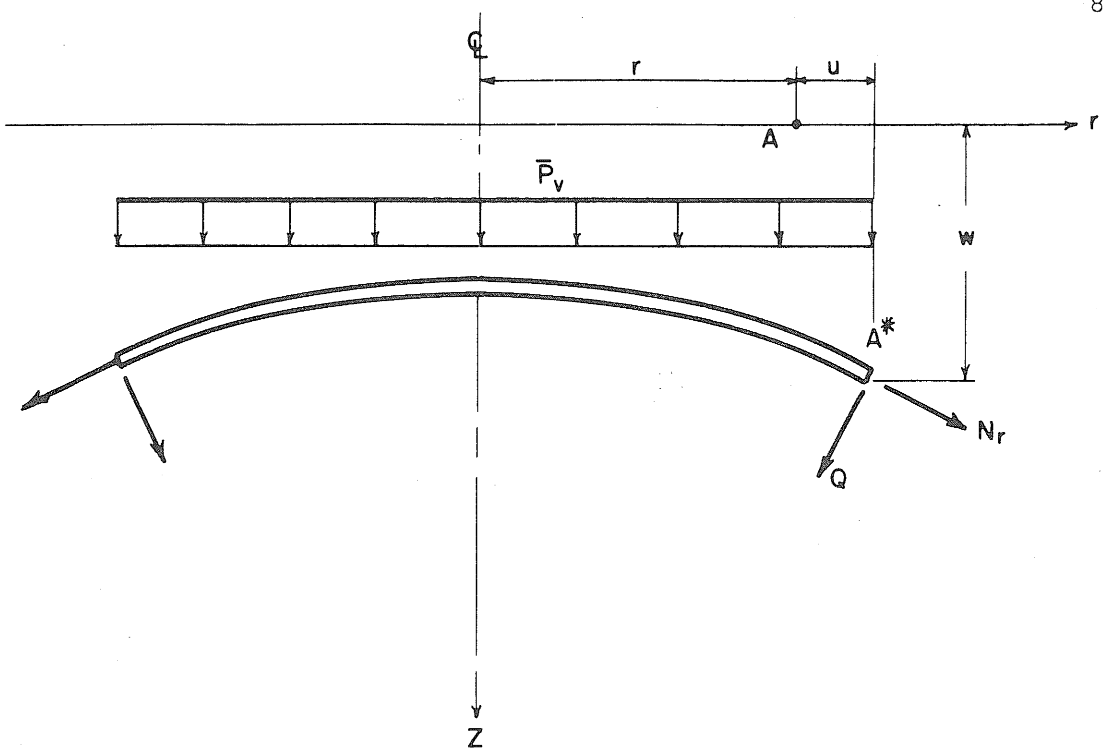


Figure 3. Section of a circular plate projected on the r-z plane.

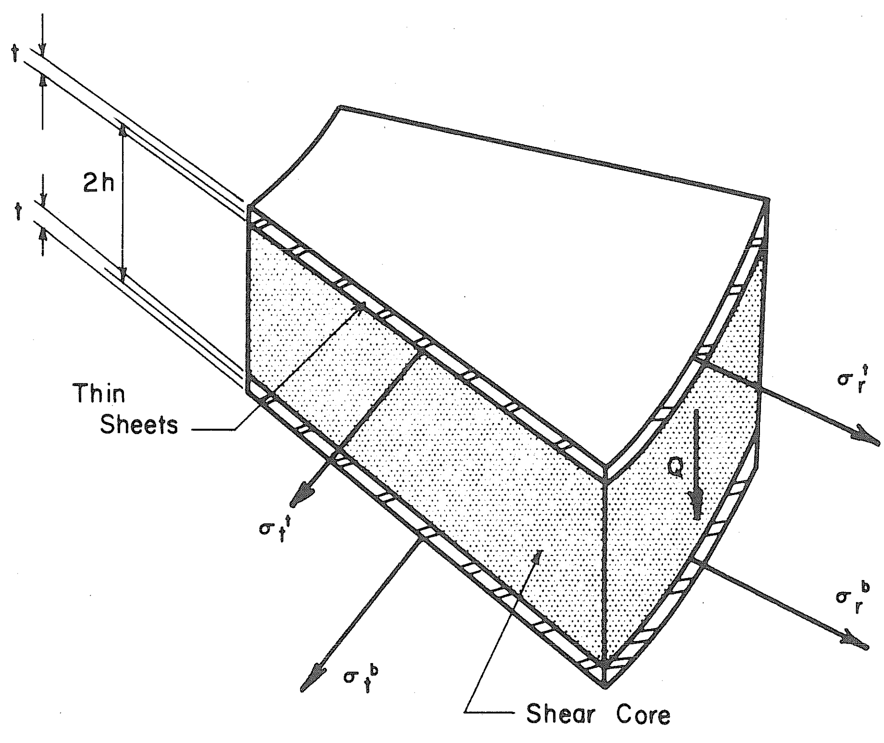


Figure 4. Sandwich configuration.

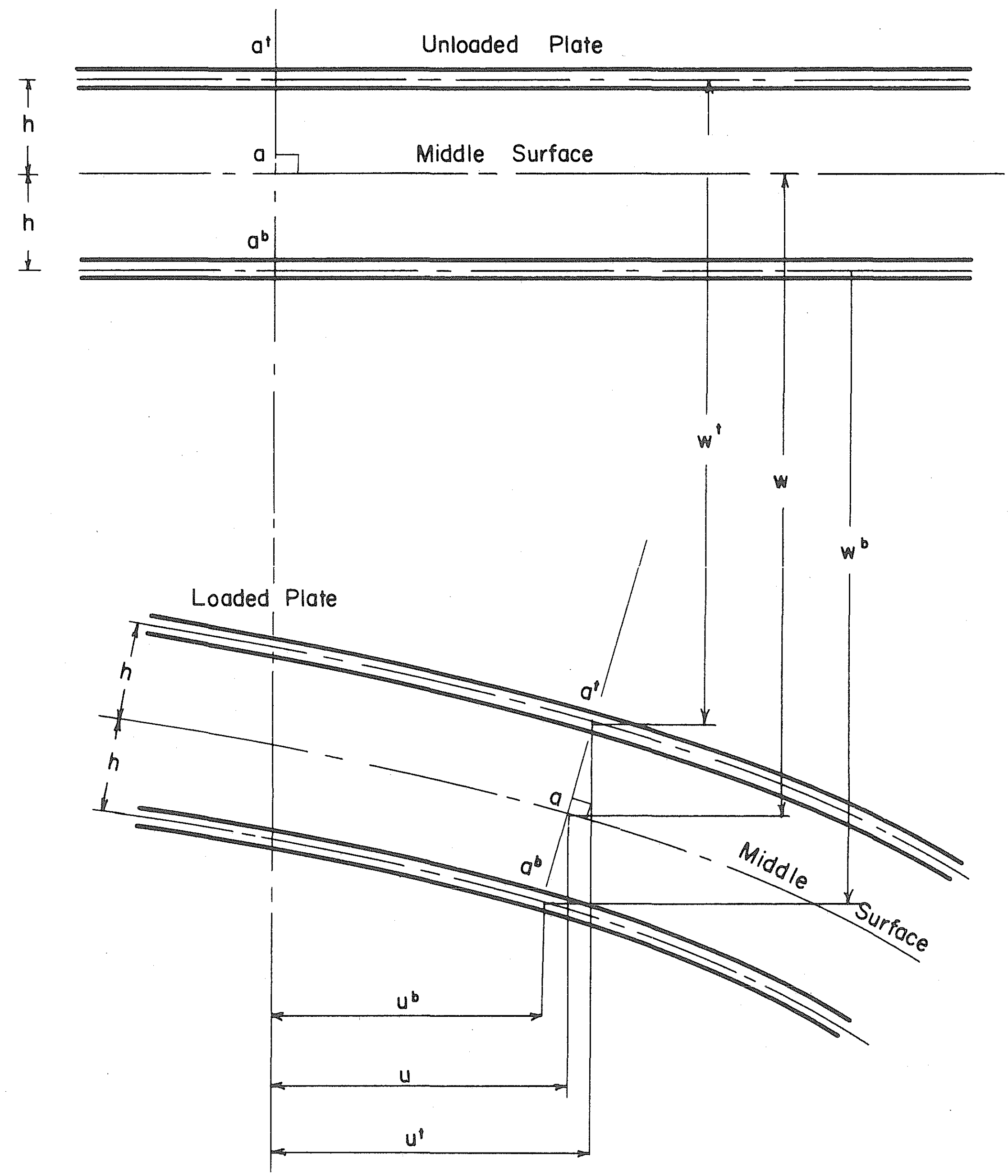


Figure 5. Transformation of displacements of the outer sheets to the middle surface.

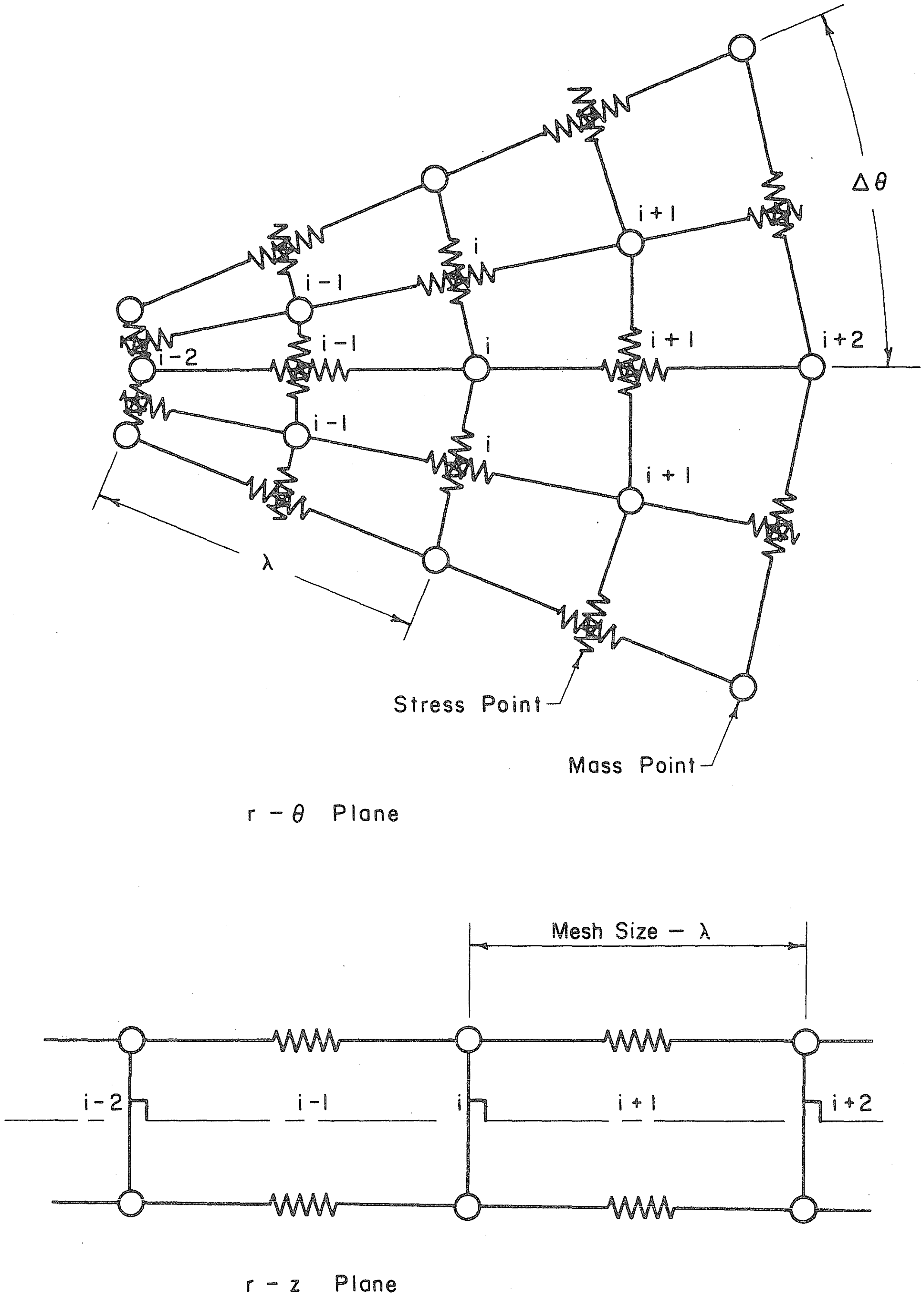


Figure 6. Schematic representation of the model.

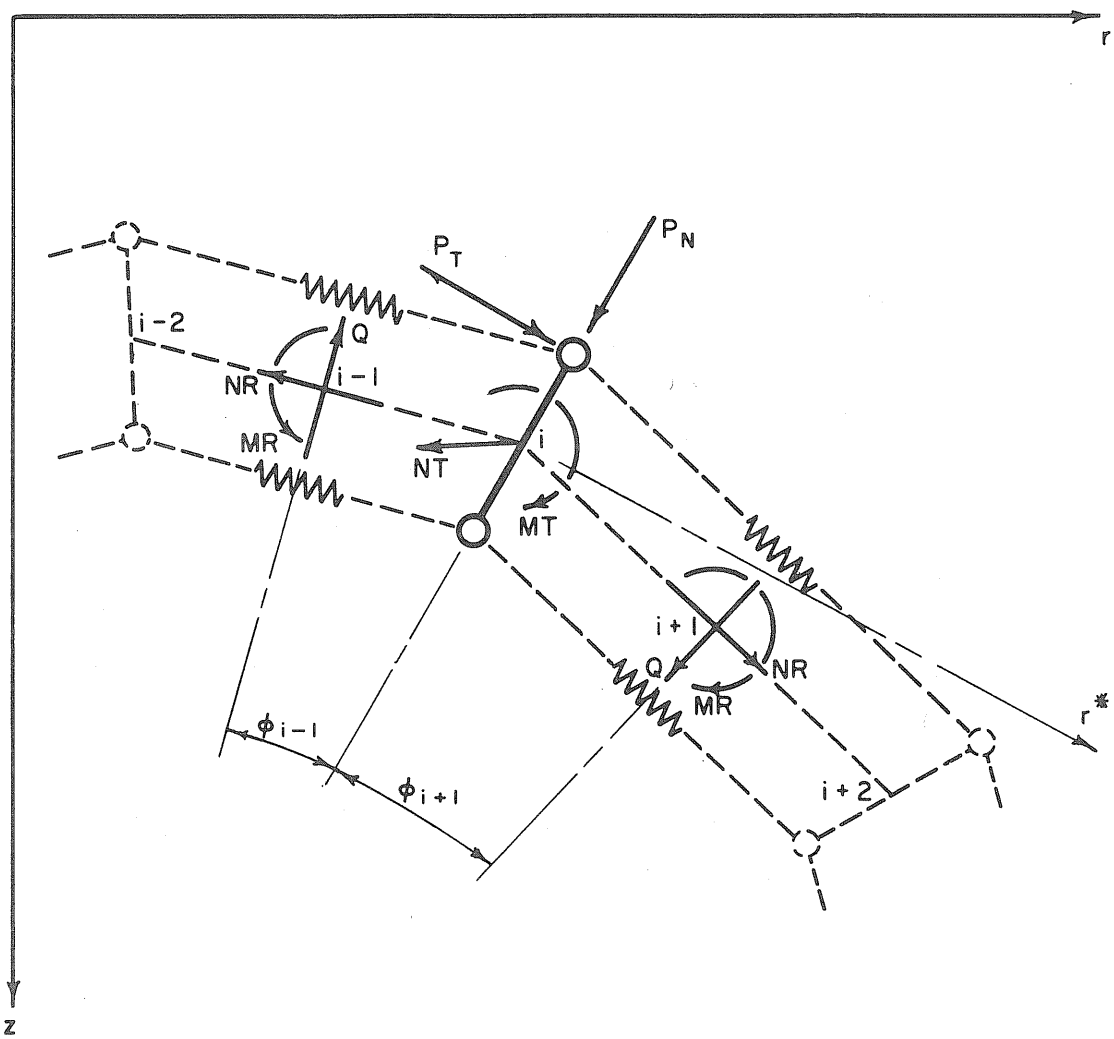


Figure 7. Equilibrium of a mass point of the model.

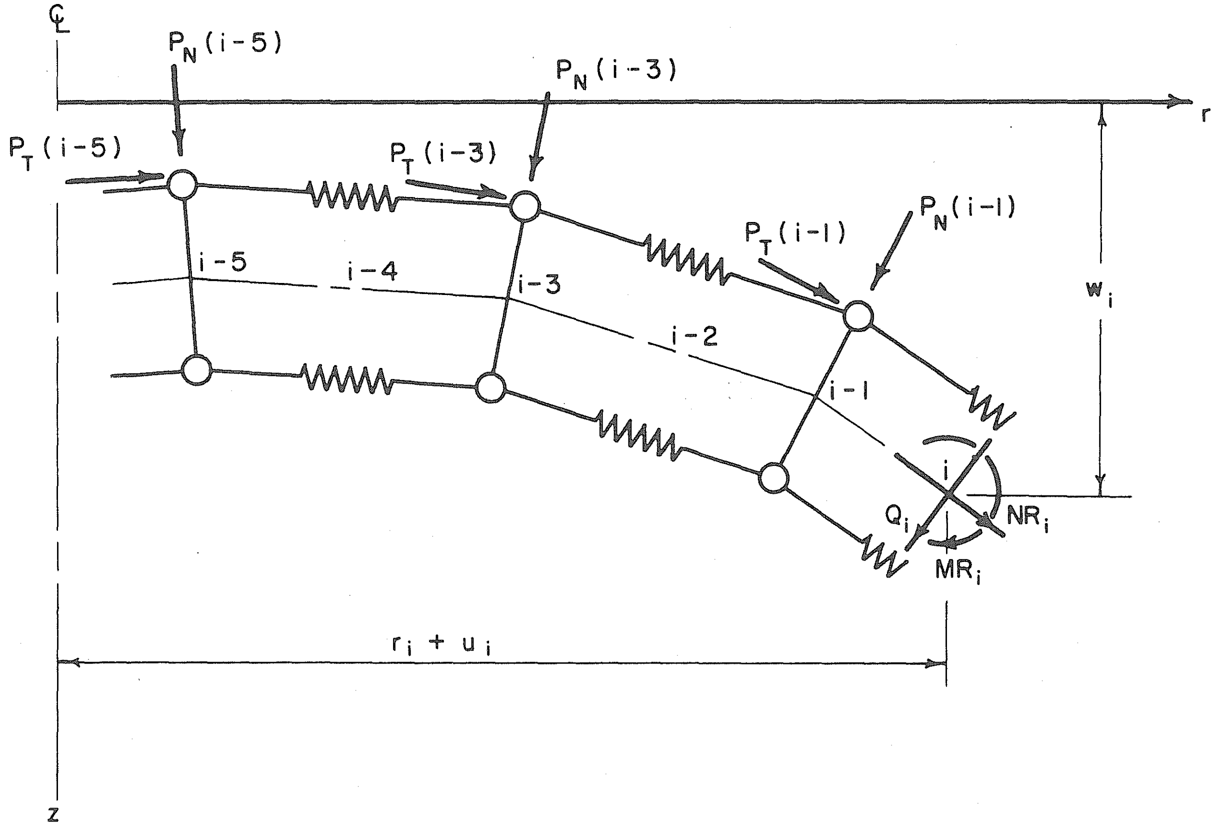


Figure 8. Equilibrium of shear forces from the model.

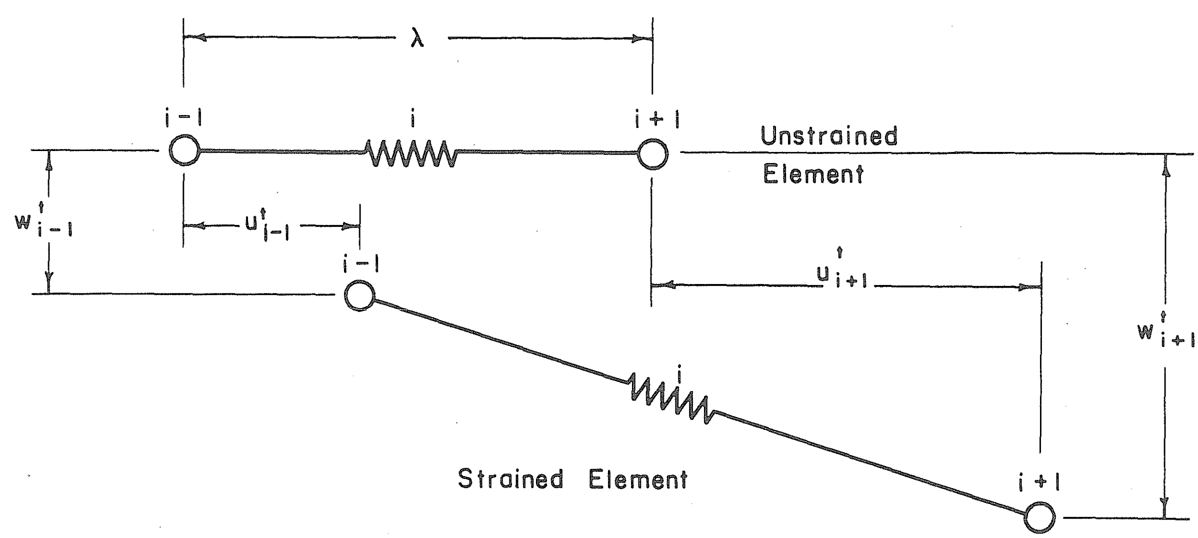


Figure 9. Strain from the model.

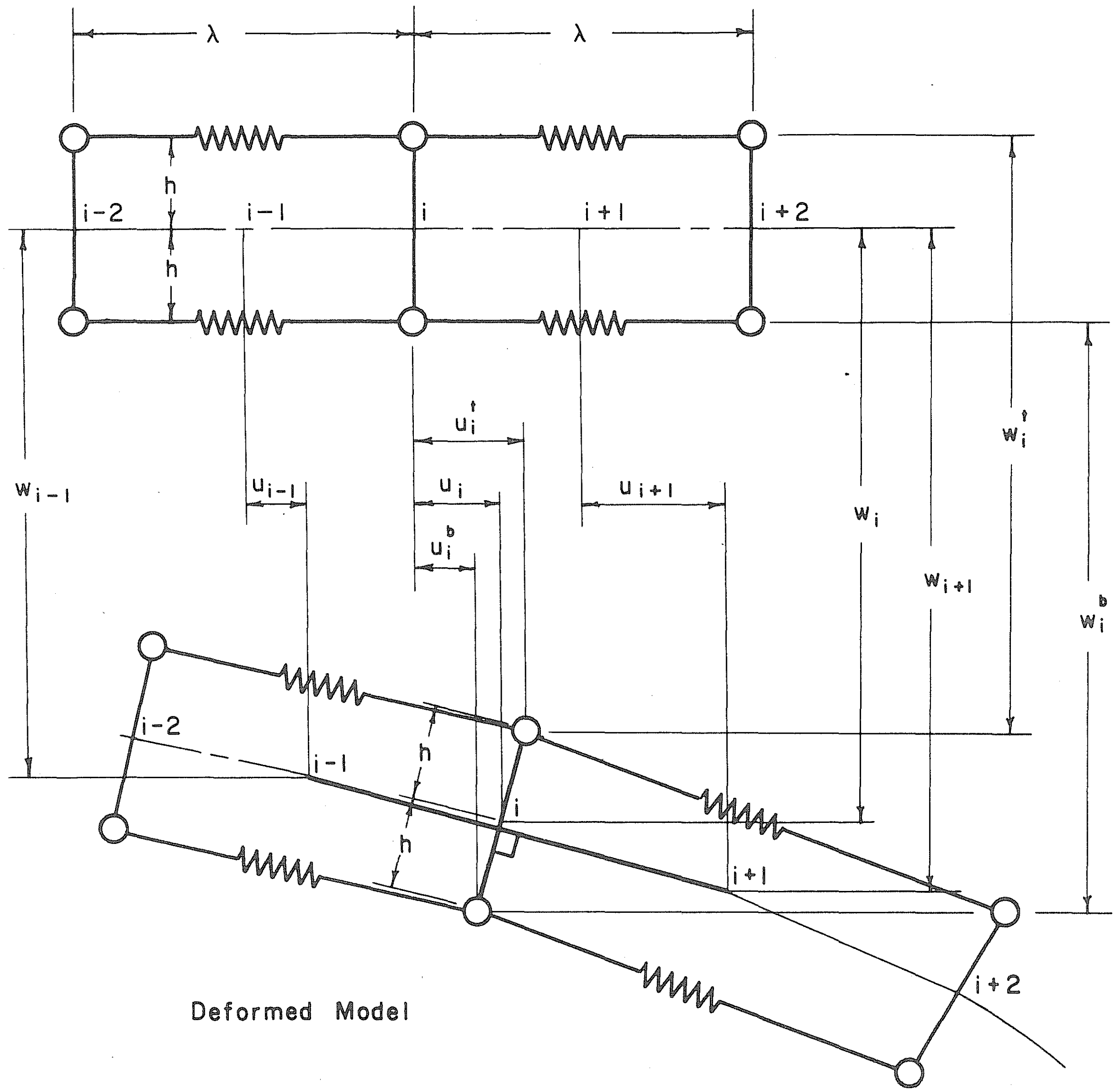


Figure 10. Transformation of displacements in the model.

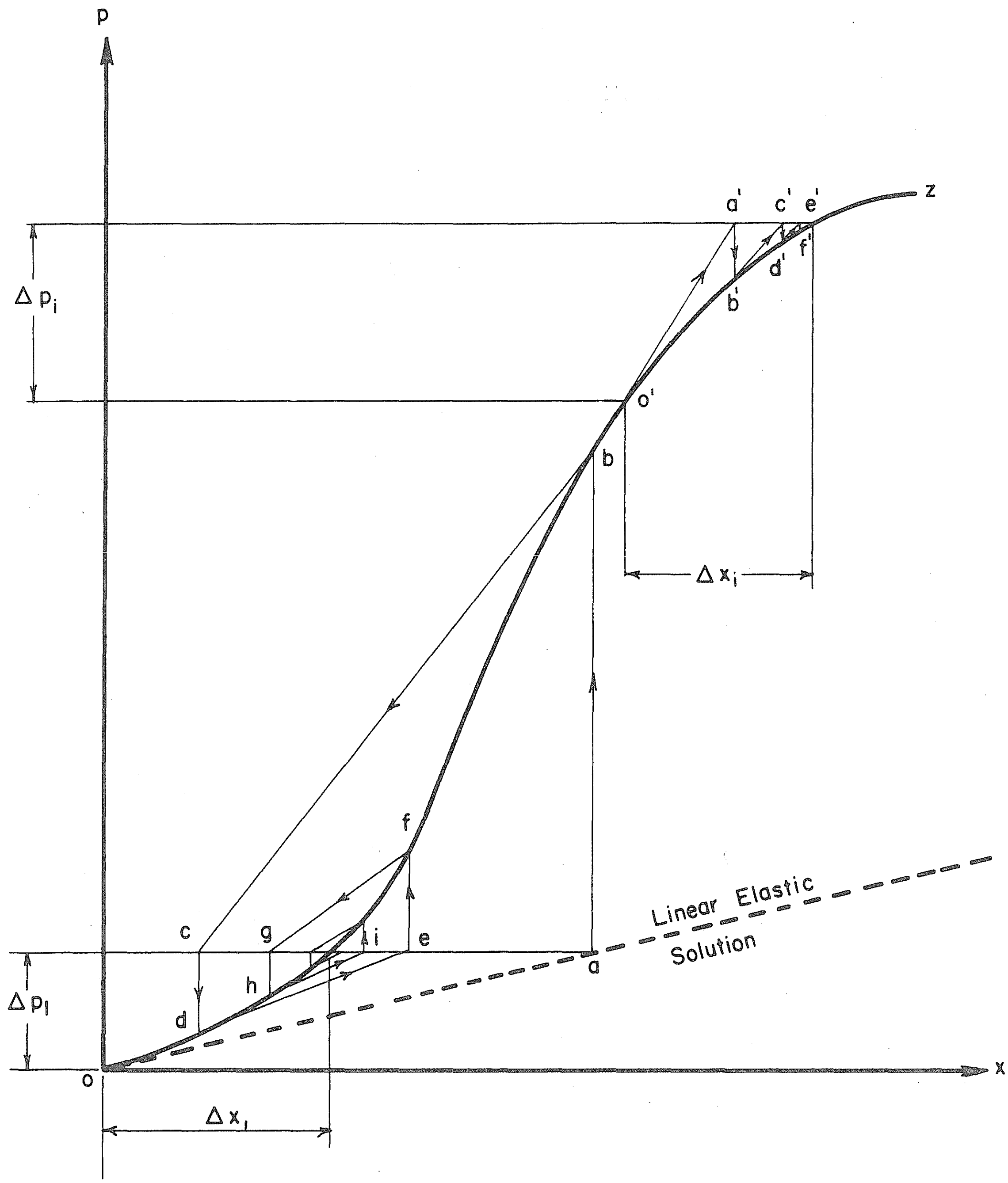


Figure 11. Solution path.

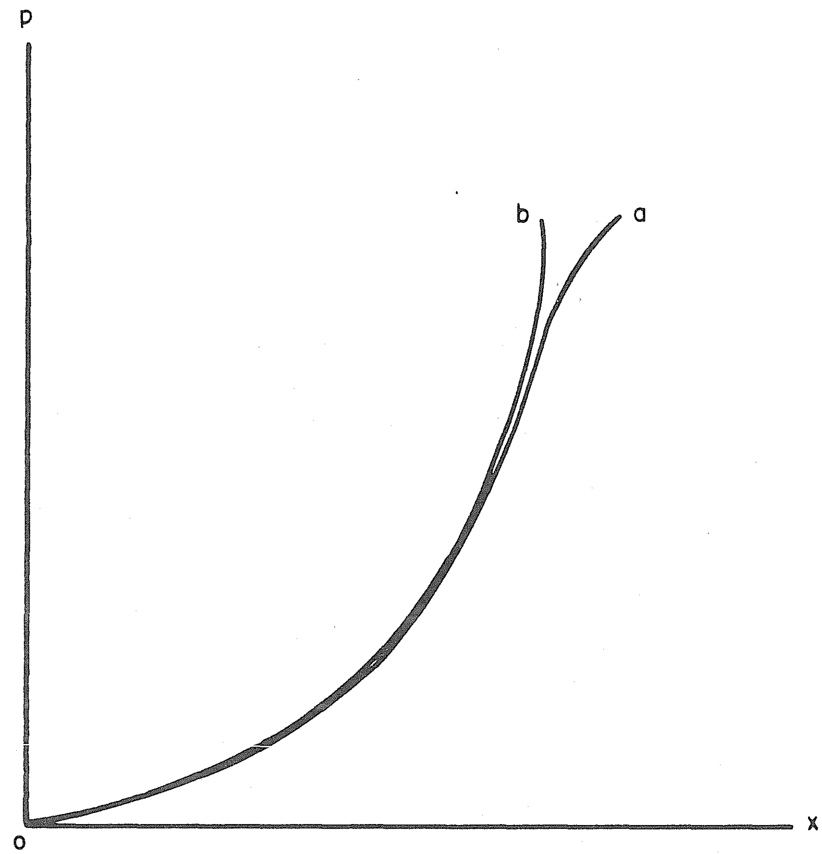


Figure 12. Separation of strings.

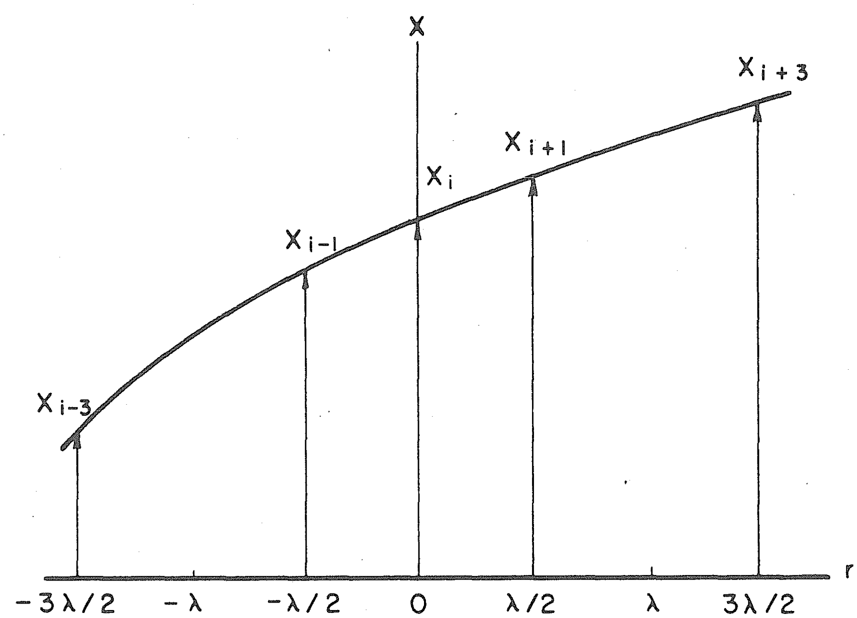


Figure 13. Fit of $x_i^2$ to a cubic through $x_{i-2}^1$, $x_{i-1}^1$, $x_{i+1}^1$ and $x_{i+2}^1$.

FLOW DIAGRAM

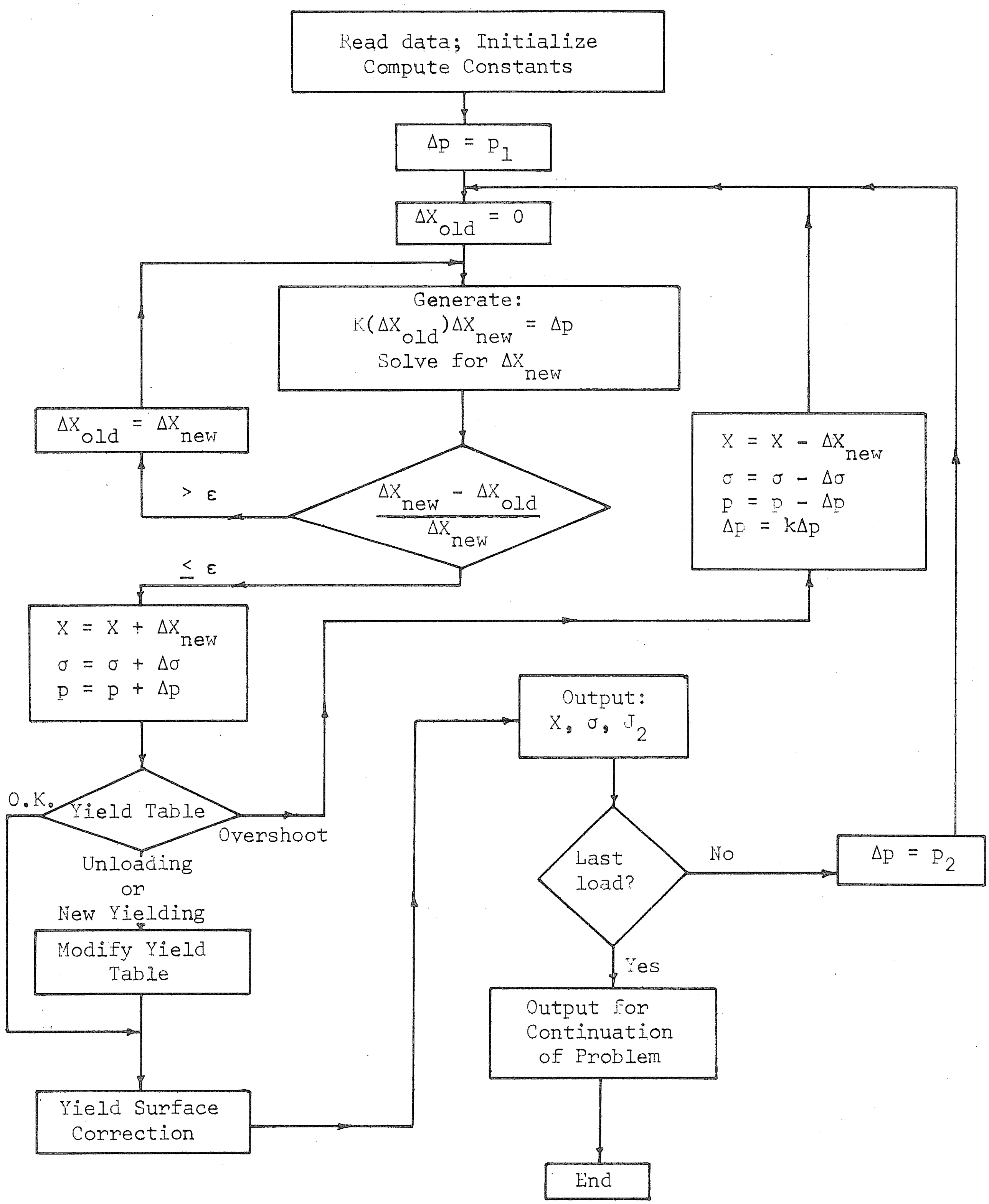


Figure 14. Flow diagram.

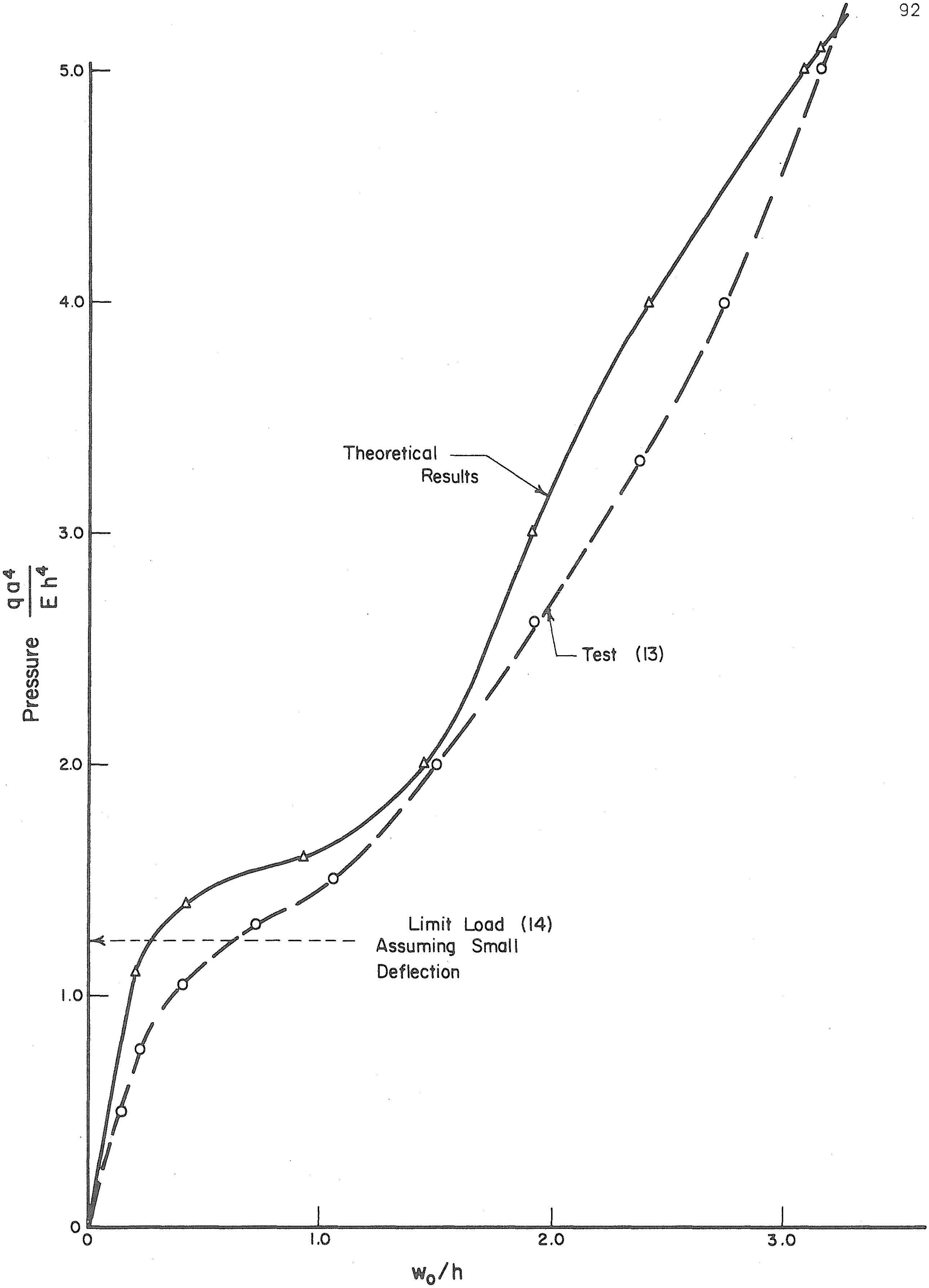


Figure 15. Load-deflection curves for a clamped plate subjected to a uniform pressure.

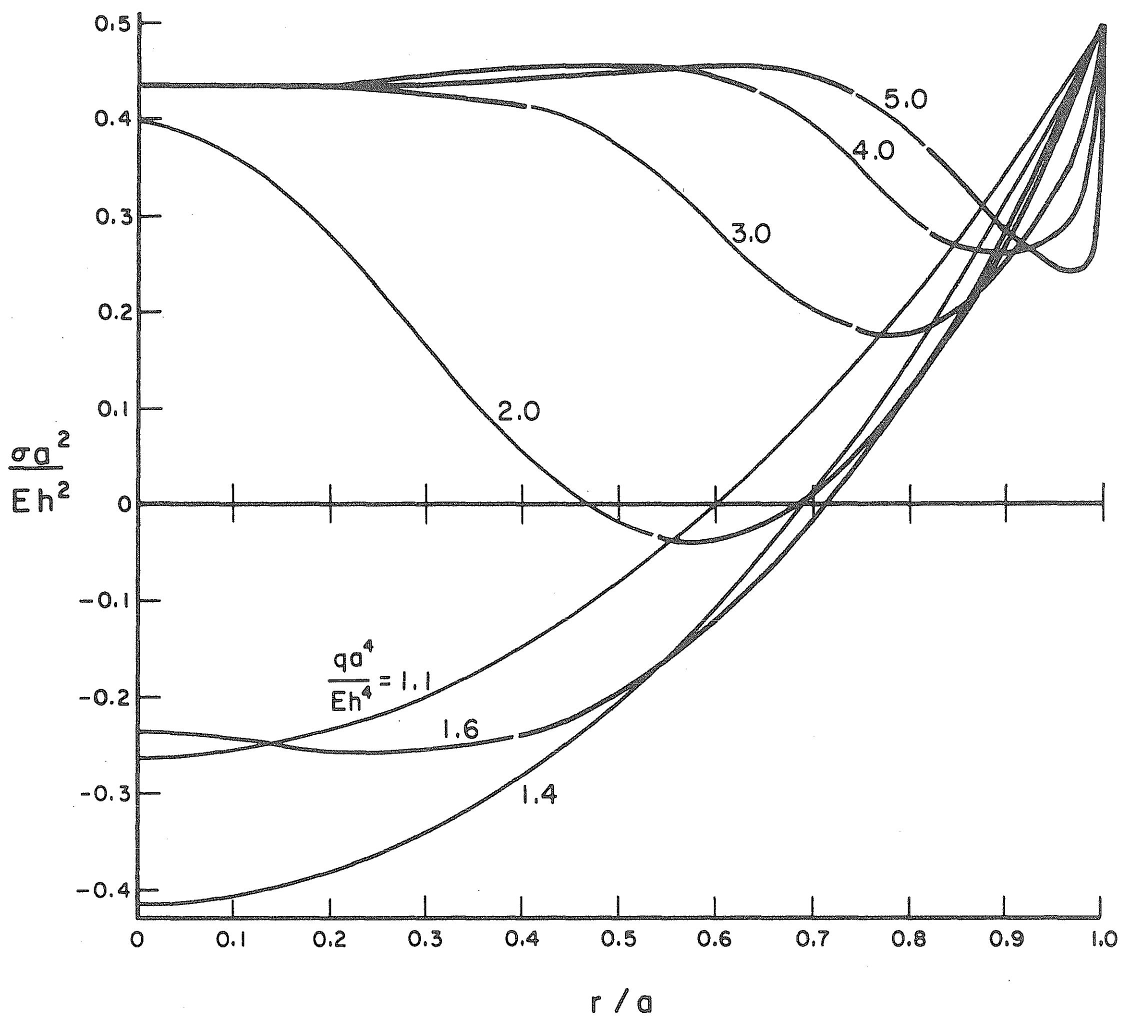


Figure 16. Radial stress in the top sheet.

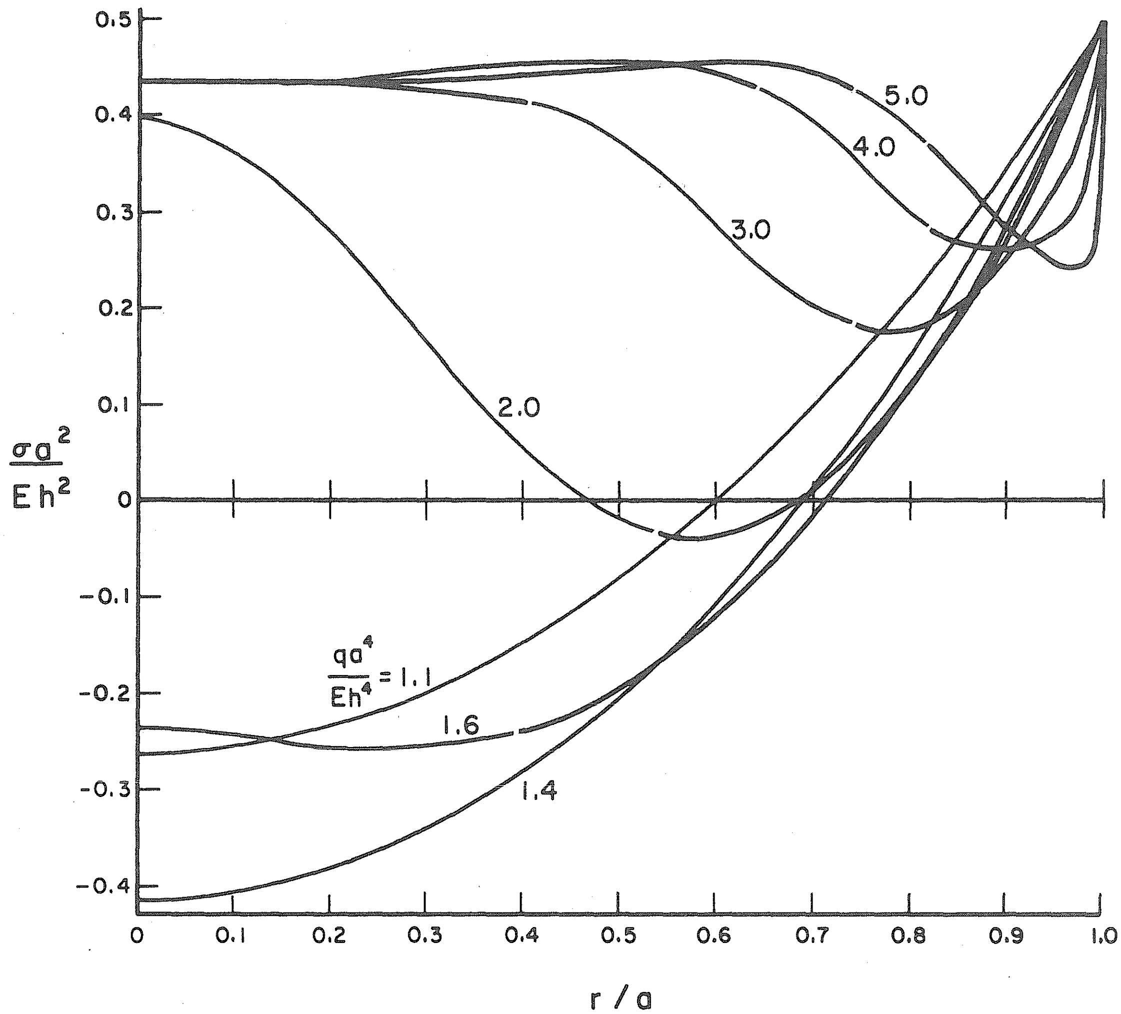


Figure 16. Radial stress in the top sheet.

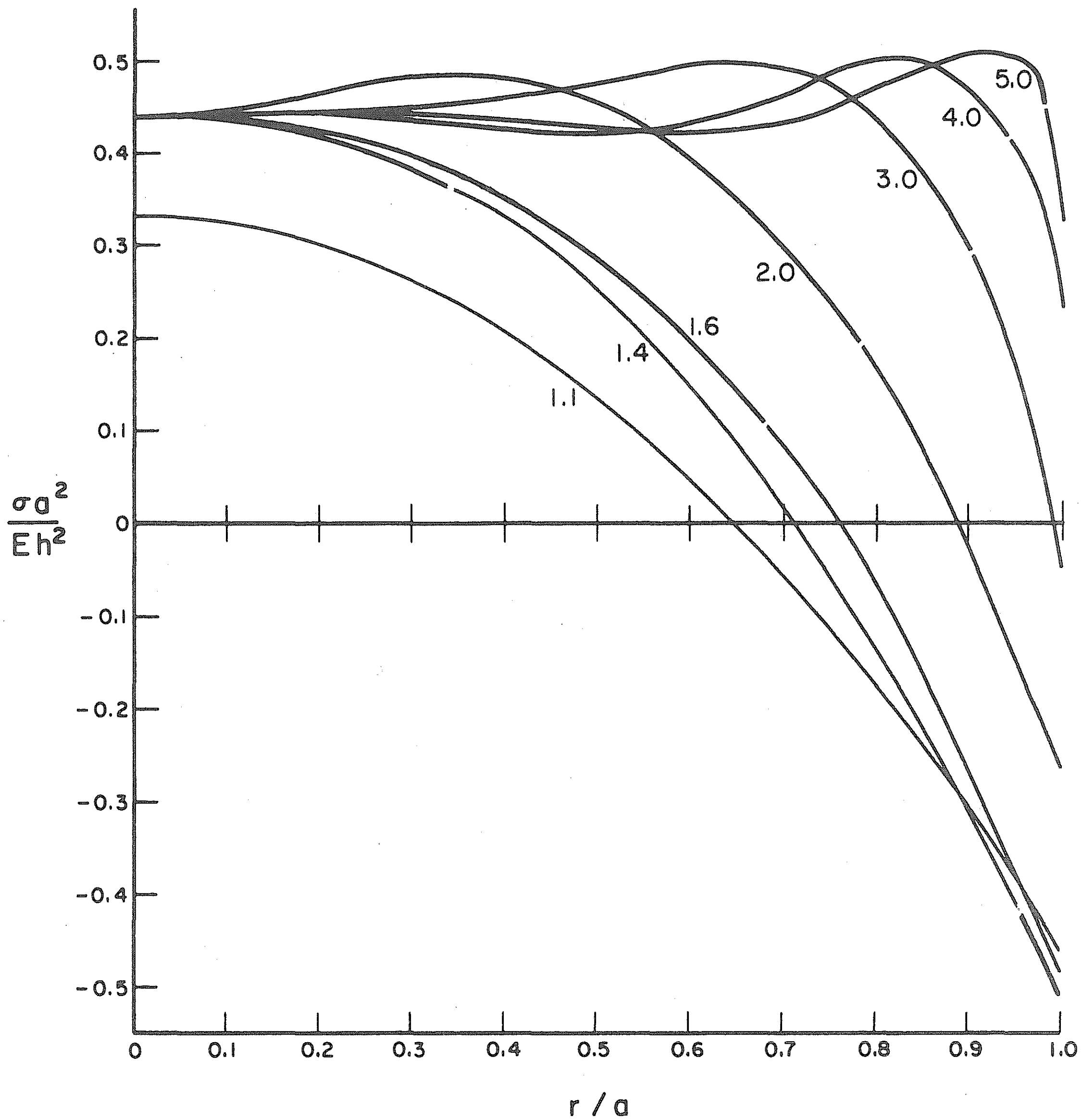


Figure 17. Radial stress in the bottom sheet.

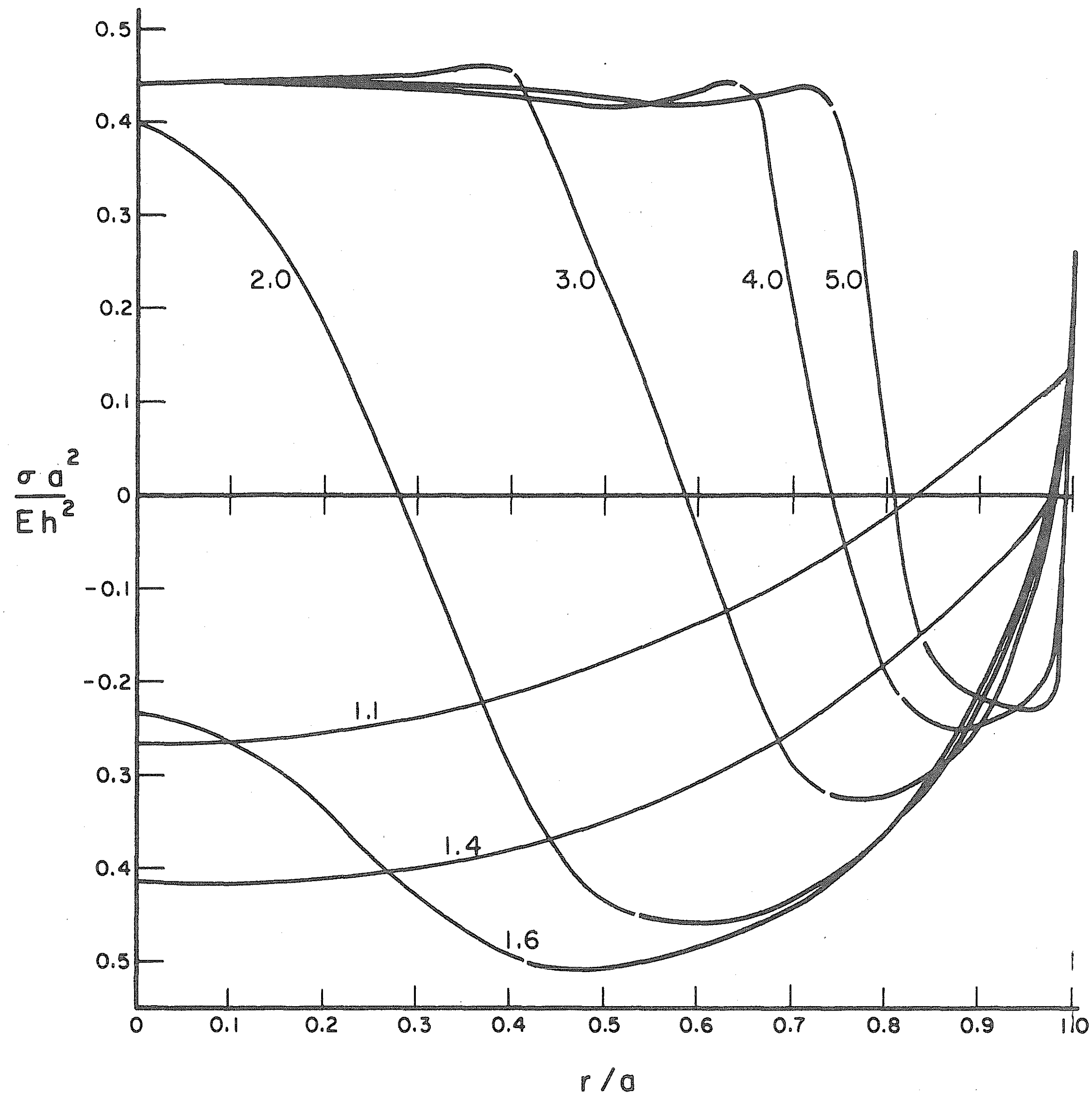


Figure 18. Tangential stress in the top sheet.

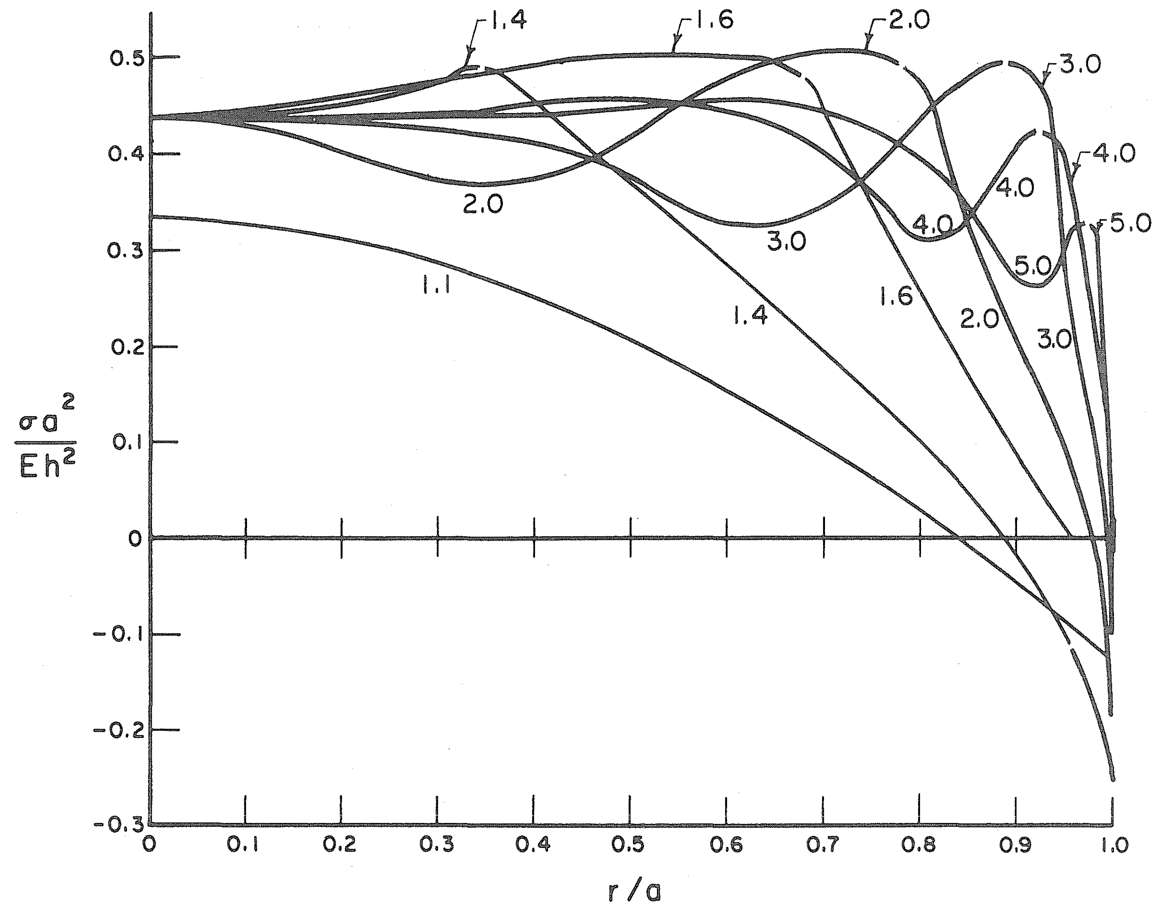


Figure 19. Tangential stress in the bottom sheet.

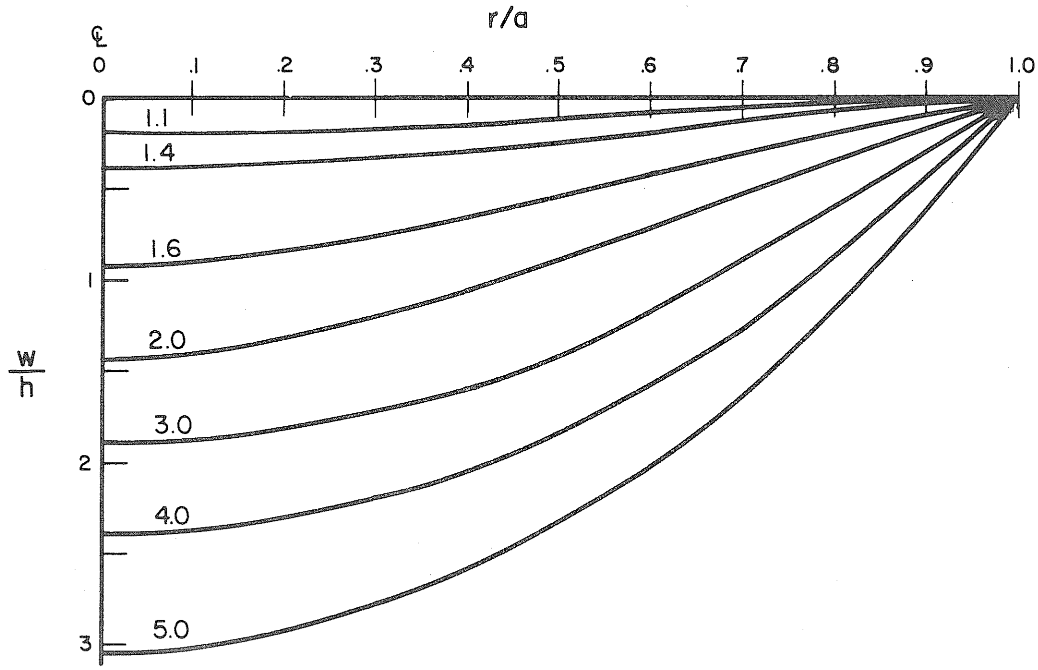


Figure 20. Vertical displacement profiles.

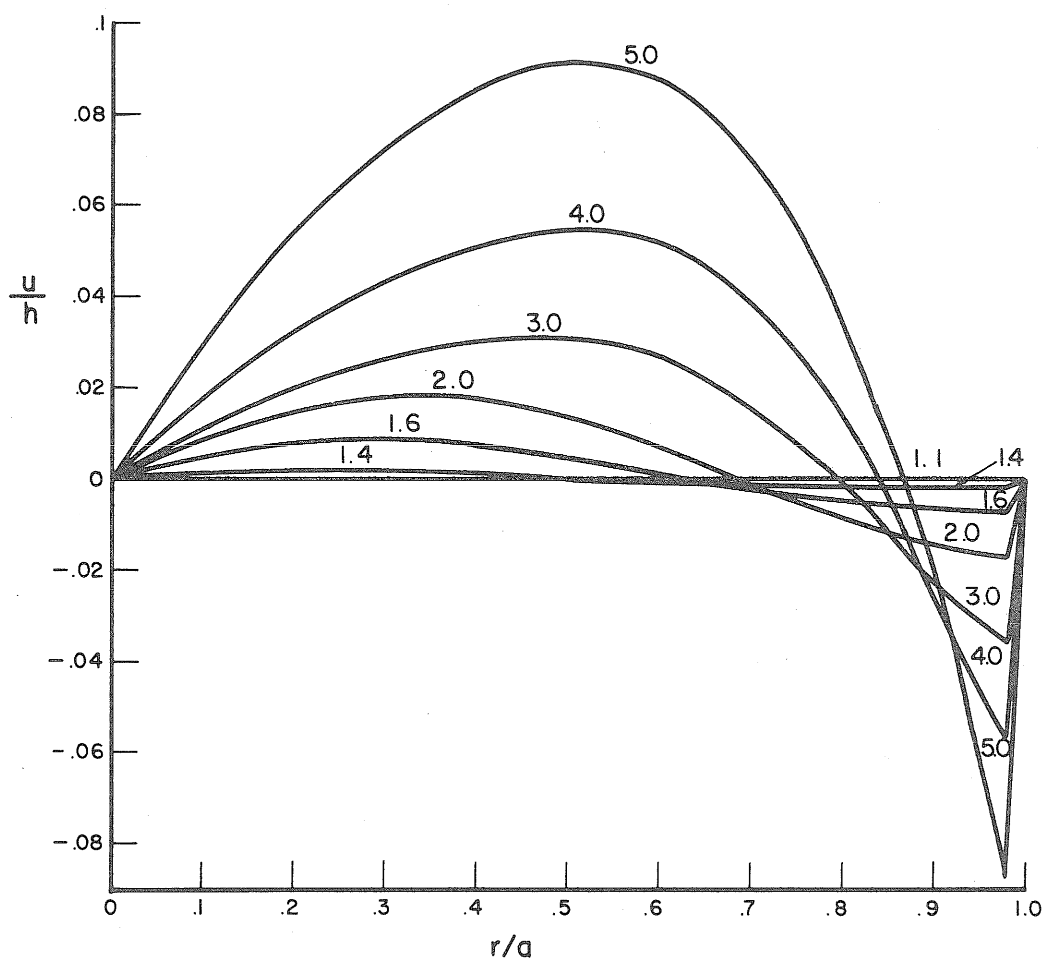


Figure 21. Horizontal displacement profiles of the middle surface.

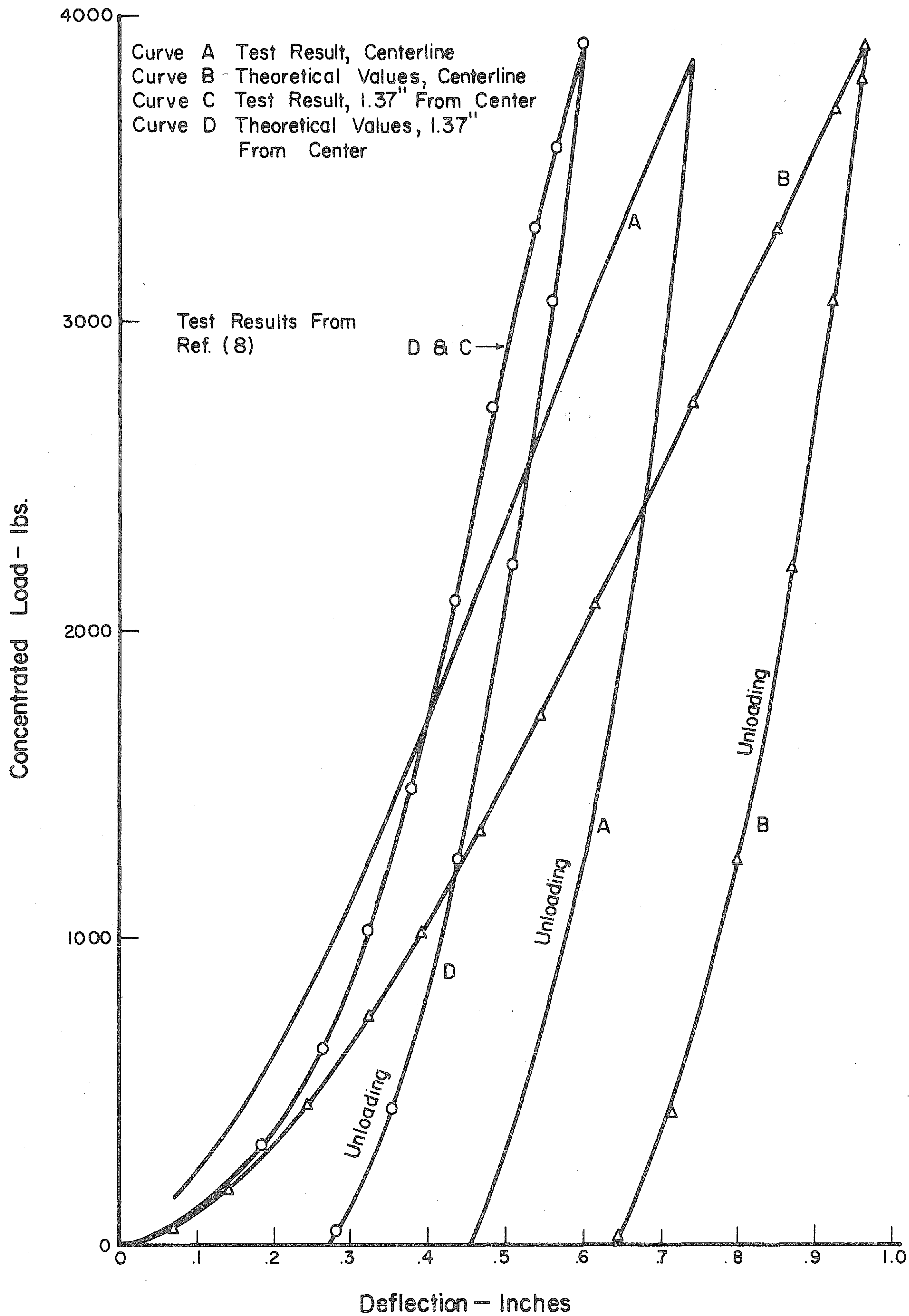


Figure 22. Load-deflection curves for a simply supported plate loaded with a concentrated load.

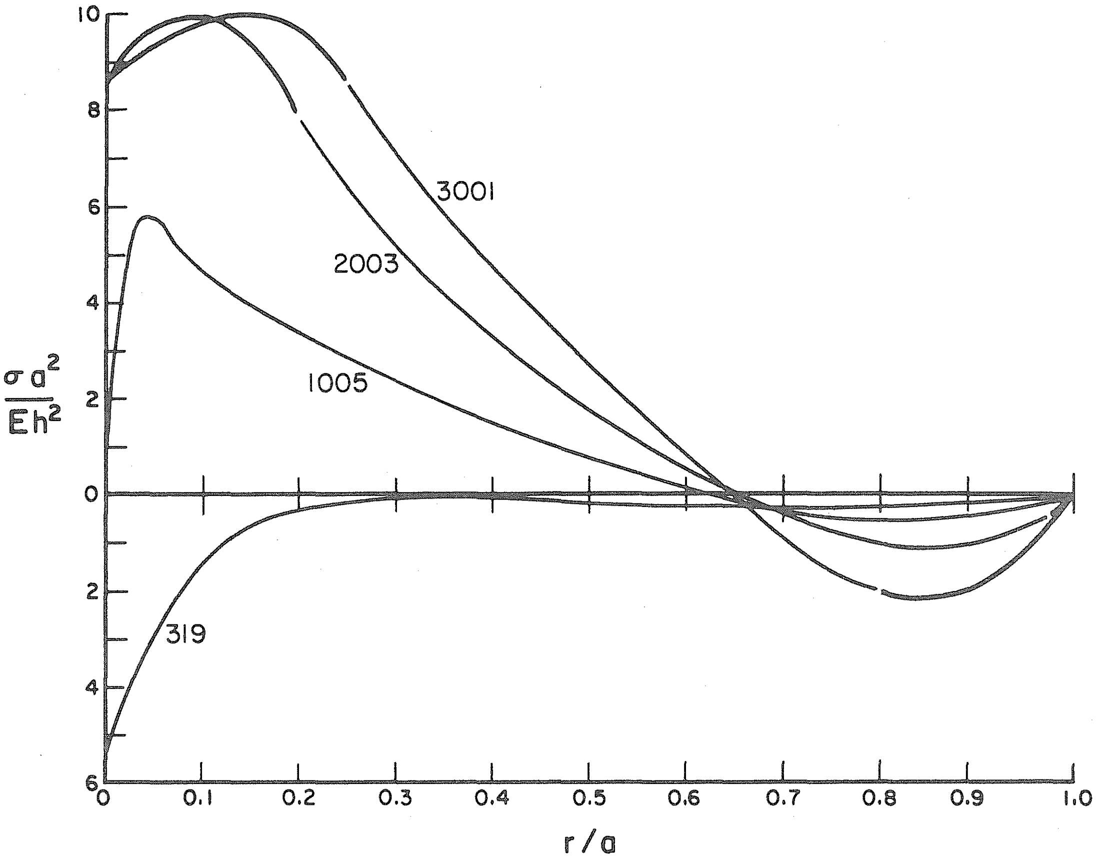


Figure 23. Radial stress in the top sheet.

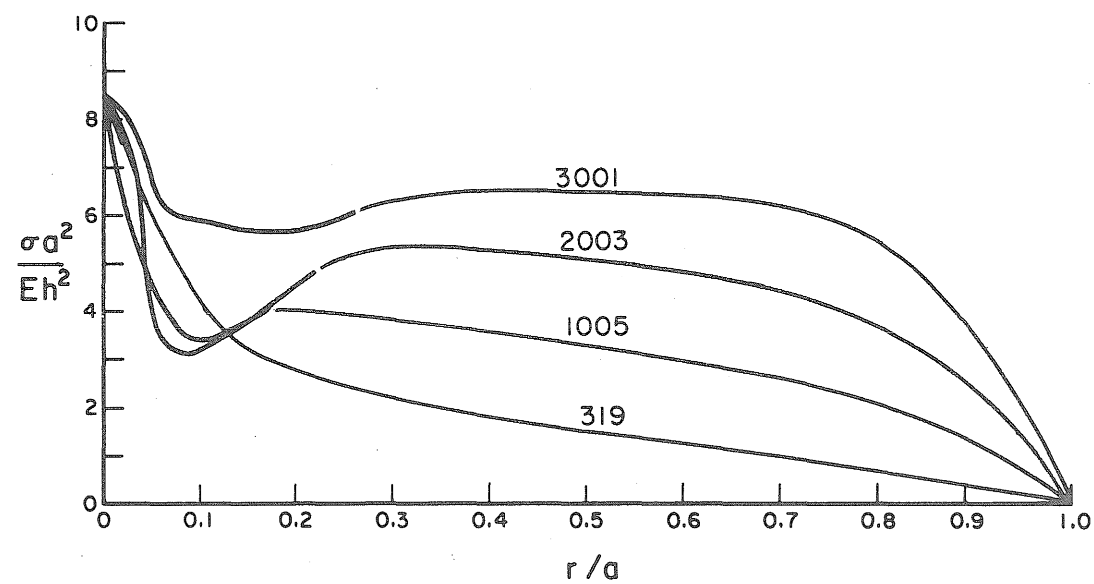


Figure 24. Radial stress in the bottom sheet.

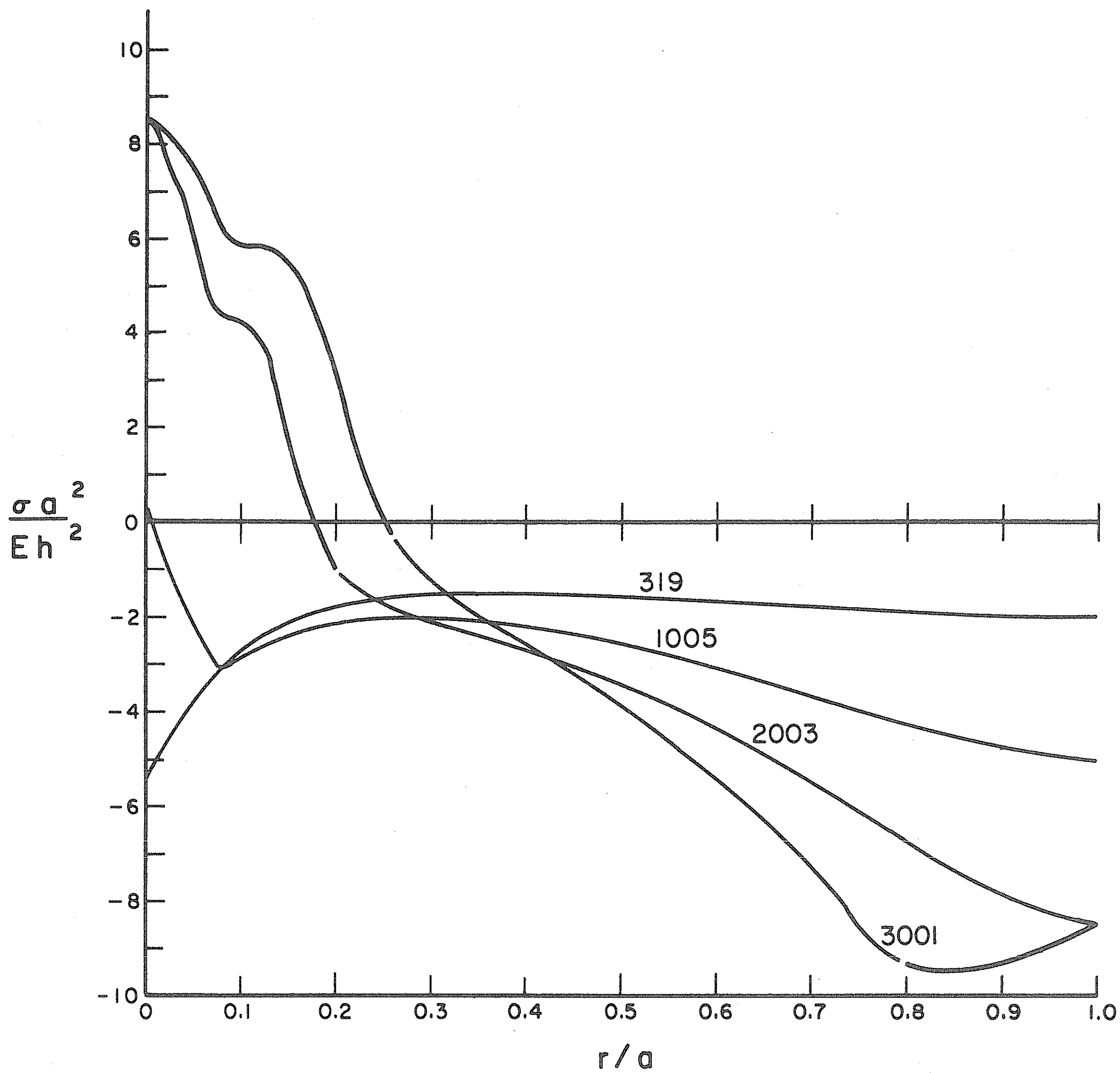


Figure 25. Tangential stress in the top sheet.

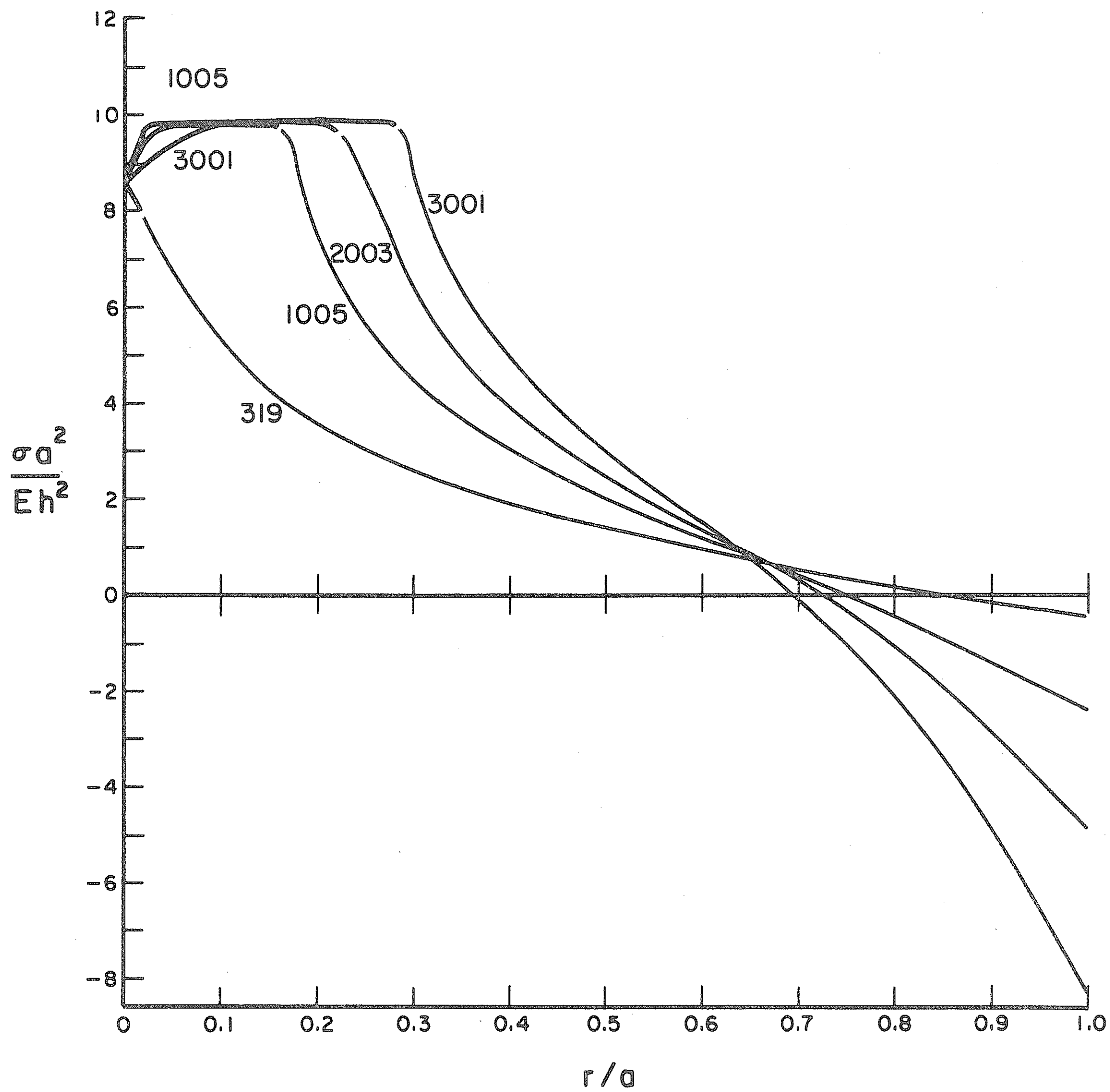


Figure 26. Tangential stress in the bottom sheet.

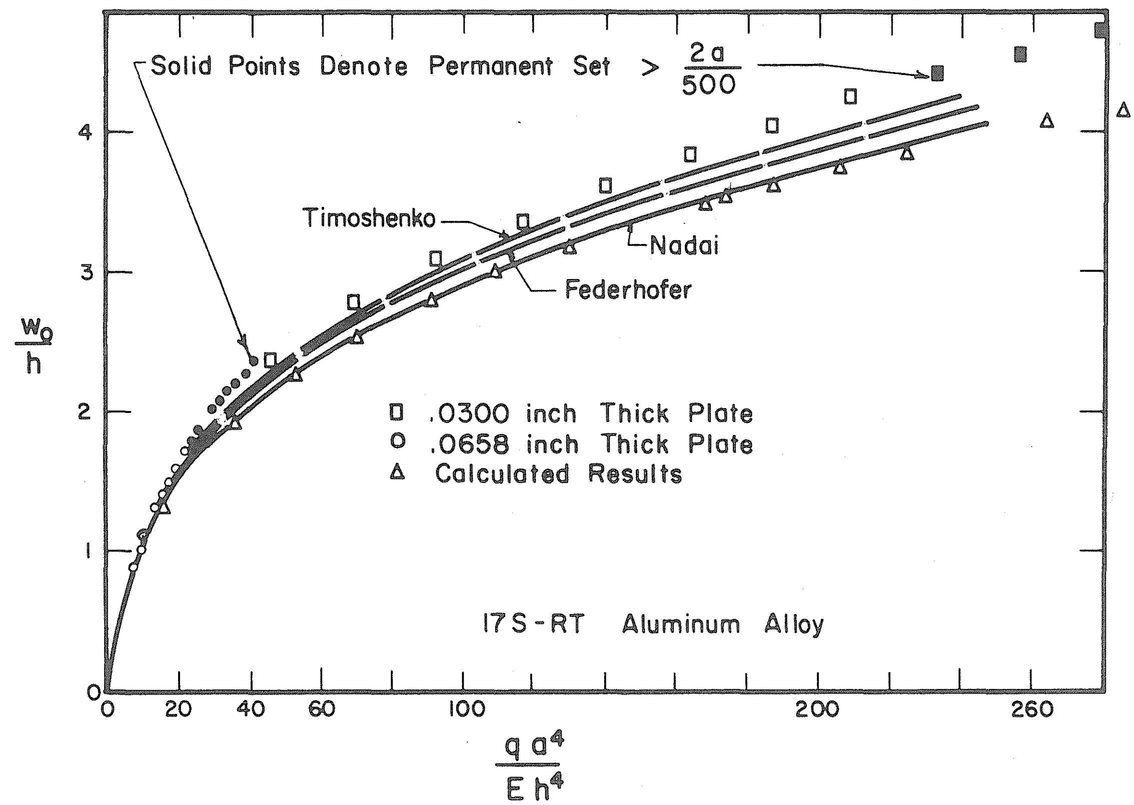


Figure 27. Load-deflection curves for a clamped plate subjected to a uniform pressure.

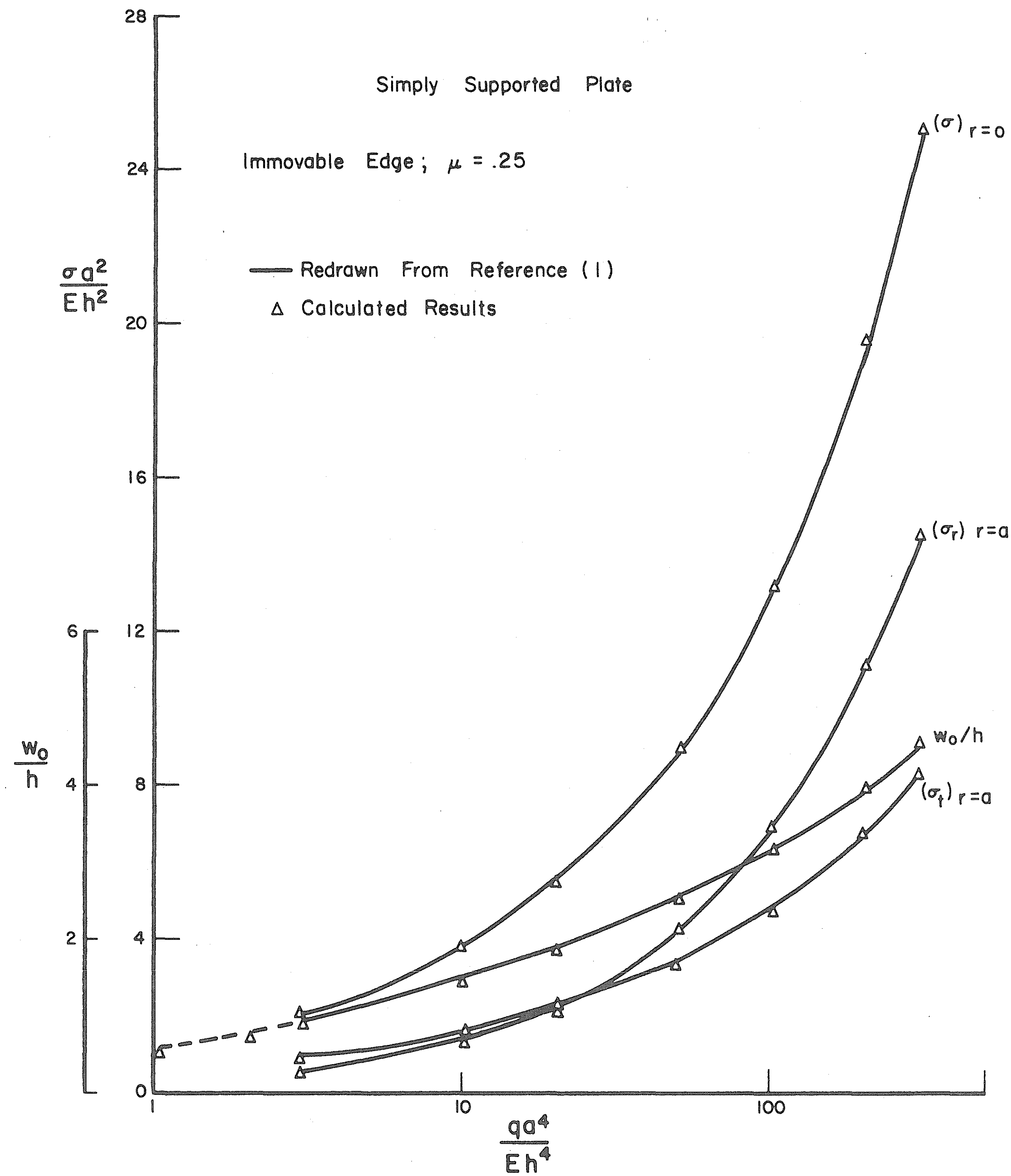


Figure 28. Displacements and stresses versus normal load for a simply supported plate with immovable edges.

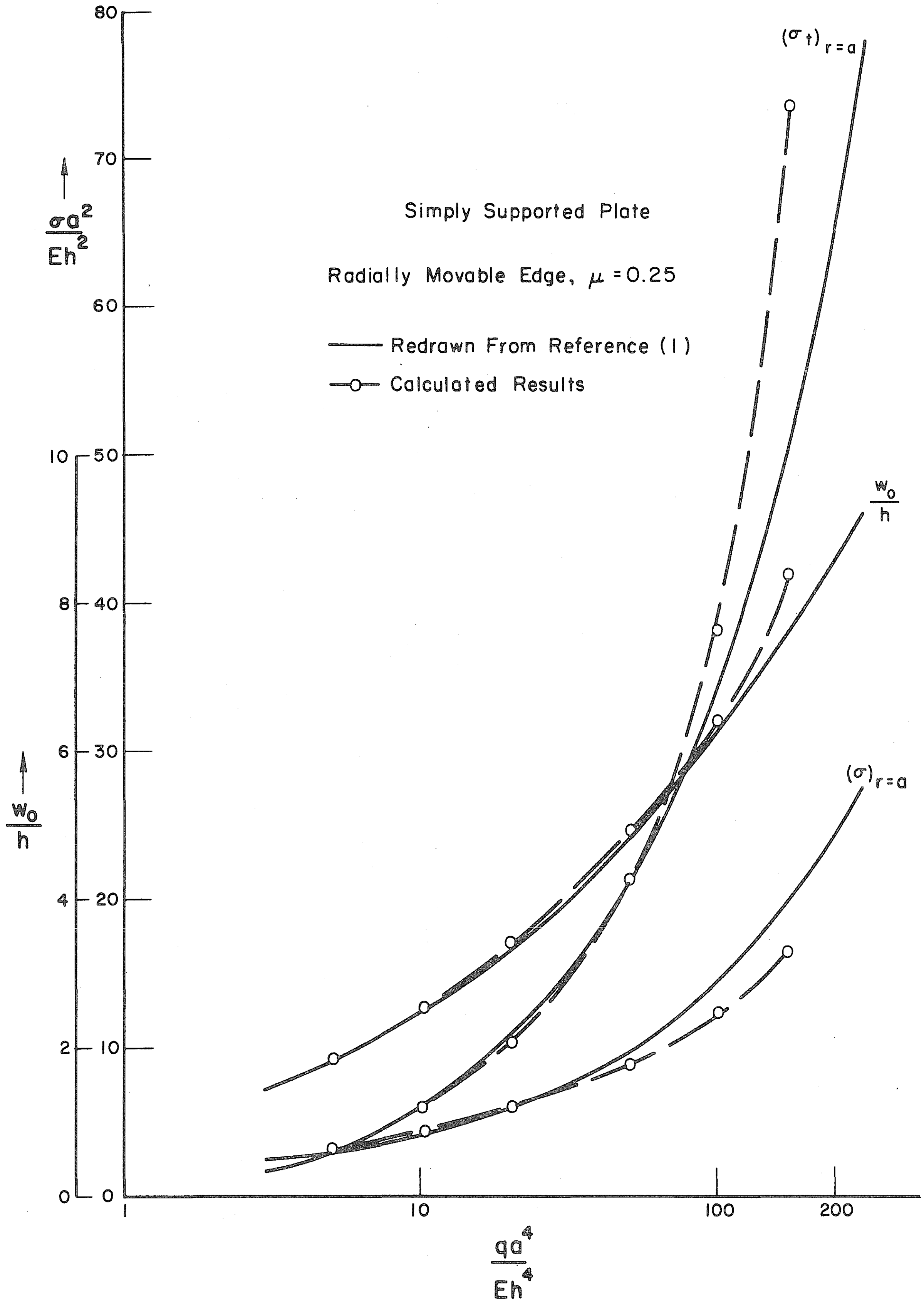


Figure 29. Displacements and stresses versus normal load for a simply supported plate with movable edges.

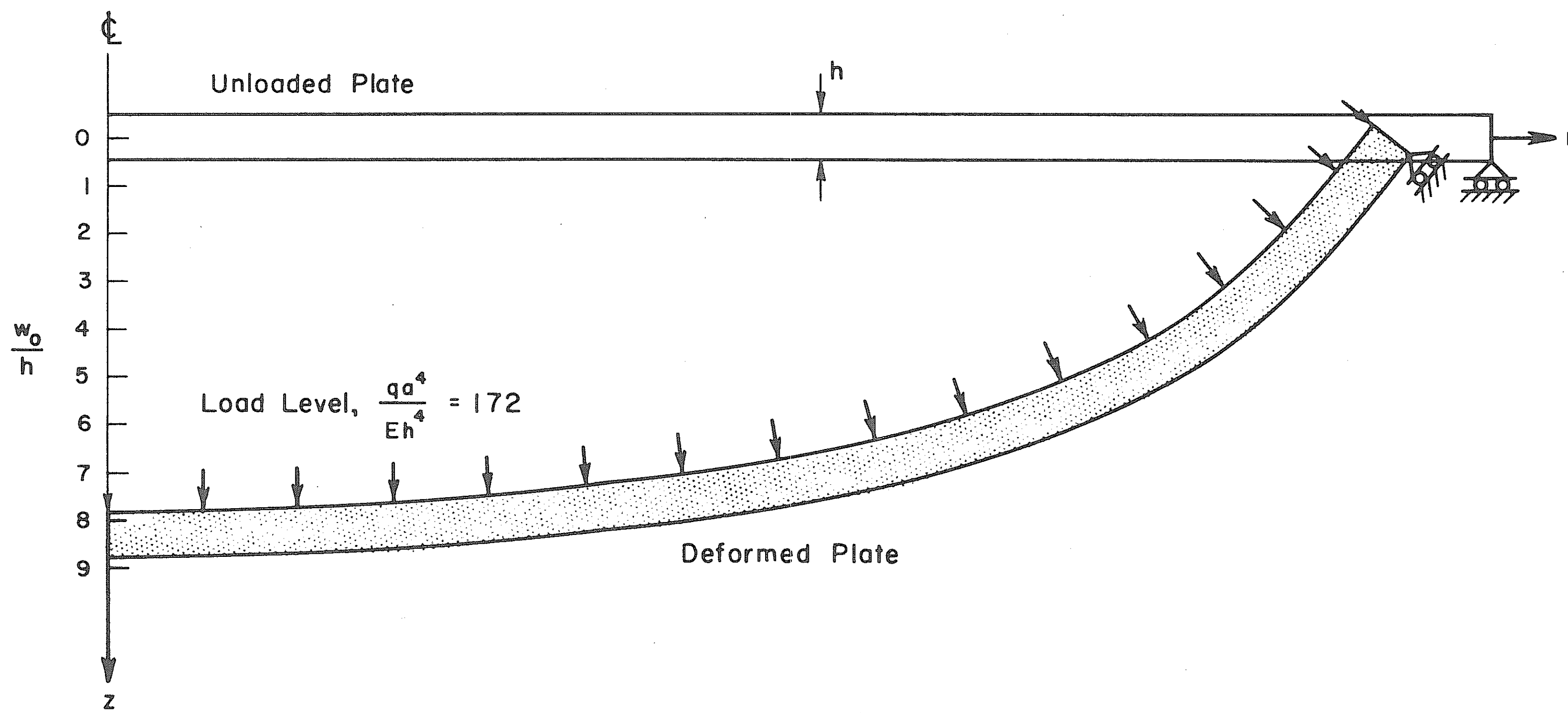


Figure 30. Cross-section of loaded plate.

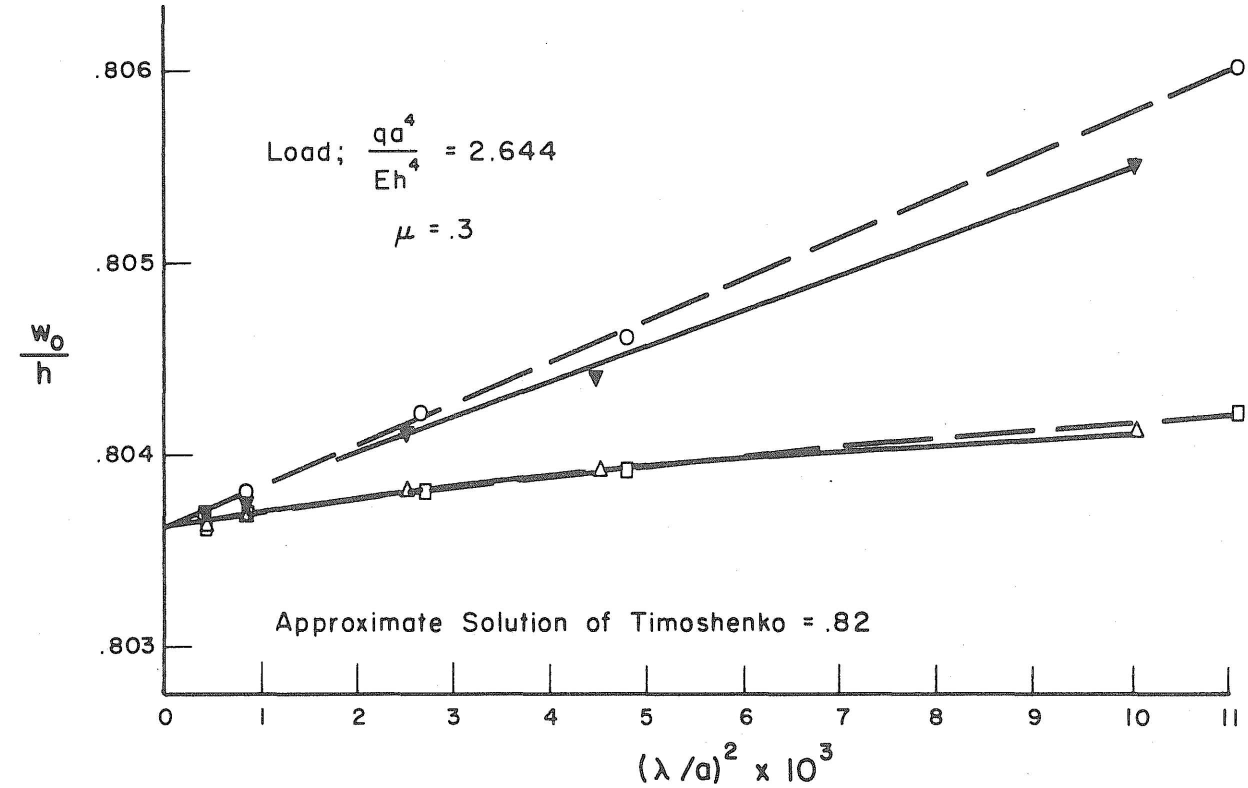


Figure 31. Convergence of displacements with decreasing mesh length.

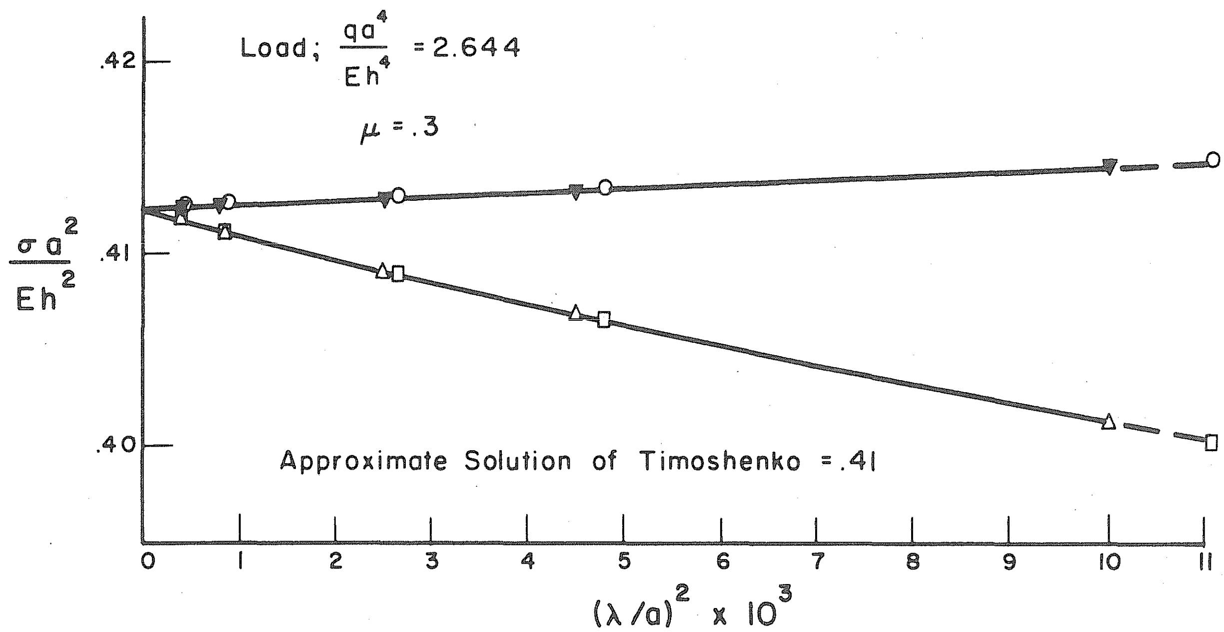


Figure 32. Convergence of radial membrane stress at the edge with decreasing mesh length.